 © 2014 Westinghouse Electric Company LLC. All Rights Reserved

Westinghouse VERA Test Stand

Zero Power Physics Test Simulations for the **AP1000®** PWR

Fausto Franceschini, Westinghouse Electric Company LLC
Andrew Godfrey, Oak Ridge National Laboratory
Joel Kulesza, Westinghouse Electric Company LLC
Robert Oelrich, Westinghouse Electric Company LLC

L3.AMA.VDT.P8.01 Milestone Report
CASL-U-2014-0012-000

March 6, 2014

Westinghouse

REVISION LOG

Revision	Date	Affected Pages	Revision Description
0	Jan 31, 2014	All	First Issue
1	Mar 6, 2014	Section 6, Executive Summary, Conclusions, Appendix A and D	VERA reactivity coefficients added, KENO reactivity coefficient uncertainties improved.

Document pages that are:

Export Controlled None

IP/Proprietary/NDA Controlled None

Sensitive Controlled None

Requested Distribution:

To: Doug Kothe, ORNL, CASL Director

Doug Burns, INL, CASL Deputy Director

Paul Turinsky, NCSU, CASL Chief Scientist

Copy: Jeff Banta, ORNL, CASL Program Manager

Jess Gehin, ORNL, CASL PHI Focus Area Lead

Scott Palmtag, CASL PHI Focus Area Deputy Lead

Bill Martin, UM, CASL RTM Focus Area Lead

Tom Evans, ORNL, CASL RTM Focus Area Deputy Lead

Zeses Karoutas, Westinghouse, CASL AMA Focus Area Lead

Steve Hess, EPRI, CASL AMA Focus Area Deputy Lead

Rose Montgomery, TVA, CASL AMA Focus Area Deputy Lead

Heather Feldman, EPRI, Industry Council Chairman

EXECUTIVE SUMMARY

Westinghouse has successfully performed simulations of zero power physics tests (ZPPT) for its state-of-the-art **AP1000**® reactor using VERA-CS. The VERA simulations were performed by Westinghouse personnel using a VERA build on a dedicated Westinghouse computer cluster within the framework of a "Test Stand" application of the CASL technology, and produced results with impressive agreement to reference calculations.

The primary objective of the CASL Test Stands is to engage industry partners to assess VERA performance on real-world industry applications through early VERA deployments at industry sites, to provide demonstrated applications of VERA and to collect feedback on potential improvements. Westinghouse is the first organization to host a VERA Test Stand.

Westinghouse selected the core physics simulation of the **AP1000** pressurized water reactor (PWR) first core for its initial focus specifically because its advanced features are challenging to core simulators, and thus provide an excellent platform for assessment of VERA performance. These features include radial and axial heterogeneities, such as five fuel regions with U^{235} concentrations from natural U to 4.8 w/o ^{235}U, to achieve a low-leakage 18-month cycle with optimum fuel cycle economics. Enrichment zoning and multiple burnable absorbers are used for power shaping and reactivity control. These burnable absorbers include the Westinghouse Integral Fuel Burnable Absorber (IFBA), a thin ZrB_2 coating deposited on the pellet surface and discrete Wet Annular Burnable Absorber (WABA) rods, inserted at selected guide thimble locations. A combination of light ("gray") tungsten control banks and standard ("black") Ag-In-Cd control banks is employed for MSHIM™, an advanced operational strategy that provides robust core reactivity and axial power distribution control with minimal changes to the soluble boron concentration in the reactor coolant during both normal operation and power maneuvering scenarios. This MSHIM strategy employs an increased presence of control clusters (gray and black) in the reactor core during full power operation. Overall, these advanced features make the **AP1000** PWR a best-in-class generation III+ design, but also challenge core simulators, making the **AP1000** PWR especially suited to qualify VERA's performance and potential benefits.

An extensive set of simulations have been performed throughout this activity with the results presented in detail in this report. The SP_5P_3 VERA solver in 23 energy groups with on-the-fly pin-homogenized cross sections generated from a 252-group SCALE library has been used throughout this work. This approach has shown excellent agreement with the results from the SCALE 6.2 continuous energy Monte Carlo code KENO-VI, which has been assumed as the numerical reference for the simulations performed.

AP1000® and MSHIM™ are trademarks or registered trademarks of Westinghouse Electric Company LLC in the United States and may be registered in other countries throughout the world. All rights reserved. Unauthorized use is strictly prohibited.

In particular, the Hot Zero Power (HZP) critical boron concentration predicted by VERA is within 3 ppm of the KENO prediction, as shown in Table 1-1. The difference in boron worth is 0.2 pcm/ppm. The Doppler, Moderator and Isothermal Temperature Coefficients, DTC, MTC and ITC, are respectively within 0.2, 0.4 and 0.6 pcm/F (Table 1-2). The temperature reactivity coefficient simulations is an area recommended for further investigation since the differences observed, while small, are not insignificant.

The root mean square (RMS) difference in rod worth between VERA and KENO is 4 pcm, with a maximum difference of 9 pcm across 11 control banks employed in the **AP1000** PWR, including gray and black absorbers (Table 1-3). A plot summarizing the rod worth comparison for VERA vs. KENO is given in Figure 1-1.

The results of the ZPPT simulations from VERA are consistent with Westinghouse predictions using in-house core physics industrial tools and licensed methods; this reinforces the confidence in the predictions for the start-up tests of the **AP1000** PWR first core, scheduled to occur within the next year.

VERA also shows remarkable agreement with KENO in regards to power distribution predictions, for simulations including radial core slices as well as a 3D multi-assembly with partially-inserted control rods. A chart summarizing the power distribution comparison for VERA vs. KENO is given in Figure 1-2, showing the RMS in power difference multiplied by 100 across the simulations performed. It can be seen that the RMS is well below 1.0% for every simulated case, including a 3x3 multi-assembly case with a partially inserted Ag-In-Cd control bank in the central position. Detailed power distribution results are given in Section 6 of this report.

It is noted that 3D core power distribution comparisons have not been performed here due to the difficulty of obtaining a low-uncertainty reference Monte Carlo solution over 3D core geometry. Work is ongoing to obtain this reference using Shift, a massively parallel Monte Carlo code under development in VERA and the results obtained with Shift for the **AP1000** PWR core will be reported separately.

In terms of practicality of use, the VERA input system, VERAIN, has been found to provide a practical and effective interface to set up simulations for commercial PWR cores. With VERAIN, it has been possible to implement a core model of the complexity of the **AP1000** PWR core in a convenient ASCII format using a common input deck.

All the VERA simulations reported have been performed on a build of VERA installed on a dedicated Westinghouse compute cluster with 48 compute nodes with 12 processing cores per node and 96 GB of RAM per node. A table summarizing VERA's computational performance is given in Table 1-4. 2D geometries up to entire core slices have been executed within minutes on a reasonable number of compute cores, e.g. 5 minutes on 144 cores for a radial slice of the **AP1000** PWR core, using the SP_5P_3 solver with 23-energy group on-the-fly cross section generation.

As expected, this approach does become increasingly resource intensive as the geometry is extended to 3D. The ZPPT calculations performed, essentially 3D core eigenvalue calculations with no coupling or depletion, could be executed in less than two hours per calculation on 320 cores. Using SP_5P_3 with the current implementation for core cycle calculations with coupling and depletion would result in impractical calculation time, and memory requirements beyond what is currently available on a mid-size industry computer platform. While use of a lower SP_N order with fewer number of energy groups should alleviate these issues, the resulting impact on accuracy remains to be ascertained.

In summary, Westinghouse has observed an impressive agreement between VERA-based ZPPT simulations and KENO-based reference numerical results for its **AP1000** PWR first core, an advanced simulation application that can be challenging for core simulators. This application is illustrative of the benefits fostered by the availability of higher-fidelity simulators to the nuclear industry to obtain reliable reference solutions for challenging simulation scenarios. The work performed in the VERA Test Stand reinforces the confidence in the start-up tests prediction for the **AP1000** PWR first core, while contributing to expansion of the validation basis of VERA with best-in-class core design and operational strategy.

The recommended, logical next step is the simulation of **AP1000** reactor cycle depletion with VERA-CS. This next step will require completion of coupling with thermal-hydraulics, depletion capabilities and related developments in VERA-CS, as well as a substantial reduction of the required computational resources to enable to perform these simulations on industry computer clusters.

In addition to the successful performance assessment of current VERA-CS tools, Westinghouse reports significant additional benefits from its hosting of the Test Stand as a CASL partner. These benefits are spurred by the direct engagement of the parties involved and are discussed in the Westinghouse Test Stand Experience in Section 2. There have also been the expected challenges in the preparation and execution of the Test Stand, which were resolved thanks to the efforts and resources that each organization and individual involved have been willing to invest on this project. The enthusiasm and dedication of the CASL and Westinghouse personnel involved have been key contributors to the success of the Westinghouse Test Stand.

Table 1-1 HZP Reactivity Results

	KENO	VERA	VERA-KENO
All rods out start-up critical boron	**1313 ppm**	**1310 ppm**	**-3 ppm (-32 pcm)**

Table 1-2 Temperature Reactivity Coefficients

	KENO	VERA	VERA-KENO
Doppler Temperature Coefficient (DTC) pcm/F	-1.54 ± 0.03	-1.72	-0.18
Moderator Temperature Coefficient (MTC) pcm/F	-1.12 ± 0.04	-1.50	-0.38
Isothermal Temperature Coefficient (ITC) pcm/F	**-2.66±0.05**	**-3.22**	**-0.56**

Table 1-3 Control bank Worth Results

		KENO	VERA-CS	
Bank	**Material**	**Worth (pcm) ± 2 pcm**	**ΔWorth (pcm)**	**ΔWorth (%)**
MA	Tungsten	258	-1	-0.5
MB	Tungsten	217	-5	-2.1
MC	Tungsten	188	-2	-1.1
MD	Tungsten	234	0	0.0
M1	Ag-In-Cd	651	-4	-0.6
M2	Ag-In-Cd	887	3	0.4
AO	Ag-In-Cd	1635	-4	-0.3
S1	Ag-In-Cd	1079	0	0.0
S2	Ag-In-Cd	1096	-9	-0.8
S3	Ag-In-Cd	1124	0	0.0
S4	Ag-In-Cd	580	-3	-0.4
		RMS	**4**	**0.8**
		Max	**9**	**2.1**

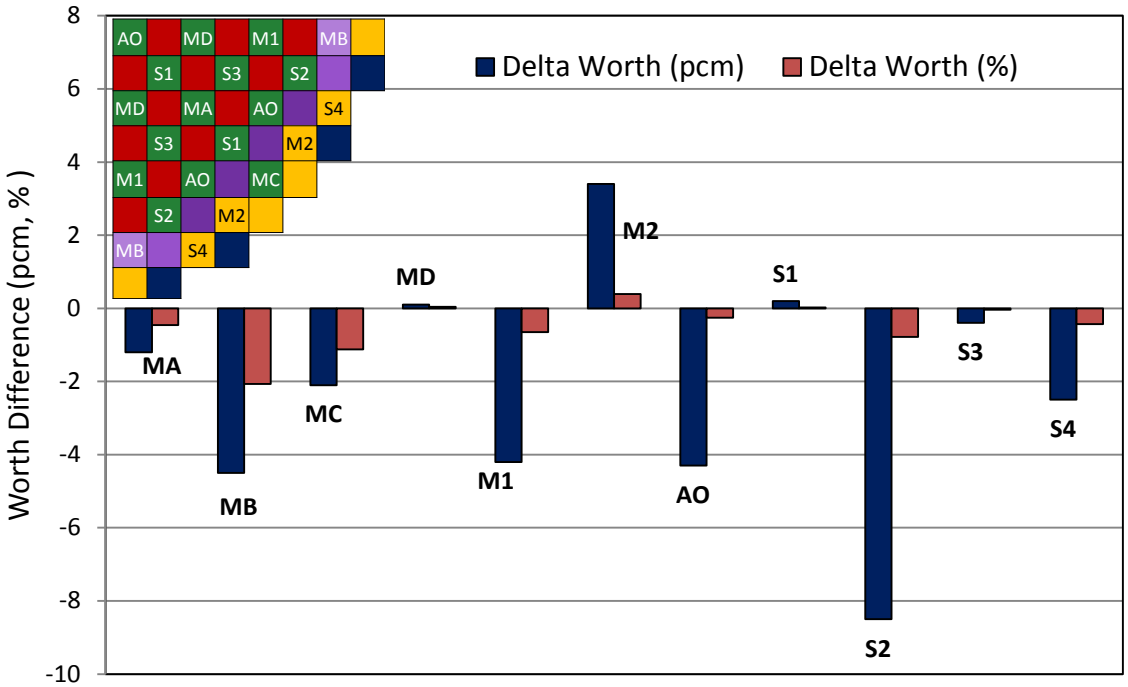

Figure 1-1 Delta in rod worth (in pcm and %) for VERA vs. KENO

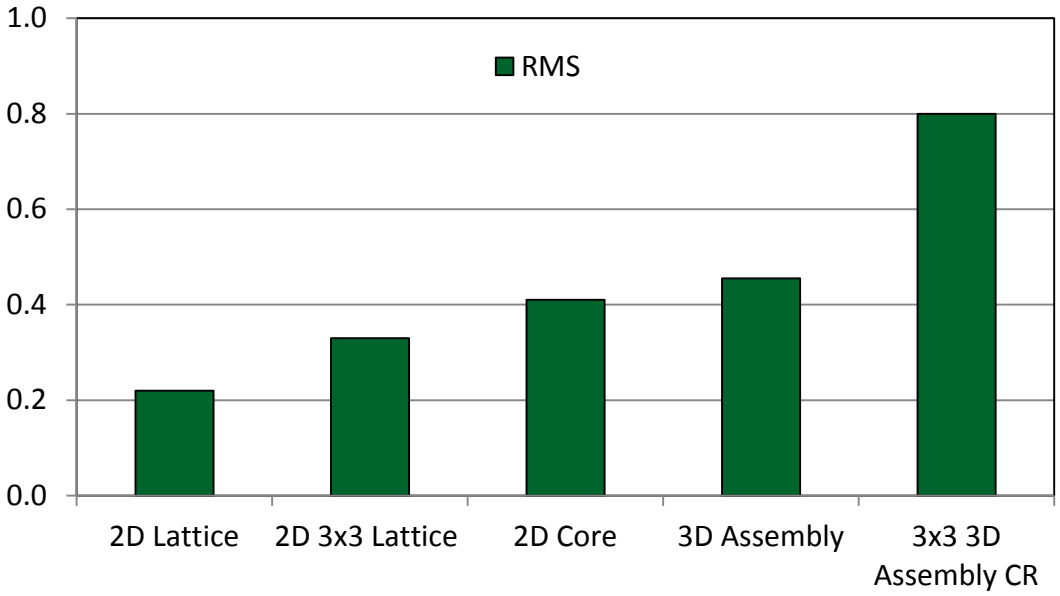

Figure 1-2 Delta power RMS (in %) VERA vs. KENO

Table 1-4 Computational performance of VERA-CS for AP1000 simulations on Westinghouse computer cluster

Case	Cores #	Cells #	Core hours	Wall Time (min)	Memory
2D Lattice	12	324	0.2	~1	<96 GB
3x3 Lattice	12	3K	0.4	~2	<96 GB
2D Core	144	86K	13	~5	<512 GB
3D Assembly	64	0.2M	32	30	<512 GB
3D 3x3 Assembly	144	1.5M	96	40	<1.2 TB
3D Core (Eigenvalue)	320	6M	0.5K	100	<4 TB

CONTENTS

EXECUTIVE SUMMARY iii

1 INTRODUCTION 15

2 THE WESTINGHOUSE TEST STAND EXPERIENCE 17

3 VERA BUILD 20
3.1 Software & Supporting Elements 20
3.2 Computing Hardware & Infrastructure 21
3.3 Key Lessons Learned 22

4 ADVANCED FIRST CORE OF THE AP1000 PWR 24

5 APPROACH TO SIMULATIONS 38
5.1 Codes used 38
5.1.1 VERA-CS 38
5.1.1.1 Cross Section Generation 39
5.1.1.2 Flux Solver 40
5.1.1.3 VERA Output 40
5.1.2 KENO-VI 40
5.1.2.1 Use of KENO in CASL 41
5.2 Westinghouse Test Stand Simulations 43
5.3 Modeling approach in KENO 44
5.3.1 KENO Model Details 44
5.4 Modeling approach in VERA-CS 46

6 RESULTS 48
6.1 2D Lattice Results 48
6.2 2D Multi-Lattice 51
6.3 2D Core 55
6.4 3D Single Assembly 63
6.5 3D Multi-Assemby 68
6.6 Zero Power Physics Tests 71

7 COMPUTATIONAL REQUIREMENTS 75

8 USABILITY OF VERA-CS 78

9 CONCLUSIONS 82

10 ACKNOWLEDGEMENTS 84

11 REFERENCES 85

APPENDIX A CE KENO-VI SIMULATIONS 88
A.1 2D Lattices 88
A.2 2D Multi-Lattice 89
A.3 2D Core 90
A.4 3D Single Assembly 92
A.5 3D 3x3 Multi-Assembly with Control Rod 95
A.6 3D Quarter Core Zero Power Physics Tests 97

APPENDIX B RADIAL REFLECTOR SENSITIVITY STUDY 103

APPENDIX C AXIAL REFLECTOR SENSITIVITY STUDY 110

APPENDIX D KENO ISOTHERMAL TEMPERATURE COEFFICIENT 114

APPENDIX E KENO VERIFICATION AGAINST MCNP 120

APPENDIX F VERA INSTALLATION GUIDE 121

APPENDIX G VERA AP1000 INPUT 125

LIST OF TABLES

TABLE 1-1 HZP REACTIVITY RESULTS VI
TABLE 1-2 TEMPERATURE REACTIVITY COEFFICIENTS VI
TABLE 1-3 CONTROL BANK WORTH RESULTS VI
TABLE 1-4 COMPUTATIONAL PERFORMANCE OF VERA-CS FOR AP1000 SIMULATIONS ON WESTINGHOUSE COMPUTER CLUSTER VIII
TABLE 3-1 SUMMARY OF PRIMARY VERA COMPONENTS ON WESTINGHOUSE TEST STAND 21
TABLE 4-1 REACTOR CORE DESCRIPTION [REF. 1] 26
TABLE 4-1 REACTOR CORE DESCRIPTION (CONT.) [REF. 1] 27
TABLE 6-1 HZP LATTICE RESULTS 49
TABLE 6-2 HZP MULTI-LATTICE RESULTS 52
TABLE 6-3 SUMMARY OF COMPARISON VERA-CS VS. KENO FOR AP1000 2D CORE 55
TABLE 6-4 3D ASSEMBLY RESULTS (REG. 3) 64
TABLE 6-5 3 D ASSEMBLY SUMMARY RESULTS FOR ALL FUEL REGIONS 66
TABLE 6-6 3D 3X3 ASSEMBLY SUMMARY RESULTS 71
TABLE 6-7 HZP REACTIVITY RESULTS 72
TABLE 6-8 TEMPERATURE REACTIVITY COEFFICIENT RESULTS 72
TABLE 6-9 AP1000 HZP CONTROL BANK WORTH RESULTS 73
TABLE 7-1 COMPUTER RESOURCES USED FOR VERA-CS AND KENO AP1000 SIMULATIONS 77
TABLE A-1 REPRESENTATIVE 2D LATTICE MONTE CARLO PARAMETERS 89
TABLE A-2 REPRESENTATIVE 2D 3X3 MULTI-LATTICE MONTE CARLO PARAMETERS 89
TABLE A-3 2D CORE MONTE CARLO PARAMETERS 92
TABLE A-4 REPRESENTATIVE 3D SINGLE ASSEMBLY MONTE CARLO PARAMETERS 93
TABLE A-5 3D 3X3 MULTI-ASSEMBLY MONTE CARLO PARAMETERS 95
TABLE A-6 REPRESENTATIVE 3D CORE MONTE CARLO PARAMETERS 98
TABLE A-7 CE KENO-VI ZPPT RESULTS FOR FIRST AP1000 STARTUP 99
TABLE B-1 INCREMENTAL DIFFERENCES IN 2D CORE MODELS FROM CASE TO CASE 105
TABLE C-1 3D SHROUD RING ANALYSIS MONTE CARLO PARAMETERS 111
TABLE D-1 MODERATOR TEMPERATURE-ONLY REACTIVITY COEFFICIENT 116
TABLE D-2 MODERATOR DENSITY REACTIVITY COEFFICIENT 117
TABLE D-3 DOPPLER TEMPERATURE REACTIVITY COEFFICIENT 118
TABLE E-1 2D 17X17 LATTICE COMPARISONS BETWEEN KENO AND MCNP 120

LIST OF FIGURES

FIGURE 1-1 DELTA IN ROD WORTH (IN PCM AND %) FOR VERA VS. KENO VII
FIGURE 1-2 DELTA POWER RMS (IN %) VERA VS. KENO VII
FIGURE 3-1 SCHEMATIC OF NEWTON SHARED WESTINGHOUSE COMPUTER SYSTEM 22
FIGURE 3-2 SCHEMATIC OF BINFORD SEGREGATED/DEDICATED WESTINGHOUSE COMPUTER SYSTEM 22
FIGURE 4-1 AP1000 PWR FIRST CORE FUEL LOADING PATTERN 28
FIGURE 4-2 ASSEMBLY LOADING PATTERN FOR REGION 4 29
FIGURE 4-3 ASSEMBLY LOADING PATTERN FOR REGION 5A 30
FIGURE 4-4 ASSEMBLY LOADING PATTERN FOR REGION 5B 31
FIGURE 4-5 ASSEMBLY LOADING PATTERN FOR REGION 5C 32
FIGURE 4-6 FIRST CORE BURNABLE ABSORBERS COLLOCATION 33
FIGURE 4-7 AXIAL FUEL STACKS FOR REGIONS 1 THROUGH 5 34
FIGURE 4-8 CONTROL ROD BANKS AND CORE PLACEMENT 35
FIGURE 4-9 REFLECTOR -RADIAL CUT 36
FIGURE 4-10 CORE SHROUD - ISOMETRIC VIEW 37
FIGURE 5-1 KENO SEMI-EXPLICIT SPACER GRID MODEL (MV GRID) 46
FIGURE 6-1 HZP DELTA K-INF VERA-CS-KENO (PCM) FOR 2D LATTICE SIMULATIONS 50
FIGURE 6-2 HZP ΔP (RMS AND MAX) VERA-KENO FOR 2D LATTICE SIMULATIONS 50
FIGURE 6-3 LOADING PATTERN FOR MULTI-LATTICE SIMULATIONS 52
FIGURE 6-4 ASSEMBLY POWER (KENO, LEFT) AND DELTA ASSEMBLY POWER (VERA-KENO X100, RIGHT) FOR THE AG-IN-CD RODDED MULTI-LATTICE SIMULATION 52
FIGURE 6-5 PIN POWER (KENO) FOR AG-IN-CD RODDED MULTI-LATTICE SIMULATION 53
FIGURE 6-6 DELTA PIN POWER (VERA-KENO)X100 FOR AG-IN-CD RODDED MULTI-LATTICE SIMULATION 54
FIGURE 6-7 AP1000 2D CORE: RADIAL SLICE AT THE AXIAL MIDPLANE 57
FIGURE 6-8 AP1000 2D CORE ASSEMBLY POWER (KENO) 58
FIGURE 6-9 AP1000 2D CORE PIN POWER (KENO) 59
FIGURE 6-10 AP1000 2D CORE DELTA ASSEMBLY POWER (VERA-CS VS. KENO) 60
FIGURE 6-11 AP1000 2D CORE PIN POWER COMPARISON 61
FIGURE 6-12 AP1000 2D CORE FORM FACTOR COMPARISON 62
FIGURE 6-13 AP1000 REG. 3 ASSEMBLY POWER DISTRIBUTION– NO GRIDS, VOID BOUNDARY CONDITIONS 64
FIGURE 6-14 AP1000 REG. 3 ASSEMBLY POWER DISTRIBUTION– W/ GRIDS, VOID BOUNDARY CONDITIONS 65
FIGURE 6-15 AP1000 REG. 3 ASSEMBLY POWER DISTRIBUTION– ENTIRE FUEL STACK AND STRUCTURE 65
FIGURE 6-16 ASSEMBLY POWER DISTRIBUTION FOR REG. 4 FUEL STACK 66
FIGURE 6-17 ASSEMBLY POWER DISTRIBUTION FOR REG. 5A FUEL STACK 67
FIGURE 6-18 ASSEMBLY POWER DISTRIBUTION FOR REG. 5C FUEL STACK 67
FIGURE 6-19 ASSEMBLY POWER DISTRIBUTION FOR REG. 5B FUEL STACK 68
FIGURE 6-20 LOADING PATTERN FOR MULTI-LATTICE SIMULATIONS 69
FIGURE 6-21 3D 3X3 ASSEMBLIES AXIAL POWER DISTRIBUTION WITH PARTIAL INSERTION OF AG-IN-CD CR 69
FIGURE 6-22 3D 3X3 POWER (LEFT), DELTA POWER VERA-KENO (BY CELL: MIDDLE, BY AXIAL NODE: RIGHT) 70
FIGURE 6-23 DELTA IN BANK WORTH (IN PCM AND %) FOR VERA VS. KENO 73
FIGURE 6-24 AP1000 PWR CORE KENO MODEL 74
FIGURE A-1 EXAMPLE 2D LATTICE MODEL FOR KENO-VI (REG. 5A) (SEE FIGURE 4-3) 88
FIGURE A-2 2D MULTI-LATTICE MODEL FOR KENO-VI 90
FIGURE A-3 KENO 2D CORE MODEL 91
FIGURE A-4 3D ASSEMBLY MODEL FOR KENO-VI - REGION 4 94
FIGURE A-5 3D 3X3 MULTI-ASSEMBLY MODEL FOR KENO-VI 96
FIGURE A-6 KENO ZPPT CORE MODEL (1 OF 2) 100
FIGURE A-7 KENO ZPPT CORE MODEL (2 OF 2) 101
FIGURE A-8 VISUALIZATION OF 3D FISSION DISTRIBUTION FROM KENO-VI 102
FIGURE B-1 KENO 2D CORE RADIAL REFLECTOR MODELS 104
FIGURE B-2 RADIAL PIN POWER EFFECTS OF THE BAFFLE 106
FIGURE B-3 RADIAL PIN POWER EFFECTS OF THE CORE BARREL, PADS, AND VESSEL 107
FIGURE B-4 RADIAL PIN POWER EFFECTS OF SHROUD RING 108
FIGURE B-5 RADIAL PIN POWER EFFECTS OF THE CORE BARREL, PADS, VESSEL, AND SHROUD RING 109

FIGURE C-1 AXIALLY SMEARED SHROUD RING MODEL 112
FIGURE C-2 AXIAL POWER DIFFERENCES BETWEEN EXPLICIT AND SMEARED SHROUD RING MODELS 112
FIGURE C-3 RADIAL POWER DIFFERENCES BETWEEN EXPLICIT AND SMEARED SHROUD RING MODELS 113
FIGURE C-4 3D POWER DIFFERENCES BETWEEN EXPLICIT AND SMEARED SHROUD RING MODELS 113
FIGURE D-1 KENO AND VERA REACTIVITY VS. MODERATOR TEMPERATURE 116
FIGURE D-2 KENO REACTIVITY VS. MODERATOR DENSITY 117
FIGURE D-3 KENO REACTIVITY VS. FUEL TEMPERATURE 118
FIGURE F-1 EXAMPLE OF VERA INSTALLATION GUIDE RESTRUCTURED TEXT FILE 122
FIGURE F-2 EXAMPLE OF VERA INSTALLATION GUIDE PDF FILE 123
FIGURE F-3 EXAMPLE OF VERA INSTALLATION GUIDE HTML FILE 124

ACRONYMS

2D	Two Dimensional
3D	Three Dimensional
ARO	All Rods Out
BOC	Beginning of Cycle
CASL	Consortium for Advanced Simulation of Light Water Reactors
CE	Continuous energy
DBW	Differential Boron (reactivity) Worth (pcm/ppmB)
DTC	Doppler Temperature Coefficient (pcm/F)
HZP	Hot Zero Power
I/O	Input/Output
INL	Idaho National Laboratory
ITC	Isothermal Temperature (reactivity) Coefficient (pcm/F)
LSF	Load Sharing Facility (a computer resource queuing system)
LWR	Light Water Reactor
MG	Multi-group (as in cross sections)
MTC	Moderator Temperature Coefficient (pcm/F)
OLCF	Oak Ridge Leadership Computing Facility
ORNL	Oak Ridge National Laboratory
PCM	Percent Mille (in this case, 10^5 times Δk or $\Delta\rho$)
PWR	Pressurized Water Reactor
QDR	Quad Data Rate (an Infiniband interconnect throughput rating)
RAM	Random Access Memory
RCCA	Rod Cluster Control Assembly
RMS	Root Mean Square
SSH	Secure Shell (computer communication protocol)
TPL	Third-party Library
VERA	Virtual Environment for Reactor Applications
Westinghouse	Westinghouse Electric Company LLC
ZPPT	Zero Power Physics Test

1 INTRODUCTION

The primary objective of the Consortium of Advanced Simulation LWRs (CASL) Test Stands is to engage industry partners to assess VERA performance on real-world industry applications through early VERA deployments at industry sites, to provide demonstrated applications of VERA and to collect feedback on potential improvements. Westinghouse is the first organization to host a VERA Test Stand.

The Westinghouse VERA Test Stand is focused on the core physics analysis of the **AP1000** PWR first core. This advanced core design, which will be deployed in all **AP1000** units currently under construction, provides a challenging application for VERA and the opportunity in the relatively near term to obtain state-of-the-art measurements to extend its validation basis.

The **AP1000** PWR first core implements an 18-month cycle low-leakage design using five fuel regions with ^{235}U concentrations from natural U to 4.8 w/o enrichment. Enrichment zoning and burnable absorbers are used for power shaping and reactivity control. In particular, the Westinghouse Integral Fuel Burnable Absorber (IFBA), a thin ZrB_2 coating on the pellet surface, and the discrete Wet Annular Burnable Absorber (WABA) rod, inserted at selected guide thimble locations, are used. Low worth “gray” tungsten control banks and standard “black” Ag-In-Cd control banks are employed for MSHIM, an advanced operational strategy that provides robust core reactivity and axial power distribution control with minimal changes to the soluble boron concentration during both normal operation and power maneuvering scenarios. This strategy necessitates an increased presence of control clusters (gray and black) in the reactor core during operation. All these features make the **AP1000** reactor a best-in-class generation III+ PWR, but they also challenge existing core simulators. This makes application of VERA to the **AP1000** PWR core especially relevant to investigate the performance and potential benefits of a high-fidelity core simulator.

For the test stand, VERA-CS has been built on a dedicated parallel-computation system within Westinghouse which currently features 576 cores distributed on 48 nodes with a total memory of 96 GB/node (8 GB/core). The deployment utilized the VERA build system and, working together with CASL staff, a process has been successfully established to streamline updates to the VERA build to incorporate changes and new features available from the VERA repository. A VERA installation guide has been produced and together with the lessons learned from Westinghouse’s test stand experience has been made available back to CASL to facilitate subsequent VERA deployments.

The activities foreseen for the **AP1000** PWR core physics analysis are simulation of the start-up core zero power physics tests (ZPPTs), with results reported here. Cycle depletion analysis is under consideration for a subsequent phase. An extensive set of simulations has been performed to support the ZPPT simulation, including 2D lattice simulations up to a radial slice of the core, and 3D assembly and multi-assembly simulations. These simulations constitute a very valuable set of benchmarks to assess the performance of VERA not only in terms of eigenvalue

but also in terms of fission rate distribution. The results of these simulations and the comparison to Monte-Carlo solution are presented in this report.

This report is organized as follows. Section 2 summarizes the Westinghouse Test Stand Experience. Section 3 describes the VERA build process and architecture of the Westinghouse compute cluster where the VERA simulations have been performed. Section 4 describes the **AP1000** PWR core design. Section 5 describes the modeling approach. Section 6 reports the results of the simulations. Section 7 summarizes VERA's computational performance. Section 8 discusses usability of VERA-CS for the Test Stand simulations. Section 9 offers concluding remarks. APPENDIX A through APPENDIX E provide additional details on the KENO simulations. APPENDIX F contains the VERA installation guide produced along this work. APPENDIX G contains the VERA input for the **AP1000** PWR core.

2 THE WESTINGHOUSE TEST STAND EXPERIENCE

The technical analysis for the Westinghouse VERA Test Stand began at the end of June 2013, with the release of the VERA build on the Westinghouse computer system. The Westinghouse experience with VERA is however broader in breadth and temporal horizon. Westinghouse has collaborated with CASL personnel for the validation of VERA-CS well ahead of the start of the Test Stand simulations, making its expertise in the design and analysis of commercial PWRs, together with its state-of-the-art in-house core physics package, available to support VERA development (Ref. 4 and 5). This fruitful collaboration has led to the conception of the VERA Test Stand, with Westinghouse being the first organization to host these activities.

The topic selected by Westinghouse for the initial phase of the Test Stand is the reactor physics analysis of the **AP1000** PWR, and in particular its start-up ZPPTs. This analysis is particularly relevant to Westinghouse, since the **AP1000** reactor features a first core with significant advancements compared to past first cores. While these advancements improve the reactor's performance, they also challenge traditional core simulators. Westinghouse has addressed these challenges by making several improvements to its in-house core physics package (Ref. 15-33). A first positive outcome of the Test Stand is the close agreement of VERA-CS and KENO with the predictions from the Westinghouse core physics package, which reinforces the confidence in the agreement with the measurements as several **AP1000** units will start operation in the next few years.

In this and prior analyses (Ref. 4), VERA has also shown the potential to go one step beyond the current tools with regards to its capability to accurately reproduce numerical benchmarks and measurements, when available, for HZP core configurations. While more extensive comparisons are required before making definitive statements, this behavior is very promising for a core simulator that the industry could use reliably to complement its production tools. The successful development of VERA-CS would make it possible to obtain high-fidelity predictions for a range of commercial reactors and operating conditions that could be used by the nuclear industry for a variety of applications, such as anticipating or mitigating operational issues, troubleshooting mispredictions with plants measurements, benchmarking new methods, or corroborating the design of advanced cores. The scope of this Test Stand and the results obtained are an example of these potential applications.

The benefits of the Test Stand go beyond those of the technical analysis performed, which is described in detail in this report, as there are significant additional benefits spurred by the direct engagement of the parties involved. A list of these benefits, while not exhaustive, is attempted in the following paragraphs. There have been also challenges in the preparation and execution of the Test Stand, which were resolved thanks to the efforts and resources that each organization and individual involved have been willing to spend for this cause.

The mutual comprehension of the respective needs and limitations has certainly been enhanced as a result of the Test Stand activities. For instance, there are certain requirements that VERA needs to fulfill to be successfully built and operated on a host organization's computer system. The installation of VERA on Westinghouse's computer system was performed

jointly by CASL and Westinghouse staff. As a result, a procedure for building VERA has been created as part of the Test Stand activities and documented in the "VERA Installation Guide". This experience benefits future and current VERA deployments. The Westinghouse VERA build has been ported to a different, more powerful, computer system since its original install, and it has been successfully updated to include VERA developments that have been crucial to the Test Stand execution. A section of this report is devoted to the VERA build on the Westinghouse' computer system, while sample sections of the VERA installation guide are given in APPENDIX F.

VERA is computationally demanding compared to typical industrial simulators, and in order to execute the Test Stand simulations Westinghouse has purchased a dedicated VERA computer cluster with about 600 computer cores. This is a significant step upwards, and forward, in the typical computational resources allocated by the industry to perform reactor physics analyses. On the other hand, it is also indicative of high-end computer platforms that could be made available for VERA in the nuclear industry, and hence of the computational resources that VERA needs to meet for its deployment at industry's sites. While it is acceptable to complement VERA's execution by tapping into HPC resources in the interim time, and it is certainly required for particularly demanding simulations that may be performed occasionally, resorting systematically to HPC computers to run VERA is not a sustainable path forward if this capability is to be used by the industry at large. This awareness has been substantiated by the Test Stand execution. Since the HZP **AP1000** PWR simulations are already at the limit of the current computational resources available on the Westinghouse VERA dedicated cluster, the computational burden required for VERA execution has to be mitigated in short order.

One important aspect, and challenge, of the Test Stand has been the validation of VERA-CS itself for the simulations performed. This has been done through painstaking simulations set up and executed independently using a development version of the KENO-VI Monte Carlo code utilizing Continuous Energy (CE) cross sections and parallel execution (Ref. 8). The validation of VERA-CS for the **AP1000** PWR core simulations, and in general, is not a trivial undertaking as the high-fidelity physics methods employed do not suffice alone to guarantee accurate results, even more so due to the limited experience and application of VERA so far. The relevant experience and plant measurements available in the nuclear industry, in synergy with the use of first-principle tools like KENO, are an asset going forward for strengthening the validation bases of VERA.

The performance of VERA for the **AP1000** PWR core simulations, and the physics methods underpinning such performance, has raised much interest within Westinghouse. This stimulated a healthy discussion between Westinghouse and CASL method developers which is mutually beneficial and will continue in the future. The Test Stand simulations have already provided numerous and valuable scenarios for code benchmarking and development, and more will come as the project moves forward to fuel cycle depletion calculations. The scale of the simulations performed for this work, the resolution in the prediction and the degree of confidence in its accuracy supported by the comparisons with KENO are an important asset of the Test Stand.

Finally, the topic selected for the Test Stand has proved engaging and pertinent. It offered the chance for CASL personnel to be exposed to a state-of-the-art advanced core design and test the prediction capabilities of VERA with a challenging core, representative of modern PWR reloads, and advanced operational features, like the MSHIM rodded operation. The enthusiasm and dedication offered to this project by the many people involved, inside and outside Westinghouse, are a testimony of their engagement and are key contributors to the success of the Westinghouse Test Stand.

3 VERA BUILD

Two main goals have been pursued when building VERA on the Westinghouse computer system:

1. A successful/complete first-of-a-kind VERA installation at an industrial partner site, and
2. A maintainable and reproducible build process to allow VERA installation at other sites.

To achieve these goals, Westinghouse and CASL worked closely to develop a VERA Installation Guide (see APPENDIX F). The result of this effort was a well-documented process to prepare a high-performance computer system administratively to receive VERA, install and configure prerequisite utilities and third-party libraries, install and configure VERA itself, and perform subsequent updates based on periodic release snapshots provided through a central repository.

The build process has been successfully validated with installation and updates on two separate Westinghouse test stand systems between June 2013 and October 2013.

3.1 Software & Supporting Elements

VERA can be characterized as a suite of physics tools working in concert to perform a calculation of interest. To capitalize on the best contemporary analysis tools at the time VERA was being developed, tools were selected from various developers based on the their appropriateness to a given calculation within the overall simulation framework. As such, these tools are varied in their origins but must operate cohesively on the same computational platform. To permit that cohesive operation, the software and supporting elements can be characterized in three areas:

1. Calculational Tools,
2. Prerequisites to Installation, and
3. Third-party Libraries (TPLs).

In each of these categories, the components installed in the Test Stand are summarized in Table 3-1. The calculation tools used for the simulations reported here are Exnihilo and SCALE.

Table 3-1 Summary of Primary VERA Components on Westinghouse Test Stand

Calculational Tool	Prerequisite	Third-party Library
COBRA-TF	CMake	Boost
Exnihilo	eg/egdist	HDF5
MPACT	GCC	Hypre
SCALE	Git	LAPACK
	OpenMPI	MOAB
		PETSc
		Qt
		SILO
		zlib

3.2 Computing Hardware & Infrastructure

The Westinghouse systems used for the Test Stand calculations are:

1. Newton, part of Westinghouse's larger shared parallel-computation infrastructure, and
2. Binford, a segregated and dedicated parallel-computation system.

Both Newton and Binford are described schematically in Figure 3-1 and Figure 3-2, respectively.

Both systems feature interactive login nodes that are Hewlett-Packard DL580s with 32 processing cores and 1 TB of RAM. These are in turn connected using quad data rate (QDR) Infiniband interconnects through a Voltaire 4036 switch to slave nodes dedicated to computational tasks. For Newton, the computation nodes are shared resources within Westinghouse managed through a company-wide LSF-based queuing system. Approximately 256 cores are typically available to be allocated on a per-job basis for CASL purposes; however, this number greatly fluctuates depending on overall system demand. For Binford, the computation nodes are dedicated CASL resources managed through a separate project-specific Maui/Torque/Moab queuing system.

Both Newton and Binford and the corresponding slave nodes have separate 1GB Ethernet connections to shared NFS file systems for bulk file storage. Both Newton and Binford and associated firewalls are configured to allow temporary SSH tunnels to be established between Westinghouse and the "casl-dev" machine at ORNL to periodically update VERA.

Both systems are based on the SUSE Linux Enterprise Server (SLES) Linux distribution. Newton is loaded with SLES Version 10, Service Pack 2 (SLES10SP2) whereas Binford (and all of its slave nodes) is loaded with SLES11SP3.

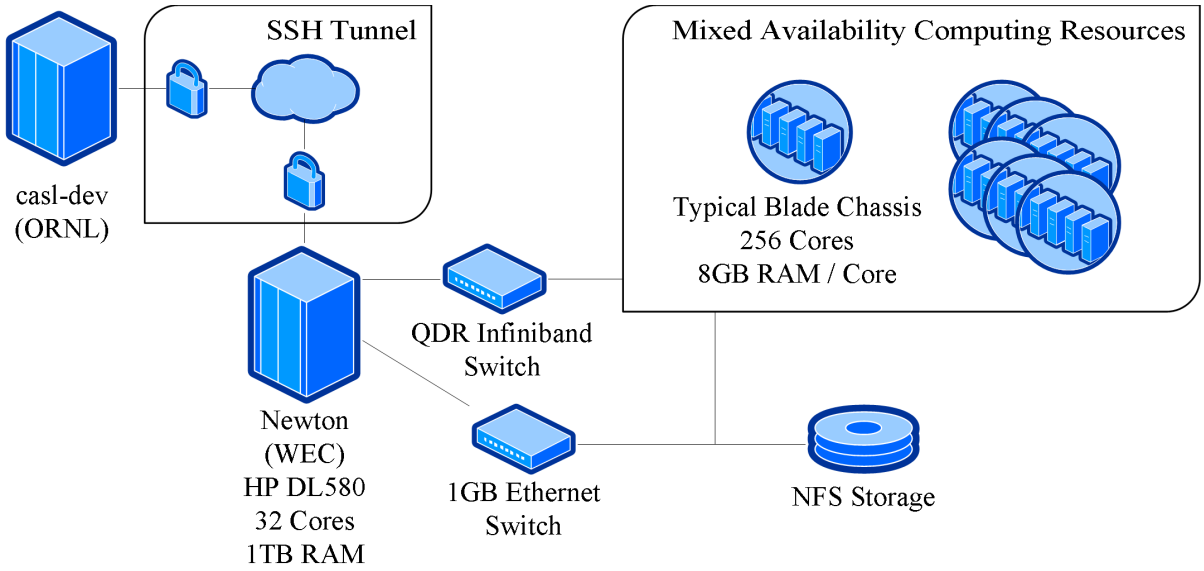

Figure 3-1 Schematic of Newton Shared Westinghouse Computer System

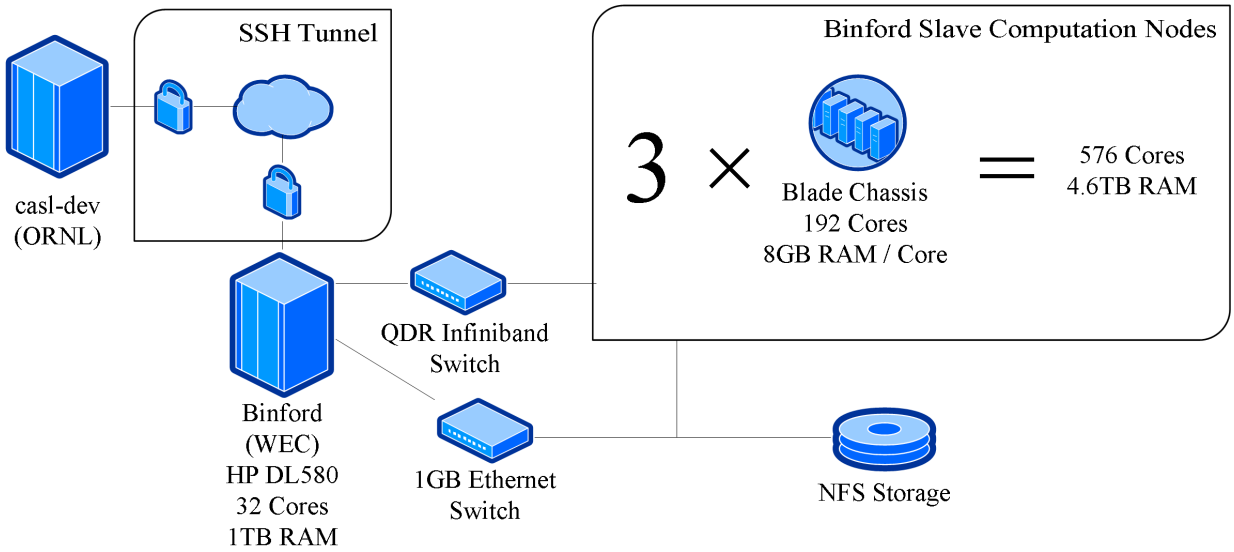

Figure 3-2 Schematic of Binford Segregated/Dedicated Westinghouse Computer System

3.3 Key Lessons Learned

Throughout the process of developing the systems described previously and the subsequent retrieval, configuration, building, and deployment of the VERA suite, several challenges were encountered. Recognizing these challenges and mitigating them in the future will benefit later recipients of VERA. The challenges encountered were in the following broad areas:

1. Computer Cluster Internet Access
2. User & System Security Protocols

3. Multiple Computer System States
4. Compiler & Prerequisite Compatibility

When the SSH tunnel was being established between the Westinghouse Test Stand and casl-dev at ORNL, a problem was encountered early whereby the Westinghouse Test Stand had no way to access computers outside of the Westinghouse intranet. Along with the necessary firewall changes to correct this, there were several administrative hurdles to surpass in order to allow even a secure tunnel to the outside to be established. The difficulty encountered here is what prompted a cautionary note in the VERA Installation Guide to encourage administrators to begin working through the process to setup this tunnel early.

Similarly, the Westinghouse computer systems are configured with a generally permissive security environment, i.e., users can see each other's files without explicit action taken to secure files. This is counter to the CASL/VERA Technology Control Plan which is restrictive by default, i.e., users must be granted access to every component of VERA with which they are expected to interact. Administrators must be aware of CASL's approach to securing information and must ensure that an adequate system is in place to abide by that approach.

Once the configuration process began for the VERA calculation tools, compilation and build tool compatibility issues were encountered. In general, Westinghouse relies heavily on the Intel compiler suite using a traditional makefile to build software. Conversely, VERA is primarily configured to use the GNU compiler suite with cmake performing the make and test operations. Therefore, the Westinghouse Test Stand did not have adequately up-to-date tools to build VERA as intended. This was reconciled by building VERA's prerequisites, third-party libraries, and calculation tools from source code using version-controlled source code for each component. This ensures that as VERA's calculational tools are distributed, the correct version of all corresponding required software is available.

Once the software was ready to be built, the heterogeneity of the Westinghouse Test Stand posed a challenge. In particular, the Newton system has access to computation nodes of varying vintages (SLES10SP2, SLES11SP1, and SLES11SP2) which leads to different library versions on the various systems. For practical purposes, since VERA was built on Newton with SLES11SP2, it can only execute parallel jobs on the SLES11SP2 nodes. This effectively limits the number of processors a job run from Newton can use to some number smaller than the total computation nodes. Therefore, as engineers and administrators are specifying systems to run VERA (or other CASL codes) and/or determining where to put those tools on existing infrastructure, the age and degree of heterogeneity of the system should be considered.

Thanks to the VERA build process developed as part of the Test Stand activities, these initial challenges have been positively resolved. The VERA build at Westinghouse is now fully operational, it has been successfully updated and ported to different computer systems, and it has been employed for generating the VERA results contained in this work.

4 ADVANCED FIRST CORE OF THE AP1000 PWR

The **AP1000** PWR features an advanced first core design, which will be deployed in all eight units under construction in the U.S. and China, with the first unit coming on line in 2015. The core and fuel characteristics are described in detail in Ref. 1, and summarized in Table 4-1. The core features five fresh fuel regions, arranged with the core loading pattern shown in Figure 4-1 and various ^{235}U enrichments. Natural U (Region 1) assemblies are employed on most of the peripheral locations to achieve a low leakage core design and improve fuel cycle economics. The checkerboard of lower/higher enriched fuel (Region 2 and 4 respectively) in the inner part of the core mimics the conditions of subsequent reloads containing irradiated fuel assemblies. The placement of the highest enriched assemblies (Region 5) slightly inboard from the periphery, as in traditional "ring of fire" core design strategies, favors radial power distribution control over the cycle.

Regions 1 to 3 feature uniform radial ^{235}U enrichment. Lower enriched axial blankets are used for Region 3. Regions 4 and 5 feature enrichment zoning with three ^{235}U enrichments per assembly, in addition to lower enriched axial blankets. The enrichment zoning, with the lowest enrichment pins located on the assembly periphery, reduces the interface effects with the neighboring lower enriched fuel assemblies. The intra assembly loading patterns for Regions 4 and 5 are shown in Figure 4-2 through Figure 4-5.

Two types of burnable absorbers are used in the **AP1000** PWR first core: the Westinghouse Integral Fuel Burnable Absorber (IFBA), a ZrB_2 coating applied on the pellet of selected fuel rods, and the Wet Annular Burnable Absorber (WABA), a discrete annular insert containing an Al_2O_3-B_4C mixture with water flowing in the inner part of the rod. These burnable absorbers are used in Regions 4 and 5, with the assembly loading patterns showed in Figure 4-2 through Figure 4-5. The burnable absorber core loading pattern is shown in Figure 4-6.

The fuel axial stacks are depicted in Figure 4-7. Region 1 and 2 fuel stacks do not feature axial blankets given their lower enrichment and the absence of burnable absorbers. Top and bottom 8-in blankets are employed in Regions 3 to 5. The blankets have lower enrichment with respect to the central part of the fuel stack and consist of solid pellets in non-IFBA fuel rods, and annular pellets in IFBA rods. The inner void of the IFBA annular blankets provides additional room for expansion of the He released from (n, alpha) reactions in ^{10}B.

The WABA rods have various axial configurations (see Figure 4-7): the short and long WABA rods used for Region 4 and the intermediate WABA featured in Region 5 feature respectively 102", 152" and 116" ^{10}B bearing central regions. This poisoned region is offset downward with respect to the fuel axial midplane. All types of WABA rods feature an unpoisoned upper plenum zone of variable length. Region 4 short WABA and Region 5 intermediate-length WABA feature an annular Zr spacer in the bottom of the stack.

There are 12 ZIRLO® grids in the **AP1000** PWR core active fuel, eight Intermediate Mixing Vane (MV) grids with a height of 2.25-in and four shorter Intermediate Flow Mixing (IFM) grids with a height of 0.66-in. Two Inconel grids are present at the top and bottom of the stack with a single protective Inconel grid above the bottom nozzle.

The core arrangement and material specifications for the control rod banks are shown in Figure 4-8. It is noted that the **AP1000** reactor operates following the MSHIM™ operation and control strategy, which relies on a combination of low worth (or gray) control cluster assemblies and standard (or black) control cluster assemblies to provide robust core reactivity and axial power distribution control with minimal changes to the soluble boron concentration in the reactor coolant during both normal operation and power maneuvering scenarios. This strategy necessitates an increased presence of control clusters (gray and black) in the reactor core during operation. Namely, out of a total of 69 rod cluster control assemblies (RCCAs), 16 gray RCCAs plus 12 black RCCAs ("M" banks in Figure 4-8) are used for MSHIM operation with additional 9 black RCCA ("AO" bank) used for axial offset control. The remaining 32 black RCCAs are used as shut-down ("S") banks. The control rod poison used for the black banks is Ag-In-Cd (AIC) while tungsten within an Inconel liner is used for the gray banks.

A radial cut of the **AP1000** PWR core which shows the core shroud, neutron pads and barrel is shown in Figure 4-9. An isometric view of the core shroud is given in Figure 4-10; it can be noticed that in addition to the baffle, the shroud features several axial rings with associated connecting structure. Currently, VERA modeling capabilities for the reflector region are li[a]mited to the baffle plus surrounding water. A detailed modeling of the reflector is possible with KENO, which enabled to perform a sensitivity study on the impact of various modeling choices. These studies are reported in APPENDIX B and APPENDIX C.

The **AP1000** PWR first core is challenging due to the presence of radial and axial heterogeneities but it is not unlike other modern LWR cores. The radial heterogeneities mimic burned cores with shuffled fuel assemblies, while radial and axially heterogeneous fuel is routinely used in BWR cores. The MSHIM operating scheme has also a counterpart in BWR operation, with insertion of selected control blades for reactivity control. IFBA and WABA are used in the majority of Westinghouse fueled cores. For the above reasons the **AP1000** PWR core simulations constitute a pertinent test stand application for VERA-CS.

[a] ZIRLO® is a registered trademark of Westinghouse Electric Company LLC in the United States and may be registered in other countries throughout the world. All rights reserved. Unauthorized use is strictly prohibited.

Table 4-1 Reactor Core Description [Ref. 1]

Active core	
Equivalent diameter (in.)	119.7
Active fuel height first core (in.), cold	168
Fuel assemblies	
Number	157
Rod array	17 x 17
Rods per assembly	264
Rod pitch (in.)	0.496
Overall transverse dimensions (in.)	8.426 x 8.426
Fuel weight, as UO_2 (lb)	211,588
Zircaloy clad weight (lb)	43,105
Number of grids per assembly	
Top and bottom	2 Ni-Cr-Fe Alloy 718
Intermediate	8 ZIRLO
Intermediate flow mixing (IFM)	4 ZIRLO
Protective	1 Ni-Cr-Fe Alloy 718
Number of guide thimbles per assembly	24
Composition of guide thimbles	ZIRLO
Diameter of guide thimbles, upper part (in.)	0.442 ID x 0.482 OD
Diameter of guide thimbles, lower part (in.)	0.397 ID x 0.482 OD
Diameter of instrument guide thimbles (in.)	0.442 ID x 0.482 OD
Fuel rods	
Number	41,448
Outside diameter (in.)	0.374
Diameter gap (in.)	0.0065
Clad thickness (in.)	0.0225
Clad material	ZIRLO

Table 4-1 Reactor Core Description (cont.) [Ref. 1]

Rod Cluster Control Assemblies	
Neutron absorber	Ag-In-Cd
Diameter (in.)	0.341
Density (lb/in.^{3})	Ag-In-Cd 0.367
Cladding material	Type 304 or 304L, cold-worked SS
Cladding OD (in.)	0.381
Cladding thickness (in.)	0.0185
Number of clusters, full-length	53
Number of absorber rods per cluster	24
Gray Rod Cluster Assemblies	
Neutron absorber	Tungsten/Alloy 718
Diameter (in.)	Tungsten 0.197 / Alloy 718 0.310
Density (lb/in.^{3})	Tungsten 0.695/ Alloy 718 0.296
Cladding material	Type 304 or 304L, cold-worked SS
Cladding OD (in.)	0.381
Cladding thickness (in.)	0.0255
Number of clusters, full-length	16
Number of absorber rods per cluster	24
Discrete Burnable absorber rods (first core)	
Number	592
Material	Alumina Boron-Carbide
OD (in.)	0.381
Inner tube, OD (in.)	0.267
Clad material	Zircaloy
Inner tube material	Zircaloy
B10 content (mg/in)	15.32
Absorber length (in.)	Variable
Integral Fuel Burnable Absorbers (first core)	
Number	5632
Type	IFBA
Material	Boride Coating
B10 Content (mg/in)	1.96
Absorber length (in.)	152

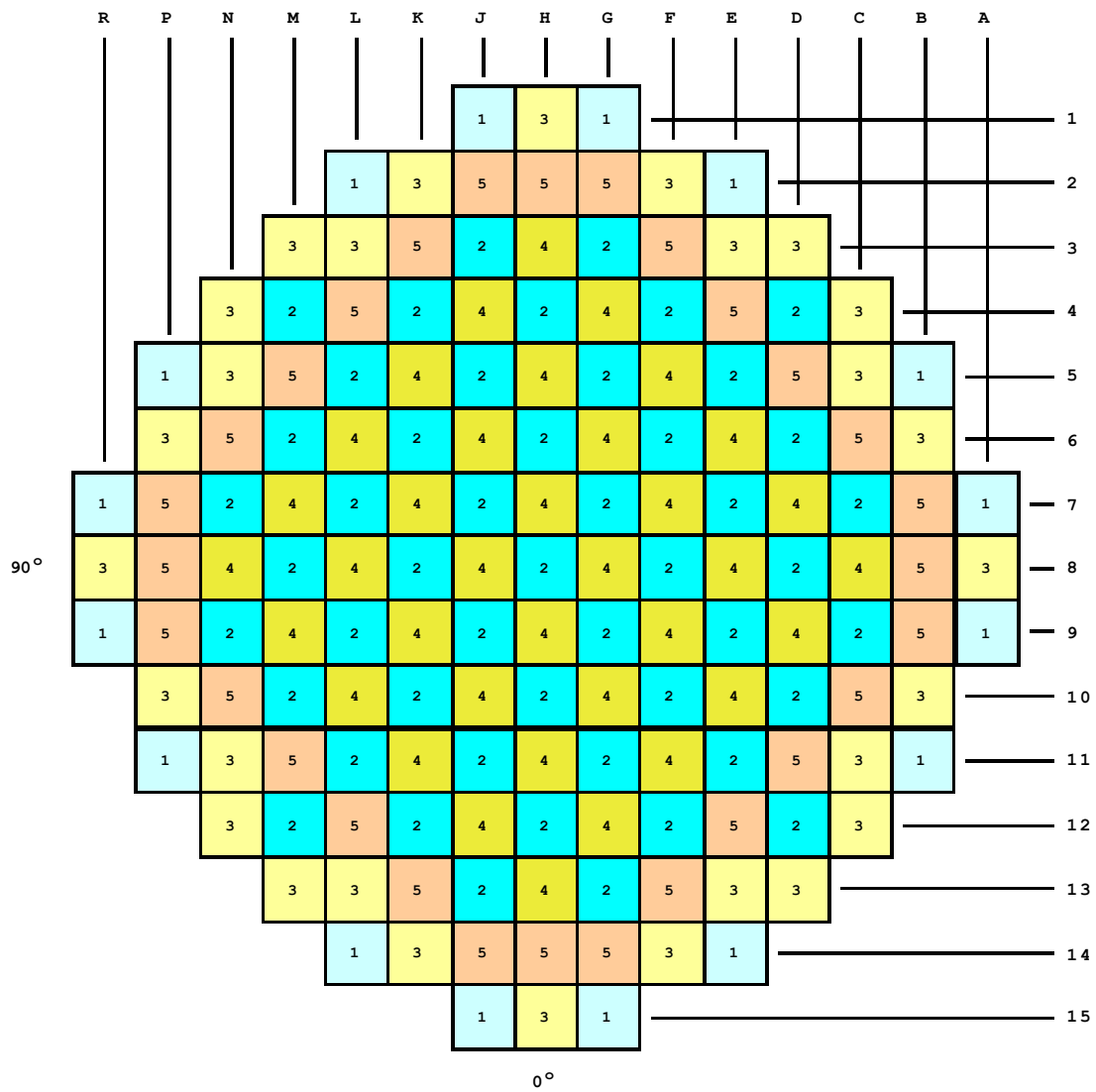

LEGEND

R Region Identifier

Region Group	Fraction of Total	U235 Midzone	U235 Blanket	IFBA Rods	WABA Rods
1	0.10	0.740	Absent	0	0
2	0.31	1.580	Absent	0	0
3	0.18	3.200	1.580	0	0
4	0.23	3.776	3.200	68	8L+4S
5A	0.05	4.376	3.200	88	4I
5B	0.03	4.376	3.200	124	0
5C	0.10	4.376	3.200	124	8I

Figure 4-1 AP1000 PWR first core Fuel Loading Pattern

LI	L	LI	L	LI	L	LI	L	LI	L	LI	L	LI	L	LI	L	LI
L	MI	M	M	M	MI	M	M	M	M	M	MI	M	M	M	MI	L
LI	M	M	M	M	GT	M	M	LW	M	M	GT	M	M	M	M	LI
L	M	M	LW	M	M	HI	H	M	H	HI	M	M	LW	M	M	L
LI	M	M	M	M	M	HI	H	M	H	HI	M	M	M	M	M	LI
L	MI	GT	M	M	GT	M	M	SW	M	M	GT	M	M	GT	MI	L
LI	M	M	HI	HI	M	HI	H	M	H	HI	M	HI	HI	M	M	LI
L	M	M	H	H	M	H	HI	M	HI	H	M	H	H	M	M	L
LI	M	LW	M	M	SW	M	M	IT	M	M	SW	M	M	LW	M	LI
L	M	M	H	H	M	H	HI	M	HI	H	M	H	H	M	M	L
LI	M	M	HI	HI	M	HI	H	M	H	HI	M	HI	HI	M	M	LI
L	MI	GT	M	M	GT	M	M	SW	M	M	GT	M	M	GT	MI	L
LI	M	M	M	M	M	HI	H	M	H	HI	M	M	M	M	M	LI
L	M	M	LW	M	M	HI	H	M	H	HI	M	M	LW	M	M	L
LI	M	M	M	M	GT	M	M	LW	M	M	GT	M	M	M	M	LI
L	MI	M	M	M	MI	M	M	M	M	M	MI	M	M	M	MI	L
LI	L	LI	L	LI	L	LI	L	LI	L	LI	L	LI	L	LI	L	LI

Region D 68 IFBA + 12 WABA

	No. Pins	Enr.	BA
L	32	3.40	No BA
LI	32	3.40	IFBA
M	140	3.80	No BA
MI	12	3.80	IFBA
H	24	4.20	No BA
HI	24	4.20	IFBA
SW	4		WABA
LW	8		WABA
GT	12		
IT	1		

Figure 4-2 Assembly Loading Pattern for Region 4

L	LI	L	LI	LI	LI	LI	LI	LI	LI	LI	LI	LI	LI	L	LI	L
LI	M	M	M	M	MI	MI	M	MI	M	MI	MI	M	M	M	M	LI
L	M	M	M	M	GT	M	M	GT	M	M	GT	M	M	M	M	L
LI	M	M	W	M	M	HI	H	M	H	HI	M	M	W	M	M	LI
LI	M	M	M	M	M	HI	H	M	H	HI	M	M	M	M	M	LI
LI	MI	GT	M	M	GT	M	M	GT	M	M	GT	M	M	GT	MI	LI
LI	MI	M	HI	HI	M	H	H	M	H	H	M	HI	HI	M	MI	LI
LI	M	M	H	H	M	H	H	M	H	H	M	H	H	M	M	LI
LI	MI	GT	M	M	GT	M	M	IT	M	M	GT	M	M	GT	MI	LI
LI	M	M	H	H	M	H	H	M	H	H	M	H	H	M	M	LI
LI	MI	M	HI	HI	M	H	H	M	H	H	M	HI	HI	M	MI	LI
LI	MI	GT	M	M	GT	M	M	GT	M	M	GT	M	M	GT	MI	LI
LI	M	M	M	M	M	HI	H	M	H	HI	M	M	M	M	M	LI
LI	M	M	W	M	M	HI	H	M	H	HI	M	M	W	M	M	LI
L	M	M	M	M	GT	M	M	GT	M	M	GT	M	M	M	M	L
LI	M	M	M	M	MI	MI	M	MI	M	MI	MI	M	M	M	M	LI
L	LI	L	LI	LI	LI	LI	LI	LI	LI	LI	LI	LI	LI	L	LI	L

Region E 88 IFBA + 4 WABA

	No. Pins	Enr.	BA
L	12	4.00	No BA
LI	52	4.00	IFBA
M	132	4.40	No BA
MI	20	4.40	IFBA
H	32	4.80	No BA
HI	16	4.80	IFBA
W	4		WABA
GT	20		
IT	1		

Figure 4-3 Assembly Loading Pattern for Region 5A

LI	LI	LI	LI	LI	LI	LI	LI	LI	LI	LI	LI	LI	LI	LI	LI	LI
LI	MI	M	M	M	MI	MI	M	MI	M	MI	MI	M	M	M	MI	LI
LI	M	M	M	MI	GT	M	M	GT	M	M	GT	MI	M	M	M	LI
LI	M	M	GT	M	M	HI	HI	M	HI	HI	M	M	GT	M	M	LI
LI	M	MI	M	M	M	HI	H	M	H	HI	M	M	M	MI	M	LI
LI	MI	GT	M	M	GT	M	M	GT	M	M	GT	M	M	GT	MI	LI
LI	MI	M	HI	HI	M	H	H	M	H	H	M	HI	HI	M	MI	LI
LI	M	M	HI	H	M	H	HI	M	HI	H	M	H	HI	M	M	LI
LI	MI	GT	M	M	GT	M	M	IT	M	M	GT	M	M	GT	MI	LI
LI	M	M	HI	H	M	H	HI	M	HI	H	M	H	HI	M	M	LI
LI	MI	M	HI	HI	M	H	H	M	H	H	M	HI	HI	M	MI	LI
LI	MI	GT	M	M	GT	M	M	GT	M	M	GT	M	M	GT	MI	LI
LI	M	MI	M	M	M	HI	H	M	H	HI	M	M	M	MI	M	LI
LI	M	M	GT	M	M	HI	HI	M	HI	HI	M	M	GT	M	M	LI
LI	M	M	M	MI	GT	M	M	GT	M	M	GT	MI	M	M	M	LI
LI	MI	M	M	M	MI	MI	M	MI	M	MI	MI	M	M	M	MI	LI
LI	LI	LI	LI	LI	LI	LI	LI	LI	LI	LI	LI	LI	LI	LI	LI	LI

Region E 124 IFBA

	No. Pins	Enr.	BA
L	0	4.00	No BA
LI	64	4.00	IFBA
M	120	4.40	No BA
MI	32	4.40	IFBA
H	20	4.80	No BA
HI	28	4.80	IFBA
W	0		WABA
GT	24		
IT	1		

Figure 4-4 Assembly Loading Pattern for Region 5B

LI	LI	LI	LI	LI	LI	LI	LI	LI	LI	LI	LI	LI	LI	LI	LI	LI
LI	MI	M	M	M	MI	MI	M	MI	M	MI	MI	M	M	M	MI	LI
LI	M	M	M	MI	GT	M	M	GT	M	M	GT	MI	M	M	M	LI
LI	M	M	W	M	M	HI	HI	M	HI	HI	M	M	W	M	M	LI
LI	M	MI	M	M	M	HI	H	M	H	HI	M	M	M	MI	M	LI
LI	MI	GT	M	M	GT	M	M	W	M	M	GT	M	M	GT	MI	LI
LI	MI	M	HI	HI	M	H	H	M	H	H	M	HI	HI	M	MI	LI
LI	M	M	HI	H	M	H	HI	M	HI	H	M	H	HI	M	M	LI
LI	MI	GT	M	M	W	M	M	IT	M	M	W	M	M	GT	MI	LI
LI	M	M	HI	H	M	H	HI	M	HI	H	M	H	HI	M	M	LI
LI	MI	M	HI	HI	M	H	H	M	H	H	M	HI	HI	M	MI	LI
LI	MI	GT	M	M	GT	M	M	W	M	M	GT	M	M	GT	MI	LI
LI	M	MI	M	M	M	HI	H	M	H	HI	M	M	M	MI	M	LI
LI	M	M	W	M	M	HI	HI	M	HI	HI	M	M	W	M	M	LI
LI	M	M	M	MI	GT	M	M	GT	M	M	GT	MI	M	M	M	LI
LI	MI	M	M	M	MI	MI	M	MI	M	MI	MI	M	M	M	MI	LI
LI	LI	LI	LI	LI	LI	LI	LI	LI	LI	LI	LI	LI	LI	LI	LI	LI

Region E 124 IFBA + 8 WABA

	No. Pins	Enr.	BA
L	0	4.00	No BA
LI	64	4.00	IFBA
M	120	4.40	No BA
MI	32	4.40	IFBA
H	20	4.80	No BA
HI	28	4.80	IFBA
W	8		WABA
GT	16		
IT	1		

Figure 4-5 Assembly Loading Pattern for Region 5C

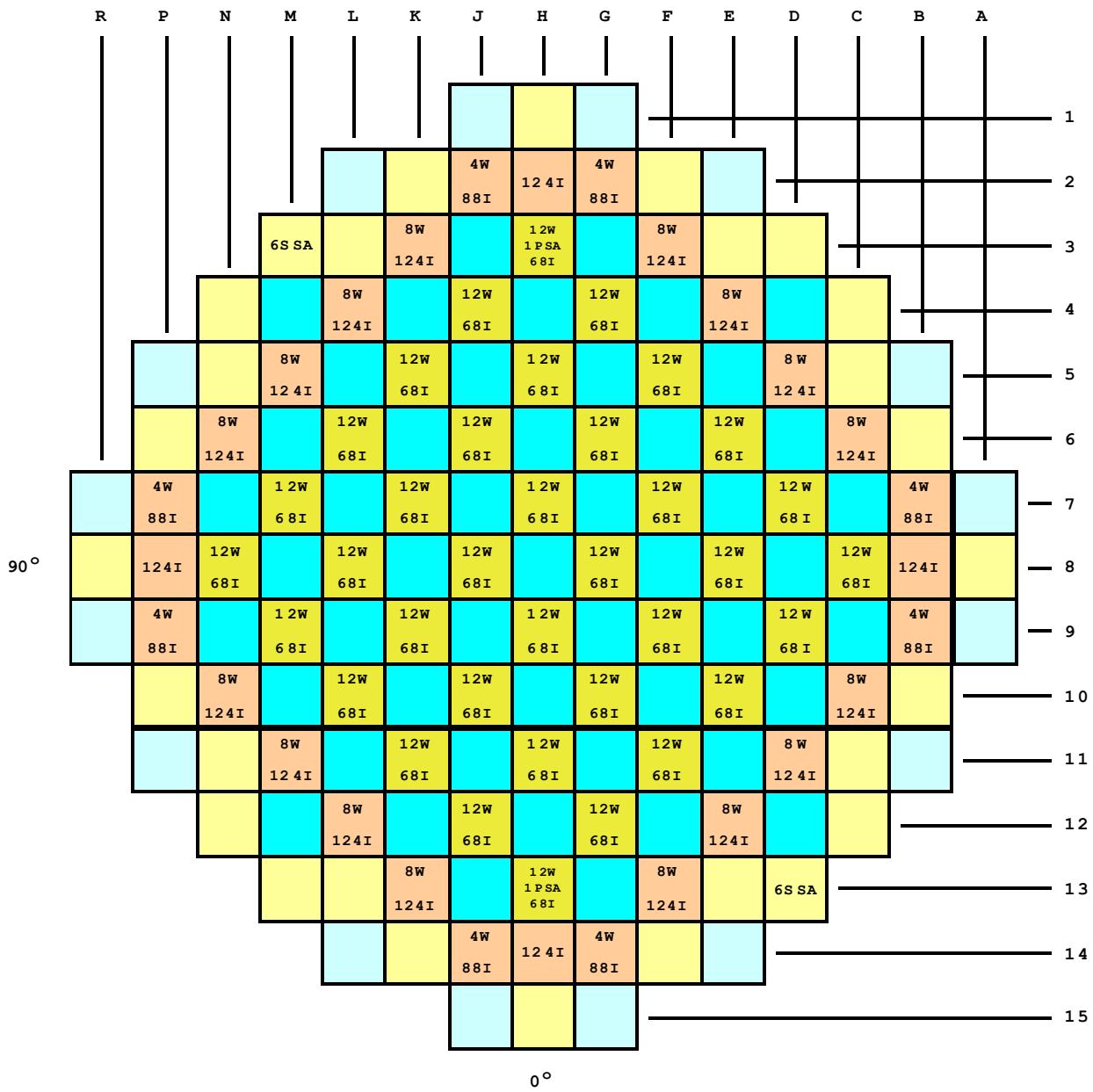

TYPE	TOTAL
##W...(NUMBER OF WABA RODLETS).....	592
##I...(TOTAL NUMBER OF FRESH IFBA RODS).....	5632
#SSA..(NUMBER OF SECONDARY SOURCE RODLETS)...	12
#PSA..(NUMBER OF PRIMARY SOURCE RODLETS).....	2

Figure 4-6 First Core Burnable Absorbers Collocation

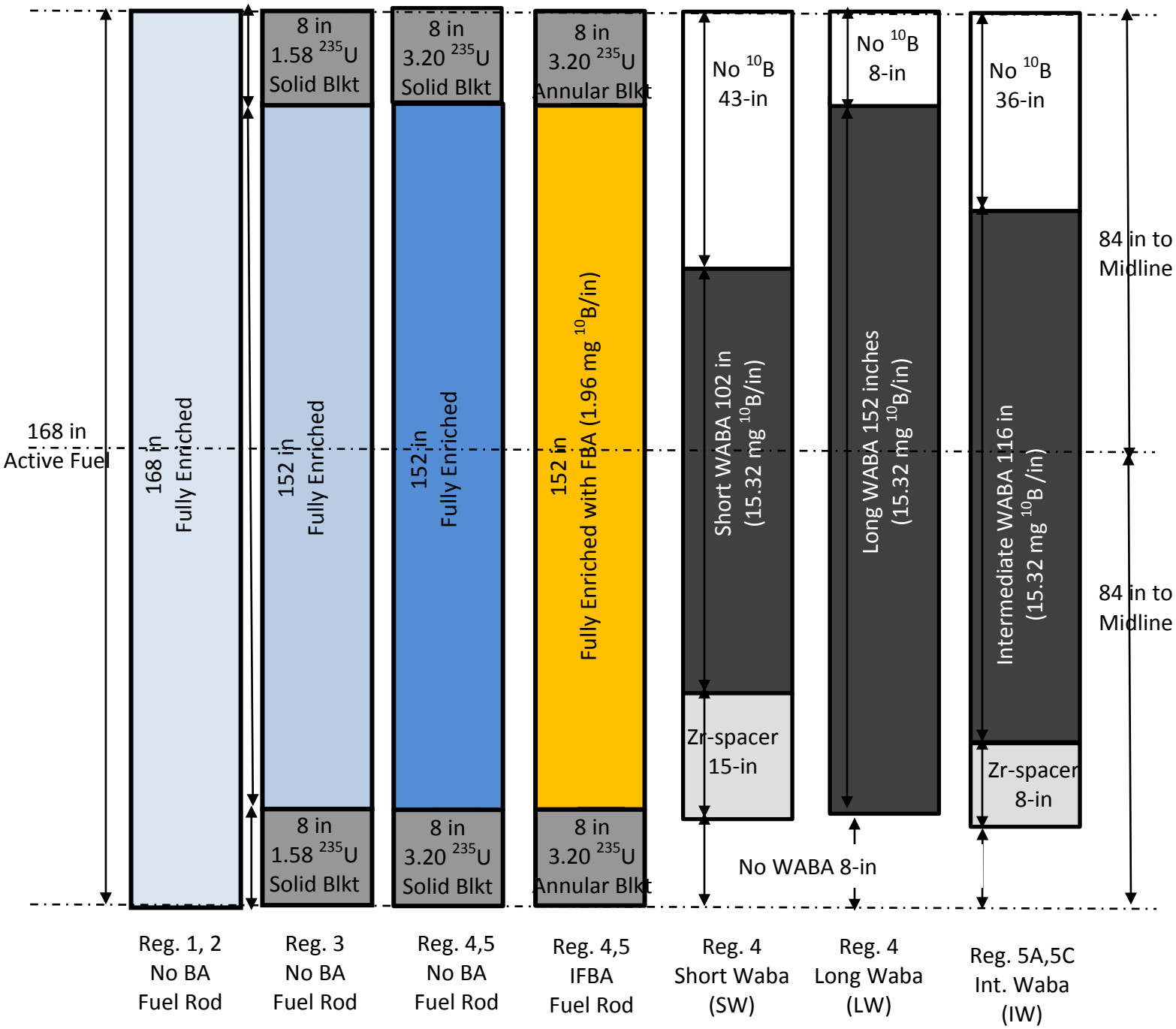

Figure 4-7 Axial Fuel Stacks for Regions 1 through 5

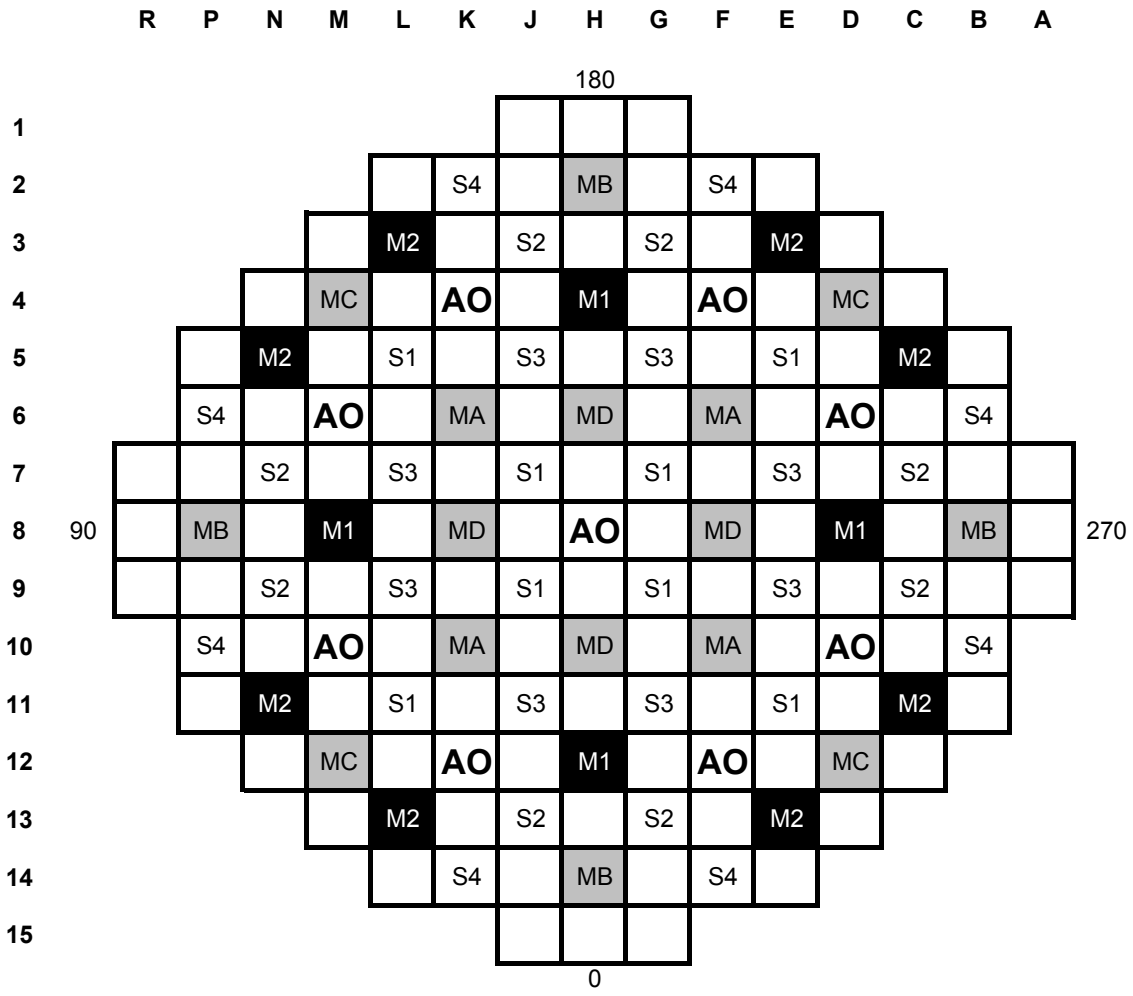

Bank ID	Group Association	Cluster Design Type	# of Clusters
MA	MSHIM Control	Gray	4
MB	MSHIM Control	Gray	4
MC	MSHIM Control	Gray	4
MD	MSHIM Control	Gray	4
M1	MSHIM Control	Black	4
M2	MSHIM Control	Black	8
AO	Axial Offset Control	Black	9
S1	Shutdown	Black	8
S2	Shutdown	Black	8
S3	Shutdown	Black	8
S4	Shutdown	Black	8
Total			**69**

Figure 4-8 Control Rod Banks and Core Placement

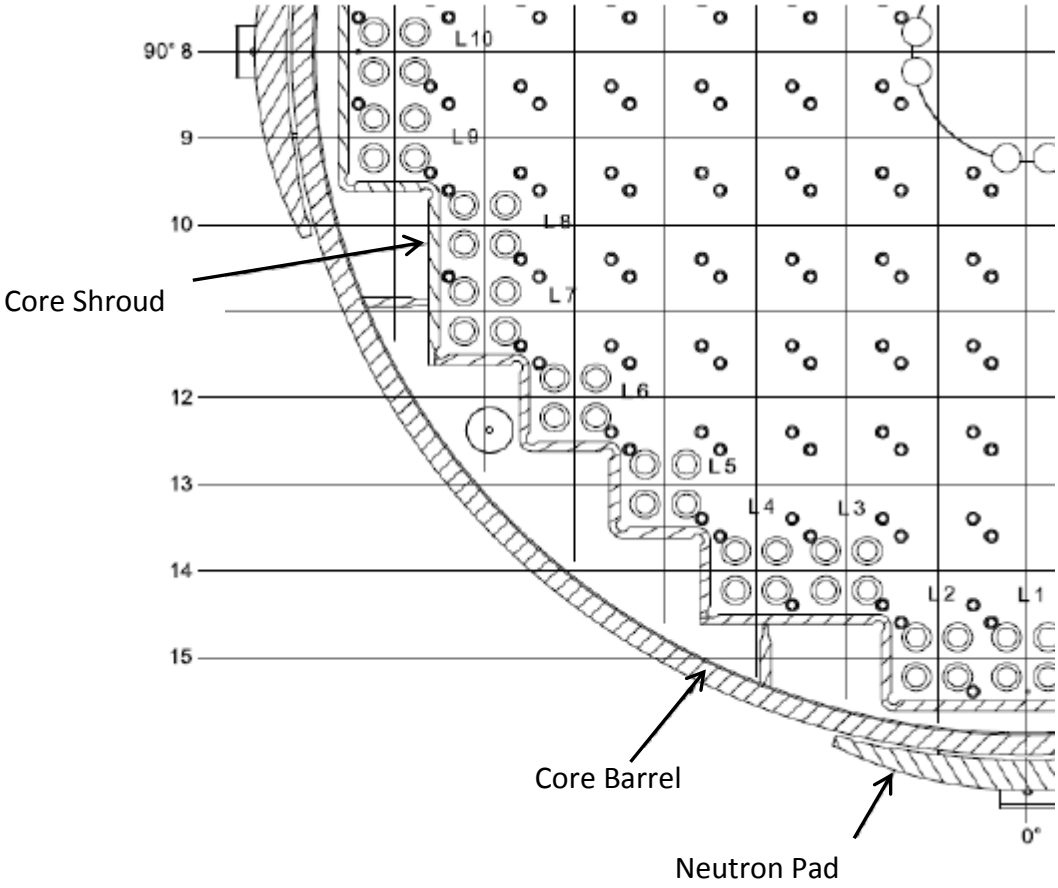

Figure 4-9 Reflector -Radial Cut

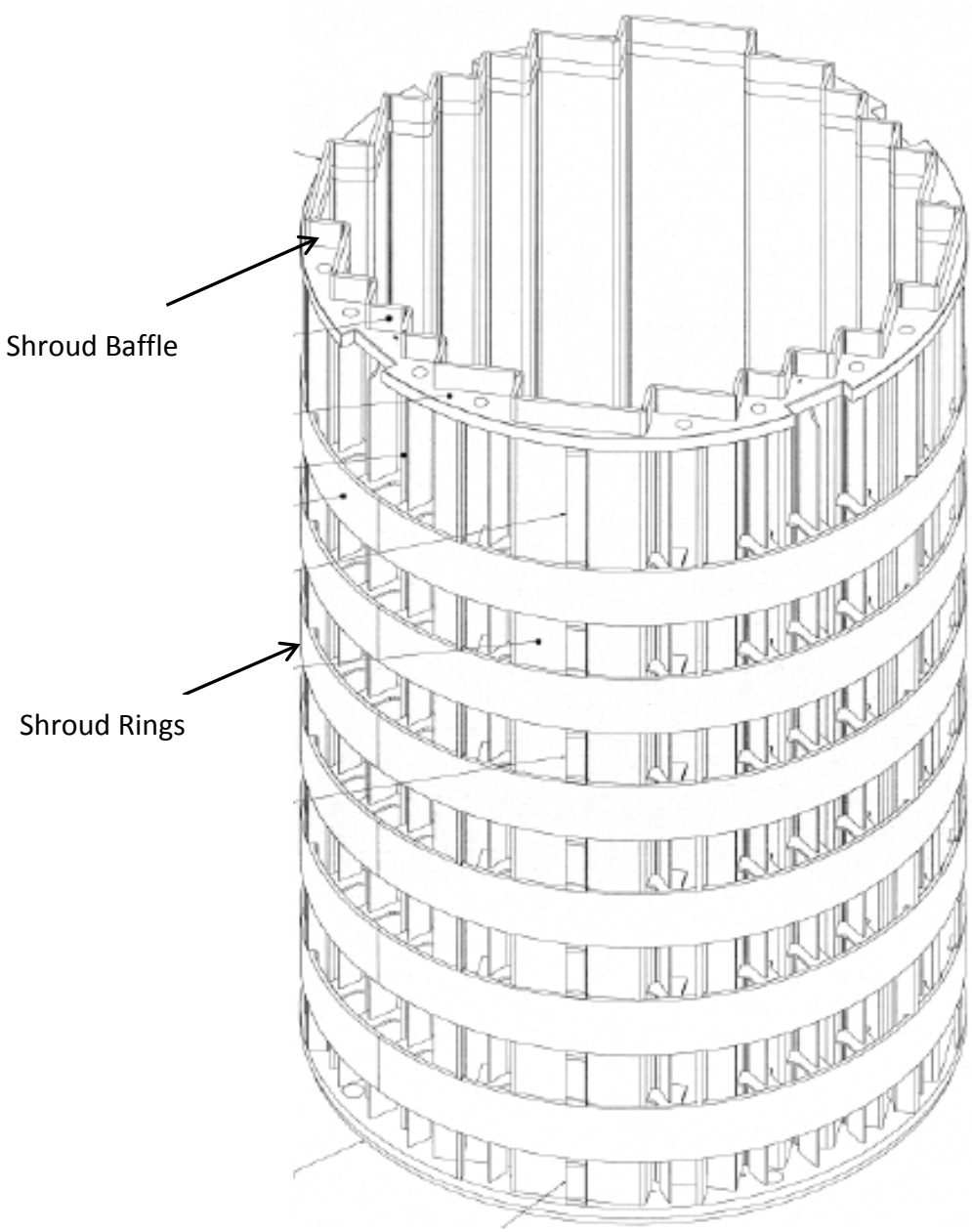

Figure 4-10 Core Shroud - Isometric View

5 APPROACH TO SIMULATIONS

This section describes the codes employed to perform the **AP1000** PWR core reactor physics HZP simulations, the modeling approach adopted and the simulations performed.

5.1 Codes used

The codes used for the work reported are listed below, together with a description of the physics methods employed in each code package:

5.1.1 VERA-CS

The core simulator of VERA, VERA-CS, with the SP_N solver and on-the-fly cell-homogenized cross sections generated using the SCALE module XSProc (Ref. 2-3) has been used. SP5 with P3 scattering and 23 energy group cross sections data collapsed from the 252 energy group ENDF/B-VII.0-based SCALE library using 1D discrete ordinate transport pin cell calculations has been used throughout this work. This package has been used in past work (Ref. 4), showing remarkable agreement with measurements (except for ITC) as well as Monte Carlo numerical solutions for HZP simulations.

In particular, the following steps are performed by VERA-CS for the simulations performed:

1. Process ASCII input file with problem specification converted into XML format
2. Convert input specification into arguments for XSProc
3. Generate a geometric representation of the reactor needed by XSProc
4. Build and partition a discrete mesh representation of the reactor geometry
5. Broadcast XSProc geometry to each processor domain
6. Run XSProc to generate pin-cell homogenized macroscopic cross sections
7. Map the cross sections to VERA-CS computational mesh cells
8. Run the SP_N solver to calculate scalar fluxes
9. Integrate scalar fluxes with fission reaction rate data to calculate power distribution
10. Perform parallel output

Further description of the main components is given below.

5.1.1.1 Cross Section Generation

The XSProc module of the SCALE code system (Ref. 3) has been incorporated into VERA and is available for use in neutronics calculations; in particular XSProc has been employed here for on-the-fly cross section generation for the VERA-CS SP_N solver.

XSProc performs resonance self-shielding with full range Bondarenko factors using the BONAMI module of the SCALE system and employing either the narrow resonance approximation or the intermediate resonance approximation. A wide variety of options are provided for different lattices and cell geometries through the use of Dancoff approximations. For uniform fuel lattices, Dancoff factors are automatically generated from the user-input geometry and material descriptions. XSProc also allows user-input Dancoff factors to treat non-uniform lattice effects, but this capability has not been used here. The fine energy group structure of the resonance self-shielding calculation can then be collapsed to a coarse group structure through a one-dimensional (1D) discrete-ordinates transport calculation internal to XSProc. In addition a spatial homogenization is employed for pin cell cross sections also using the flux results from the 1D transport solution. These XSProc results are then used for the SP_N transport calculation.

The SCALE 6.2 252 group ENDF/B-VII.0 neutron cross section data library utilized for the **AP1000** PWR core calculations contains data for 417 nuclides and 19 thermal-scattering moderators. Thermal scatting data for most nuclides are available at five temperatures, where other nuclides provide data for as many as ten temperatures. Bondarenko factors are tabulated at five different temperatures and thirty background cross sections.

The SCALE Material Information Processor capabilities are included in XSProc to: convert user input material data into atom number densities needed for cross section processing; convert user-input of fuel lattices, region-wise, and infinite medium into a form suitable for cross section processing; calculate Dancoff factors for uniform lattices; allow user input Dancoff factors for non-uniform lattices; and generate an appropriate spatial mesh for 1D transport calculations.

The SCALE XSDRNPM transport solver (Ref. 3) provides flux-weighting of cross section data and generates energy group collapsed and cell-homogenized data for subsequent multi-dimensional transport calculations. XSDRNPM is a discrete-ordinates code that solves the 1D Boltzmann equation in slab, cylindrical, or spherical coordinates.

5.1.1.2 Flux Solver

The SP_N method is a low-order space-angle approximation of the Boltzmann equation that, unlike S_N, will not converge to the true transport solution as angle (represented by Legendre moments) and space are refined. The advantage of SP_N is that the matrix representing the transport operator can be explicitly formed. The ability to form the matrix opens many possibilities for parallel decomposition, preconditioning, and solvers. The SP_N solver uses a second-order accurate finite volume spatial discretization where the number of unknowns is

$$N_c \times \left(\frac{N+1}{2}\right) \times N_g$$

where N_c is the number of computational cells, N is the SP_N expansion order (currently supported options are 1, 3, 5, or 7), and N_g is the number of groups. Even though SP_N will not converge to the true transport solution as the SP_N expansion is increased, it has been widely used and shown to be a significant improvement over diffusion theory for reactor problems.

SP_N has been implemented in VERA-CS to provide a low-order transport option. It has been shown to be accurate (except for ITC) when using pin-homogenized cross sections for ZPPT analysis (Ref. 4) and has thus been used for this work.

5.1.1.3 VERA Output

The VERA standard output is a binary HDF5 (hierarchical data format) file type (Ref. 6). Many codes and converters are being developed to use this format, including industry tools, like the Westinghouse NEXUS/ANC9 package (Ref. 15). One of the advantages of the HDF5 format is availability of software tools to view and modify the data. One such tool is HDFView (Ref. 7). Several utilities to compare multiple files and perform typical statistical analyses associated with core design and methods validation and benchmarking have been developed by CASL and were used for this work. A utility has also been developed to convert the HDF5 file data into a SILO file format suitable for various visualizations with VisIt (Ref. 14) and used to generate many of the plots and 3D images contained in this report.

5.1.2 KENO-VI

The Beta version of the Monte Carlo criticality code KENO-VI (Ref. 8) to be released in SCALE 6.2 with parallel transport capabilities and using continuous energy (CE) energy treatment has been used to obtain reference numerical solutions. While KENO has been historically employed for criticality applications, it has been successfully applied to core physics problems by CASL (Ref. 5,9) and validated against the Monte Carlo code MCNP5 (Ref. 10), as well as the startup measurements of Watts Bar Nuclear Unit 1 Cycle 1 (Ref. 4), by CASL.

ENDF/B-VII.0 CE cross section libraries generated by the AMPX code system (Ref. 11) have been used. A CE cross section library at the HZP temperature of 565 K has been utilized.

More details on the role of KENO in CASL and specifically for the **AP1000** PWR core Test Stand simulations are given in the following section as well as in APPENDIX A.

5.1.2.1 Use of KENO in CASL

CASL has extensively tested VERA for PWR HZP geometries using independent Monte Carlo CE neutron transport simulations to generate reference numerical solutions (Ref. 4, 5). The Core Physics Benchmark Progression Problems in Ref. 9 consists of approximately 50 neutronics simulations with both eigenvalue and fission rate distribution results. The analysis of the Watts Bar Nuclear 1 Cycle 1 startup physics tests reported in Ref. 4 included various Monte Carlo core calculations for criticality and control rod bank worth. The Isothermal Temperature Coefficient (ITC) has also been predicted, as reported later. Throughout this work the Monte Carlo code KENO-VI with CE cross section data and methods has been shown to provide a reliable and accurate numerical reference and has thus been adopted to provide numerical reference solutions for the **AP1000** PWR simulations.

Monte Carlo tools in the SCALE 6 (Ref. 3) system, which has been developed and maintained by ORNL since 1969, are commonly used in criticality safety and shielding calculations as well as sensitivity and uncertainty (S/U) analyses, depletion, and criticality alarm system analyses. The SCALE code system includes the KENO V.a and KENO-VI (Ref. 8) Monte Carlo criticality codes; both offer continuous energy (CE) and multi-group (MG) energy treatments to calculate physical parameters of fissile systems. The major difference between these two codes is their geometry processors; KENO V.a uses very simple geometric components but KENO-VI uses the SCALE Generalized Geometry Package (SGGP) which allows more complex geometric modeling.

KENO-VI is typically used within SCALE's CSAS6 control sequence, which was originally developed to provide automated multi-group cross section processing for MG KENO-VI transport. Later, CSAS6 was redesigned to support CE KENO-VI calculations for transport as an input and material preprocessor. More recently, KENO-VI has been extensively applied to lattice physics problems and compared successfully to the Monte Carlo code MCNP5 (Ref. 5). Some recent representative comparisons are provided in APPENDIX E.

The KENO-VI version used for this work is a development version to be released in SCALE 6.2 (Beta 2). The development version was utilized to take advantage of several new features and bug fixes, the most important to this effort being parallelization of the particle transport and improvements in the CE data and methods. All of the KENO cases were executed on INL's Fission machine using approximately 150-300 cores.

ENDF/B-VII.0 CE cross section libraries generated by the AMPX code system (Ref. 11) have been used for the **AP1000** PWR core KENO cases, consistently with the 252-group SCALE library used in the VERA-CS simulations. A CE cross section library with a temperature of 565 K was generated for the CASL Watts Bar ZPPT analysis in Ref. 4 and was also used for the **AP1000** PWR core simulations. Other libraries were also generated by ORNL staff to support reactivity

coefficient analyses (APPENDIX D). Recent enhancements to SCALE CE data libraries in SCALE 6.1 have improved both S(α,β) neutron scattering data, resulting in significant bias reduction for thermal systems, and the probability tables that provide CE treatment in the unresolved resonance range, resulting in reduced biases for systems that are sensitive to the intermediate energy range. All these updates improve the data accuracy and enhance the solution's fidelity.

In summary, KENO-VI was selected to generate the neutronics reference solution for the **AP1000** PWR core Test Stand simulations due to:

- The KENO Monte Carlo approach to particle transport has no geometric approximations, unlike deterministic solution techniques that resort to spatial discretization approaches. For the **AP1000** PWR core, the general geometry input has allowed accurate modeling of the structure surrounding the core (shroud, barrel, neutron pads, etc.) as well as other structure (plates, springs, thimble plugs etc.) to infer the impact on reactivity and power distribution vs. simpler models employed in the deterministic calculations. This is particularly relevant due to the complexity of the **AP1000** PWR core design, enabling precise modeling of selected components and performing sensitivity studies vs. simplified models. Examples of these studies performed for the reflector regions are given in the Appendixes.

- The use of Continuous Energy (CE) cross sections in KENO, which is more rigorous than self-shielding cross section methods and multi-group (MG) treatments typically used in deterministic codes. Traditional shielding methods rely on approximate geometries (1D infinite pin cells in VERA) to calculate MG cross sections in resonance regions. Additionally, the accuracy of deterministic approaches to particle transport is sensitive to the selected energy group structure. The use of CE data and methods eliminate these approximations.

- The parallel capability in the new KENO-VI (SCALE 6.2) version, which permits simulations with the high number of particle histories required to obtain low reaction rate uncertainties on large geometries. Using INL's Fission supercomputer, KENO-VI cases have been run utilizing up to 300 processors at a time.

- KENO-VI allows solutions for large, geometrically complex, problems whose computer storage requirements and geometric complexity preclude solution by previous versions of KENO. In addition, recent versions of KENO-VI and CE data enhancements have led to significant improvements in accuracy and performance.

- Familiarity and proximity between analysts and developers for support. The SCALE development team has been an asset to support the Westinghouse Test Stand activities, through partnership with ORNL, and the availability of KENO to obtain numerical reference solutions has been a key component to its success.

5.2 Westinghouse Test Stand Simulations

The **AP1000** PWR simulations performed for the Westinghouse Test Stand are summarized below. All calculations have been performed with VERA-CS and KENO, which in the absence of measurements has been assumed as the reference solution throughout this work.

All the VERA-CS simulations have been performed on the Westinghouse compute clusters described in Section 3. The KENO calculations have been performed at the INL "Fission" HPC.

1. **2D Lattices (eigenvalue and power distribution analysis)**
    - Single Lattice (Unrodded)
    - Multi Lattice (Unrodded and Rodded)
    - 2D Core with radial reflector

2. **3D Assemblies (eigenvalue and power distribution analysis)**
    - Single assembly
    - Multi Assembly (Partial Control Rod Insertion)

3. **3D Core– Zero Power Physics Tests (eigenvalue only)**
    - HZP Critical Boron Concentration
    - Rod Worth for each bank
    - Boron Worth
    - ITC, MTC and DTC

Firstly, 2D lattice calculations for each fuel type employed in the first core have been performed, amounting to twenty lattice types in total. The main objective of this set of calculations was to ensure model consistency in VERA-CS and KENO as well as assess reactivity and pin power distribution agreement between the codes using a simple but representative geometry of each fuel type used in the first core. The comparison was then extended to multiple lattices up to a radial slice of the core, including insertion of gray and black control rods, and adding the radial reflector to the model.

As a second step, the models have been extended to 3D assembly and multi-assembly geometries. The Intermediate Mixing Vane (MV) and Intermediate Flow Mixing (IFM) grids have been implemented to the model, which also includes the axial structure above and below the active fuel.

Finally, 3D core calculations have been performed, simulating the Zero Power Physics Tests (ZPPTs) of interest for this comparison. These simulations include calculation of the HZP Critical Boron Concentration, control banks reactivity worth (eleven banks in total), soluble boron worth as well as the Isothermal Temperature Coefficient (ITC), the Moderator Temperature Coefficient (MTC) and Doppler Temperature Coefficient (DTC). More details on the KENO ITC, MTC and DTC simulations are given in APPENDIX A and APPENDIX D of this report.

5.3 Modeling approach in KENO

The KENO model for the **AP1000** PWR core has been produced using the SCALE Generalized Geometry Package, which permits construction of detailed PWR models by combining geometric shapes such as cylinders and cuboids, or any volume that can be constructed with quadratic equations. For larger models, this input can become complicated, but software has been developed to translate the basic fuel and core design parameters into the large input files required for the corresponding KENO model. KENO input files exceeding eight million lines have been created in a reasonably efficient way through this process. The models were all constructed using quadrant symmetry to decrease the computer resources required to obtain reasonable power distribution uncertainties. Reflective boundaries are used for the lines of symmetry, while vacuum boundaries are applied outside of the core radial and axial reflector regions at appropriately long distances to not impact the calculated core leakage.

In addition to reactivity, KENO-VI can also provide reaction rate tallies by region, allowing the user, with some post-processing efforts, to extract the normalized fission reaction rate distribution for reactor physics problems. A post-processing procedure has been developed for extracting the calculated fission rates and uncertainties for each unique fuel region and calculating the volume-weighted normalized power distribution for comparison to other codes, including pin, assembly, radial, and axial powers, for example. These results are placed into the same output file format (HDF5) as VERA, allowing numerical and visual data interrogation through the available post processing tools. For geometries with octant symmetry, the fission tallies are combined for symmetric power locations. This effectively doubles the sampling, and the estimated uncertainty is then reduced accordingly.

To reduce the uncertainty in the fission rates of particular fuel rod locations, especially low powered locations, an extremely large number of particles is required. Power distributions and uncertainties were calculated for all problems and are reported in APPENDIX A[c]. For all cases but the 3D core, the cell-wise power uncertainties are reasonably low. For the 3D core, the problem size is such that reducing cell-wise uncertainties below a few percent is impractical with the current KENO. However, for ZPPTs a cell-wise low-uncertainty power distribution is not required to obtain accurate reactivity results; namely, the core eigenvalues (k-effective) and derived quantities obtained for the KENO models are an appropriate reference solution.

5.3.1 KENO Model Details

For the **AP1000** PWR 3D core models, the KENO-VI pre-processor developed by CASL generates eight million line ASCII input files containing 688,000 unique geometry units. This is partially

[c] It is noted that the KENO-VI power distributions are based on fission rate only and do not consider any redistribution due to gamma sources and neutron kinetic energy.

because KENO is limited to providing unique tallies only for unique units. Future KENO versions will provide the ability for mesh tallies and this will significantly reduce the number of geometry units needed for these types of models. Most core features are modeled explicitly, while regions above and below the fuel rods are treated as homogenized regions. A detailed listing of the features of the KENO-VI model for the **AP1000** PWR simulations are described below.

- Explicit representation of the fuel rod stack, plenum, and end plugs, included solid and annular axial blanket regions. The IFBA ZrB_2 coating is also treated explicitly. The end plug geometry is modeled as a cylinder, and is similar for fuel rods, WABA rods and control rods. The plenum spring is modeled as a shell of equivalent inner and outer radius and mass.

- Semi-explicit representation of all spacer, mixing, and protective grids using the 'equal cell' model, by distributing the grid mass uniformly amongst the 289 lattice cells in each assembly slice, and placing that mass in an equivalent volume box on the periphery of each cell. The axial locations of the spacer grids are modeled according to Ref. 1. The mass of the spacer sleeves is included as part of the grid mass, but the sleeves are not explicitly represented. Figure 5-1 depicts the KENO-VI spacer grid model.

- Guide tubes and instrument tubes are assumed to extend from the bottom nozzle to the top nozzle. The dashpot region of the guide tubes is modeled explicitly.

- Homogenization of the top and bottom nozzles of each assembly, and the upper and lower core plates.

- Explicit modeling of WABA (poison, bottom Zr spacer, and upper plenum), control rods, end plugs, and plenum regions below the top nozzle. Regions of inserts in and above the top nozzle are ignored. Fully withdrawn control rods are also included in the model up to the upper nozzle, which results in the rod tips being located in the fuel rod upper plenum region.

- Explicit thimble plugs in the upper regions of the guide tubes which do not contain control or WABA rodlets. The plugs are approximated as solid cylinders with equivalent length to the actual plug.

- Explicit inclusion of in-core detector instrumentation thimbles. These were not used in every case, but the capability was included in order to calculate the effect on core average reactivity for startup criticality.

- Exclusion of any source rods for startup calculations.

- Explicit treatment of the core baffle, barrel, neutron pads, and vessel. Both smeared and explicit modeling of the shroud region has been performed for sensitivity analyses in APPENDIX C.

- Material number densities for fuel, poison, and structure have been generated using Westinghouse in-house licensed codes and employed in KENO.

- Proper positioning of each of the eleven control rod banks for rod worth calculations and other operating configurations.

While the above applies to 3D core ZPPT configurations, the smaller models, such as 2D lattices, 2D multi-lattice, 2D core, 3D assembly, and 3D multi-assembly, have been generated as subsets of the 3D core cases to maintain consistency and ensure correct modeling to the extent possible. Confidence in the 3D core model was established by progressing from the smaller to the larger configurations while verifying consistency in the comparison of the results against the corresponding VERA-CS simulations, as described in Section 6.

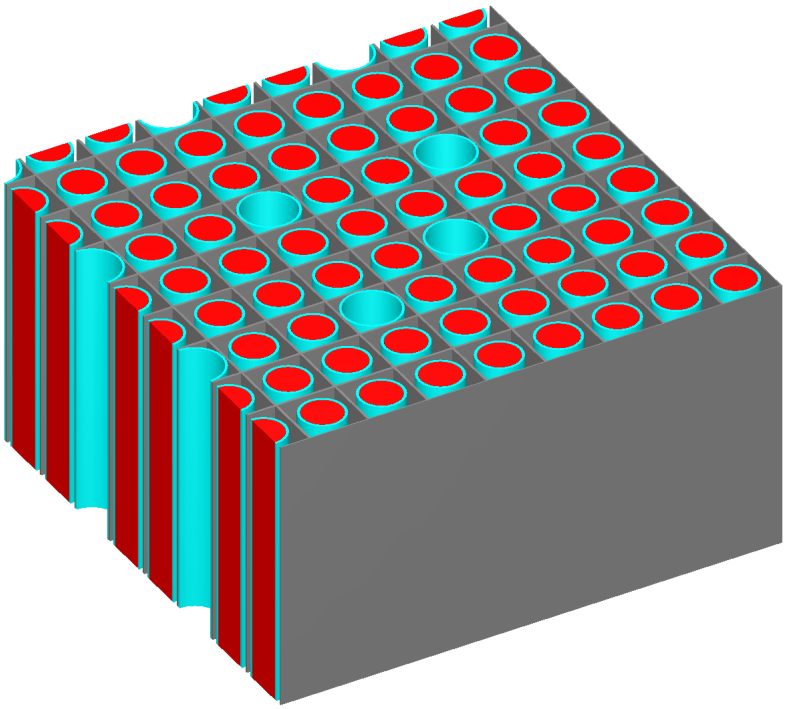

Figure 5-1 KENO Semi-Explicit Spacer Grid Model (MV Grid)

5.4 Modeling approach in VERA-CS

The VERA-CS AP1000 models have been set up through VERAIN, the VERA common input. This common ASCII-based input has been found practical and effective for building neutronic models of commercial PWRs, including the **AP1000** PWR first core. The input deck for the 3D core model of the AP1000 PWR is intuitive and compact (<1,000 lines). It contains all the fuel,

control rod, and structure specifications required to perform the HZP ZPPT analysis, with only minor modifications required to run each specific case (e.g. change of a control bank position to measure its worth, analysis of a 2D core slice or a single lattice or a single 3D assembly, etc.). Once the base input had been validated for consistency with the core design specification, setting up and running the various cases reported here has required a relatively minor effort.

A few limitations in performing reactor analysis using the current VERA-CS should be mentioned and resolved in the future. These are also discussed in Section 8.

- There is no automatic thermal expansion capability to account for the expansion of the structures going from cold to operating temperature conditions. The VERA-CS results reported here refer to models with cold dimensions and the KENO results have been generated to be consistent with VERA-CS

- The only available radial core structure model in VERA-CS consists of baffle plus water, while more complex reflectors with additional structure materials of varying geometry and thickness may be employed. The VERA-CS results reported here utilize a 1-in thick axially uniform stainless steel baffle reflector surrounded by water. A sensitivity study has been performed with KENO on the impact of various reflector models to assess the reactivity and power distribution impact of the simple 1 inch baffle approximation vs. the actual **AP1000** PWR reflector. The results of this sensitivity study are presented in APPENDIX B and APPENDIX C.

- VERAIN does not currently have to capability to accept material input in the form of atomic number density. The material compositions were provided by the Westinghouse core analysis tools in this format, and input directly into KENO. However, VERA-CS required some manual manipulation of the materials composition HDF5 file and the input material density to ensure consistency with the other codes. This process was somewhat time consuming and prone to errors.

The VERA-CS deck for the first core All-Rods-Out HZP simulation is given in APPENDIX G.

6 RESULTS

6.1 2D Lattice Results

A comparison of the reactivity and power[d] distribution for VERA-CS vs. KENO for the 2D lattices comprising the **AP1000** PWR core is given in Table 6-1. The leftmost column indicates the fuel region of pertinence for each lattice, while the "Case" column contains a succinct description of the lattice configuration. The table then shows the k-infinity value obtained from CE KENO calculations and the difference between VERA-CS and KENO. The two rightmost columns summarize the agreement in power distribution for VERA-CS vs. KENO. In particular, two representative parameters are chosen: "ΔP RMS", that is the root mean square (RMS) of the power difference (VERA-KENO) multiplied by 100, weighted by the fuel rod volumes of a given lattice, and the maximum absolute difference "ΔP Max". The delta in k-infinity is also plotted in Figure 6-1, while the RMS and Max ΔP are plotted in Figure 6-2.

The results show excellent reactivity agreement for VERA-CS vs. CE KENO across all lattices at HZP conditions, with an average difference of -34 pcm and a standard deviation of ~40 pcm. Therefore, based on 2D lattice analysis, it is reasonable to expect close, slightly lower, reactivity predictions for VERA-CS vs. KENO when extending the geometry, unless 3D transport effects and interaction between assemblies will predominate.

A comparison of the eigenvalue prediction for the various lattices is given in Figure 6-1. Lower enrichment lattices in VERA-CS are less reactive than KENO, while at higher enrichment without zoning the agreement becomes virtually perfect. Enrichment zoning, and/or use of IFBA, seems to slightly deteriorate the agreement, with some favorable compensation of errors from localized strong absorbers (e.g. WABA). These biases however are small and the comparison appears overall consistent and more than satisfactory throughout the simulations performed. VERA-CS agrees well with KENO also in the power distribution prediction, as shown in Figure 6-2, showing only a mild deterioration for localized strong absorbers, IFBA, and enrichment zoning lattices.

More details on the KENO simulations supporting this analysis are given in APPENDIX A, Section A.1.

[d] The term "power" instead of "normalized fission rate" is used for brevity in the remainder of this report.

Table 6-1 HZP lattice results

Region #	Case	KENO	VERA-CS		
		k_{inf} (+/- 3 pcm)	Δk_{inf} (pcm)	ΔP RMS (%)	ΔP Max (%)
1	^{235}U @ 0.74	0.66846	-102	0.13	0.30
2	^{235}U @ 1.58	0.95127	-38	0.15	0.31
3	^{235}U@ 3.20	1.18998	-7	0.19	0.40
3	^{235}U@ 1.58 (BLKT)	0.95226	-21	0.15	0.27
4	^{235}U@ 3.78 - 68 IFBA 12WB	1.03710	28	0.25	0.58
4	^{235}U@ 3.78 - 68 IFBA 8WB-4ZR	1.06471	61	0.25	0.60
4	^{235}U@ 3.78 - 68 IFBA 8WB-4TP	1.06583	-5	0.25	0.54
4	^{235}U@ 3.20 - 68 IFBA 12TP	1.18570	-14	0.23	0.40
4	^{235}U@ 3.20 (BLKT, 68 ANLR, 12TP)	1.18525	-10	0.24	0.42
5A	^{235}U@ 4.38 - 88 IFBA 4 WB	1.12083	-46	0.26	0.49
5A	^{235}U@ 4.38 - 88 IFBA 4 ZR	1.14851	-39	0.24	0.52
5A	^{235}U@ 4.38 - 88 IFBA 4 TP	1.14997	-65	0.24	0.51
5A	^{235}U@ 3.20 - 88 IFBA 4TP	1.18379	-26	0.24	0.42
5A	^{235}U@ 3.20 (BLKT, 88 ANLR, 4TP)	1.18348	-12	0.23	0.42
5B	^{235}U@4.38 124 IFBA	1.10339	-106	0.25	0.58
5B/C	^{235}U@ 3.20 (BLKT, 124 ANLR)	1.18063	-43	0.28	0.55
5C	^{235}U@ 4.38 - 124 IFBA 8 WB	1.04637	-36	0.28	0.50
5C	^{235}U@ 4.38 - 124 IFBA 8 TP	1.10191	-90	0.25	0.55
5C	^{235}U@ 4.38 - 124 IFBA 8 ZR	1.10025	-70	0.25	0.56
5C	^{235}U@ 3.20 (BLKT, 124 ANLR, 8TP)	1.18086	-32	0.26	0.48
		Average	-34	0.22	0.45
		Standard Deviation	40		

Notes: BLKT stands for solid blanket, ANLR stands for annular blanket, WB stands for WABA, ZR indicates the presence of Zr-spacers in selected WABA rods, TP indicates the unpoisoned He-filled top of the WABA rod. The enrichment reported for Reg. 4 and Reg. 5 is the average lattice enrichment (enrichment zoning is used for these regions, with U-235 at 3.4, 3.8 and 4.2 w/o for Reg. 4 and U-235 at 4.0, 4.4 and 4.8 for Reg. 5). No enrichment zoning is used for Reg. 1,2 and 3. Δk is the delta reactivity VERA-CS vs. KENO in pcm, calculated as $10^5 * \ln(k_{VERA\text{-}CS}/k_{KENO})$. ΔP is the delta in normalized fission rate VERA-CS-KENO multiplied by 100, with ΔP RMS calculated as the root mean square of the differences and ΔP Max as the maximum absolute difference.

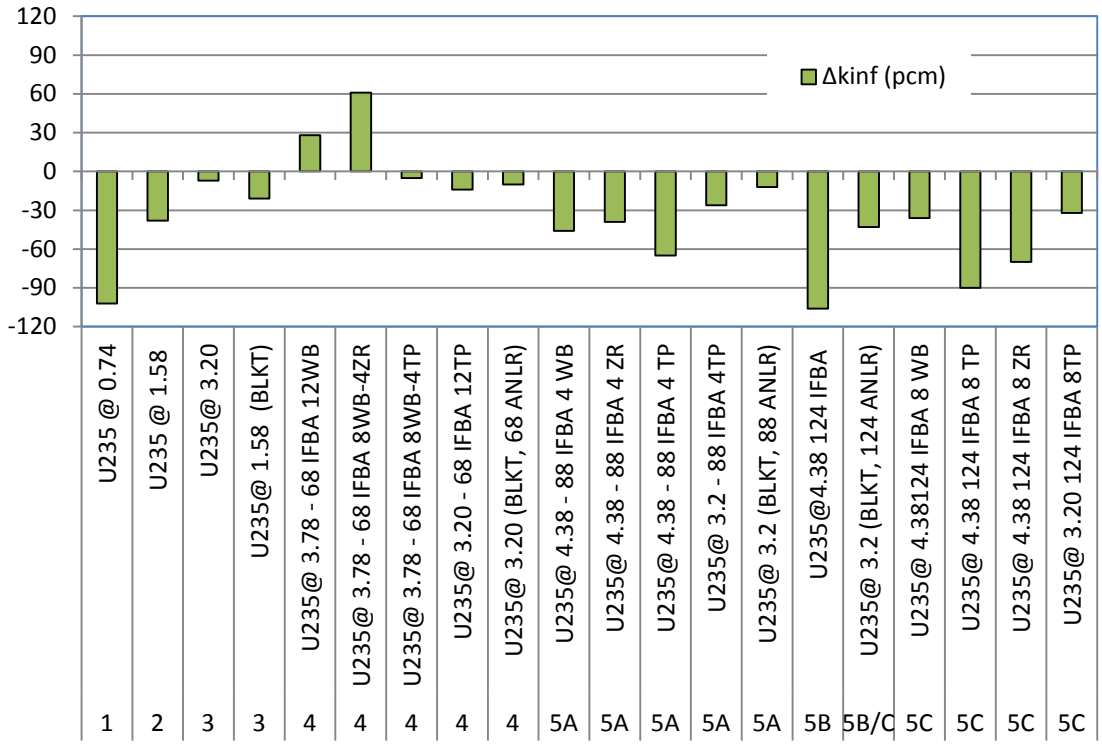

Figure 6-1 HZP delta k-inf VERA-CS-KENO (pcm) for 2D lattice simulations

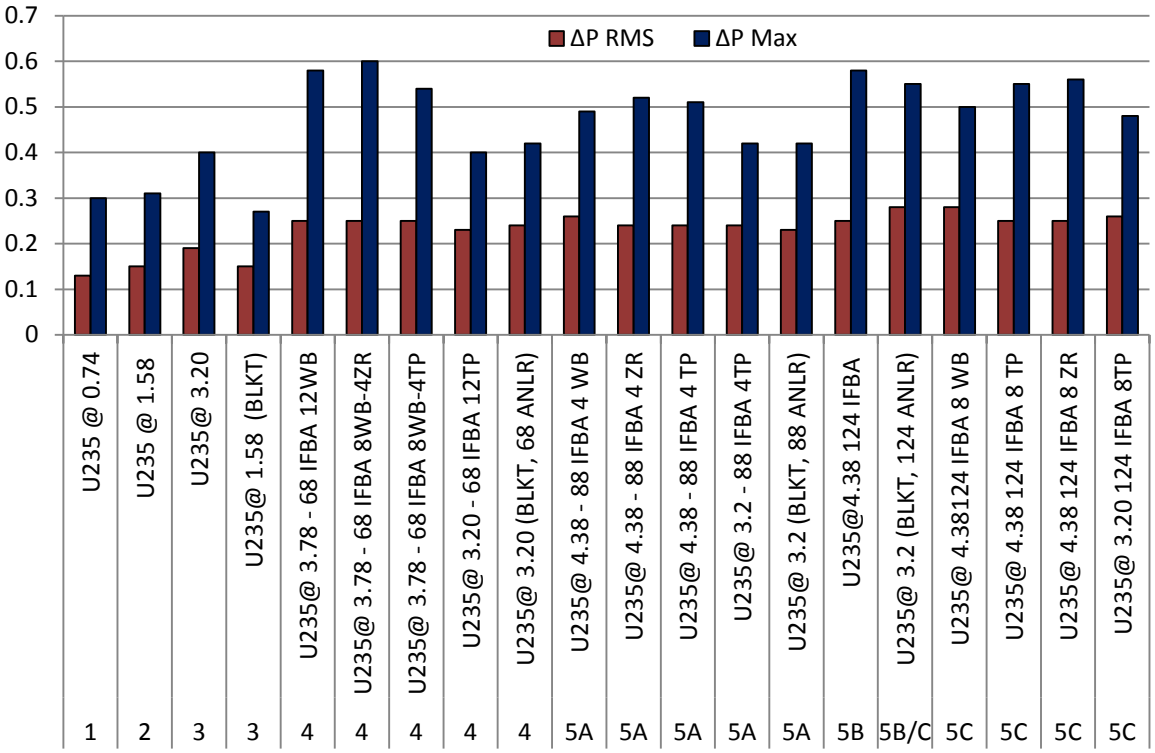

Figure 6-2 HZP ΔP (RMS and Max) VERA-KENO for 2D lattice simulations

6.2 2D Multi-Lattice

The main objective of multi-lattice calculations was to verify that the agreement in reactivity and power distribution observed in single-lattice calculations was maintained when considering the effect of neighboring assemblies. This is particularly relevant as the **AP1000** PWR first core has a checkerboard of higher/lower enriched fuel assemblies leading to relatively large power gradients across interfacing assemblies. The simulations reported here refer to a 3x3 multi-lattice configuration with fuel lattices belonging to Reg. 2 and Reg. 4 fuel. This configuration is depicted in Figure 6-3 and is representative of the inner core of the **AP1000** PWR at the axial mid-plane (see also Figure 4-1).

Three simulations have been performed for the 3×3 multi-lattice, with results reported in Table 6-2: one simulation without control rods ("unrodded"), one with Ag-In-Cd (black) control rods inserted in the central lattice of the 3x3 and one with tungsten (gray) control rods inserted in the central lattice. The eigenvalue predicted by VERA is very close to KENO and slightly lower ~-20 to -40 pcm, consistent with the single lattice results. The power distribution comparison is slightly worse than for single lattice cases but still satisfactory, with pin RMS <0.4% and Max <1%. This includes rodded cases which present specific challenges due to the local power suppression in the rodded assembly and power redistribution to the other assemblies.

A more detailed results analysis for the Ag-In-Cd rodded case is given in Figure 6-4 through Figure 6-6. Namely, Figure 6-4 shows the assembly and delta-assembly power VERA-CS vs. KENO, while Figure 6-5 and Figure 6-6 show respectively the pin power and delta pin power. The power suppression in the rodded assembly, with the power redistributing primarily to the higher enriched Reg. 4 fuel lattice, is notable. The fuel rods resulting in the highest power are located at the interface with Reg. 2 fuel, close to the water gap between the assemblies and further away from the control rods (and WABA rods) - see Figure 6-5

The power distribution comparison in Figure 6-6 shows a very satisfactory agreement, in general and for these assembly-interface locations, which are challenging due to the impact of local asymmetric spectral conditions not explicitly accounted for during the on-the-fly XSProc cross section generation step. It is not clear at this point if this agreement will hold during burnup calculations with the current cross section collapsing methodology and further investigation is recommended in this regard. A slight deterioration of the agreement in the locations adjacent to one or more strong localized absorbers (e.g. Control Rods or WABAs) is noted but the resulting discrepancy is still below 1%, which is certainly adequate to establish some degree of confidence in the power prediction capabilities of VERA-CS.

In summary, the analysis of these multi-lattice simulations solidifies the remarkable agreement shown by VERA-CS vs. KENO in the single-lattice calculations.

More details on the KENO simulations supporting this multi-lattice analysis are given in APPENDIX A, Section A.2.

Table 6-2 HZP multi-lattice results

		KENO	VERA-CS				
Case	soluble boron (ppm)	K_{inf} (+/-2 pcm)	ΔK_{inf} (pcm)	RMS ΔP Asm (%)	Max ΔP Asm (%)	RMS ΔP Pin (%)	Max ΔP Pin (%)
Unrodded	1244	1.00199	-37	0.20	0.24	0.31	0.82
Ag-In-Cd	955	1.00235	-47	0.24	0.53	0.36	0.98
Tungsten	1130	1.00227	-19	0.21	0.31	0.32	0.89

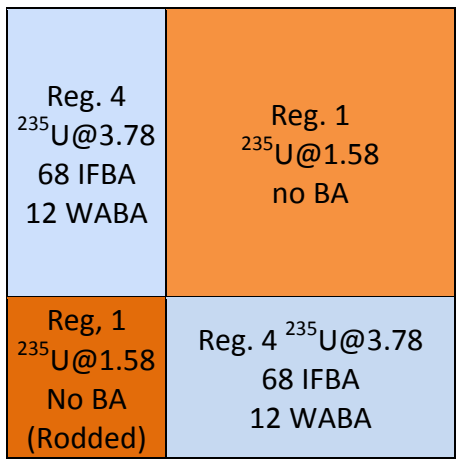

Figure 6-3 Loading Pattern for Multi-Lattice Simulations
(with Rodded and Unrodded Central Position – 1/4th geometry)

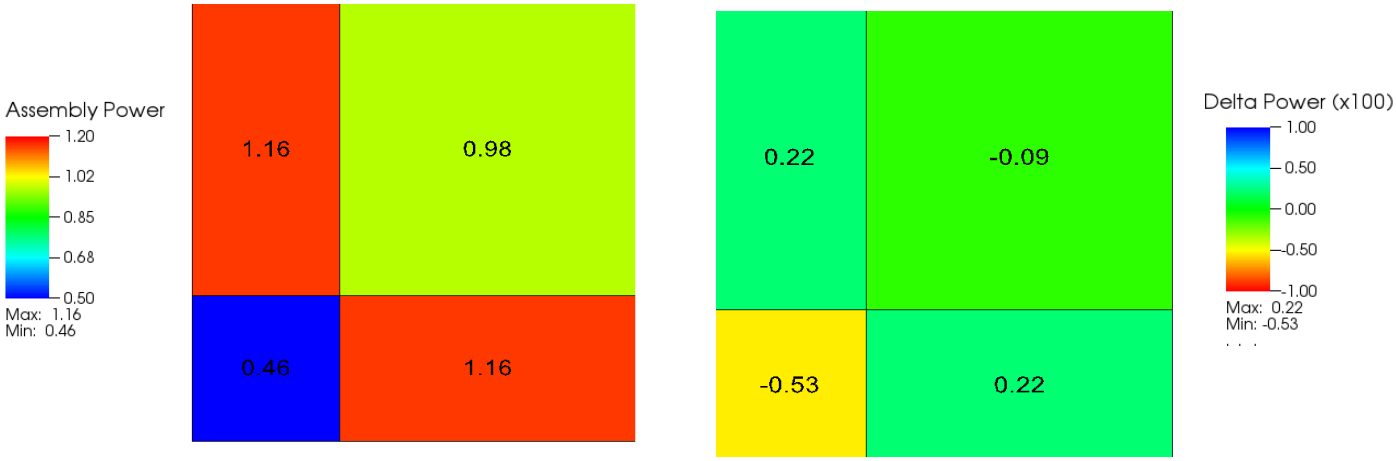

Figure 6-4 Assembly Power (KENO, left) and Delta Assembly Power (VERA-KENO x100, right) for the Ag-In-Cd Rodded Multi-Lattice Simulation

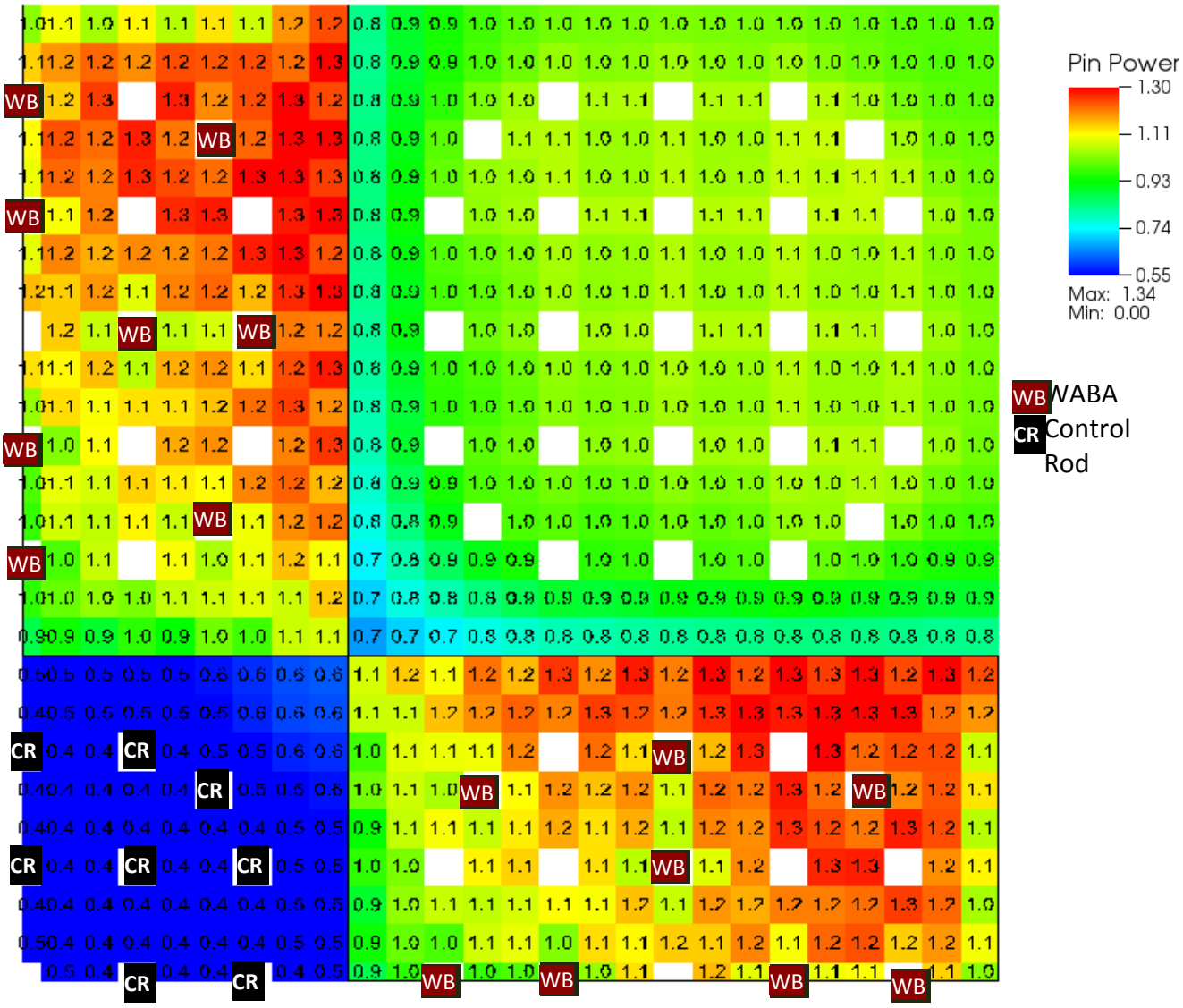

Figure 6-5 Pin Power (KENO) for Ag-In-Cd Rodded Multi-Lattice Simulation

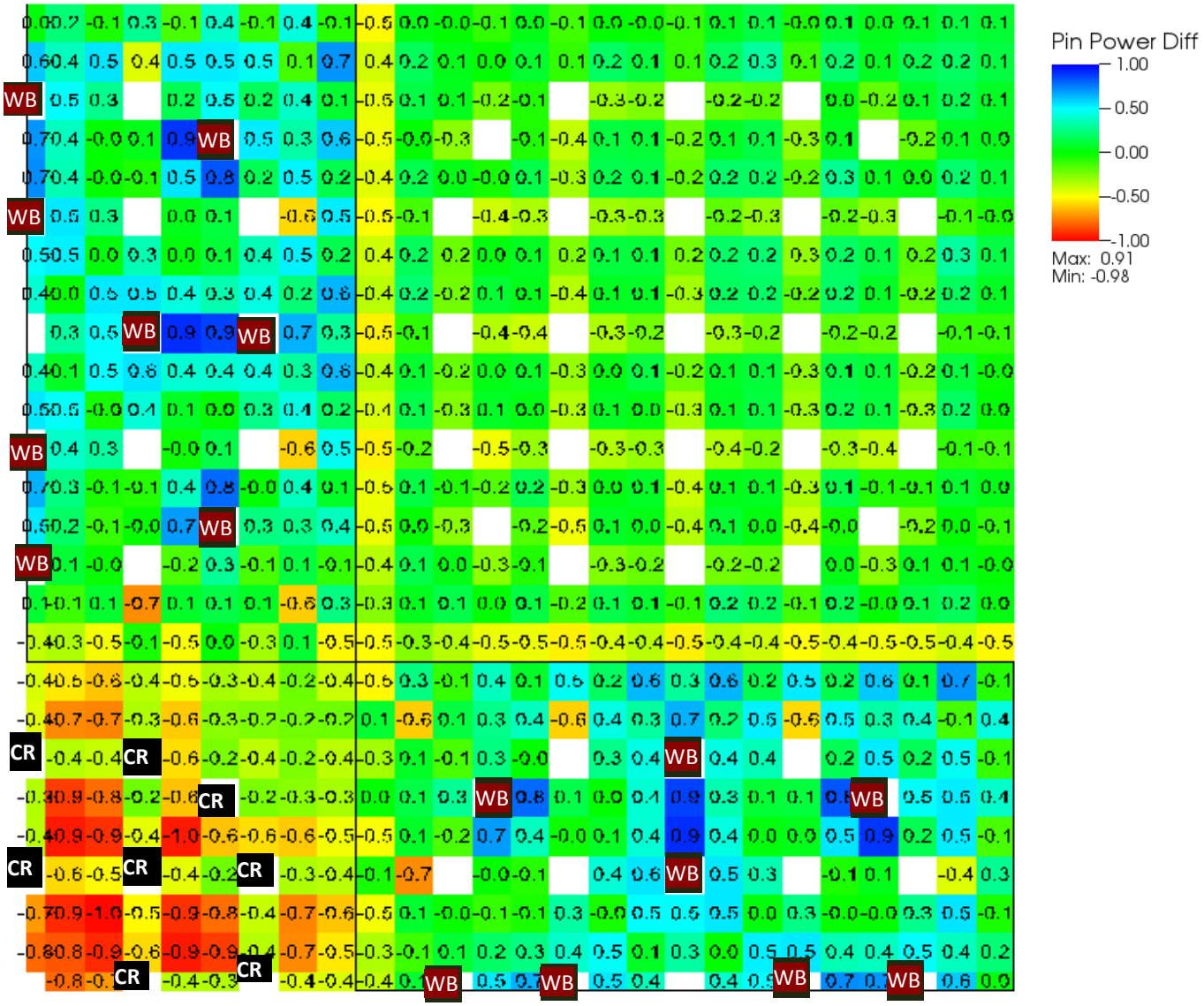

Figure 6-6 Delta Pin Power (VERA-KENO)x100 for Ag-In-Cd Rodded Multi-Lattice Simulation

6.3 2D Core

The results presented in this section refer to a radial core slice, including the reflector, at the core axial mid-plane of the **AP1000** PWR core. The geometry and material specifications for this case are displayed in Figure 6-7. Note that the reflector chosen consists of a 1 inch stainless steel baffle surrounded by water, as this can be modeled consistently in VERA-CS and KENO and thus obtain a meaningful power distribution comparison. More details on the KENO model for the 2D core can be found in APPENDIX A, and the worth of various radial reflector models is discussed in APPENDIX B.

A plot of the reference assembly power distribution obtained with KENO for this simulation is given in Figure 6-8; the KENO pin power distribution is shown in Figure 6-9. The relative comparisons for VERA-CS vs. KENO are given in Figure 6-10 (delta assembly power vs. KENO) and Figure 6-11 (delta pin power vs. KENO). A summary of the results can be found in Table 6-3.

Table 6-3 Summary of comparison VERA-CS vs. KENO for AP1000 PWR 2D core
(radial slice at axial midplane)

KENO	VERA-CS					
K_{inf} (+/-1 pcm)	Δk_{inf} (pcm)	RMS ΔP Assembly (%)	Max ΔP Assembly (%)	RMS ΔP Pin (%)	ΔP Hot Pin (%)	Max ΔP Pin (%)
1.00097	0	0.21	0.42	0.39	0.78	3.1

Notes: coolant soluble boron of 1316 ppm. "Hot pin" is the pin showing the highest relative power in this simulation. "Max assembly" and "Max pin" refer to the largest (absolute) difference in respectively assembly and pin power predictions for VERA-CS vs. KENO.

The agreement between VERA-CS and KENO for this 2D core geometry is remarkable, and consistent with the results reported for the lattice and multi-lattice simulations. The eigenvalue prediction is virtually identical. The agreement in the assembly power distribution is excellent, with RMS and maximum differences of 0.2% and 0.4% respectively. The agreement in the pin power prediction is also notable, with a delta power RMS of ~0.4% and an absolute delta power of 0.8% (<0.5% in terms of relative difference) for the hot pin.

The maximum difference in the pin power prediction is ~3.0%, occurring in the very low power pins at the edge, and especially corners, of the core (red color locations in Figure 6-11). This is possibly caused by the strong asymmetry in the local spectral conditions for these pins compared to the assumed symmetric conditions for the XSProc cross section collapsing step prior to performing the SP_N calculation. This is confirmed analyzing the delta pin form factors[e] for VERA-CS vs. KENO in Figure 6-12. This plot, in addition to the pins at the edge of the core, show other locations where the simple geometry assumed in the first energy collapsing step

[e] The form factors are the pin powers of a given assembly normalized by the power of the assembly. The normalization step effectively takes away any potential bias deriving from differences in the assembly power prediction between two codes, thus facilitating the analysis of the intra-assembly power shape prediction.

may be problematic, e.g. at the interface, and especially corners, of the natural U assemblies with the neighboring higher-enriched assemblies. However all these potentially problematic locations have very low power and are typically discharged at the end of the cycle; in addition the agreement in the overall assembly power including the peripheral assemblies is excellent. Therefore the mispredictions observed are not expected to lead to tangible inaccuracies in the prediction of the core performance.

In summary, the reactivity as well as power distribution prediction from VERA-CS for an entire slice of the **AP1000** PWR core compares remarkably well with KENO except for a few outliers of little significance. It is therefore proper at this point to extend the comparison to the axial dimension to verify that VERA-CS is capable of adequately simulating also the axial heterogeneities present in the **AP1000** PWR first core.

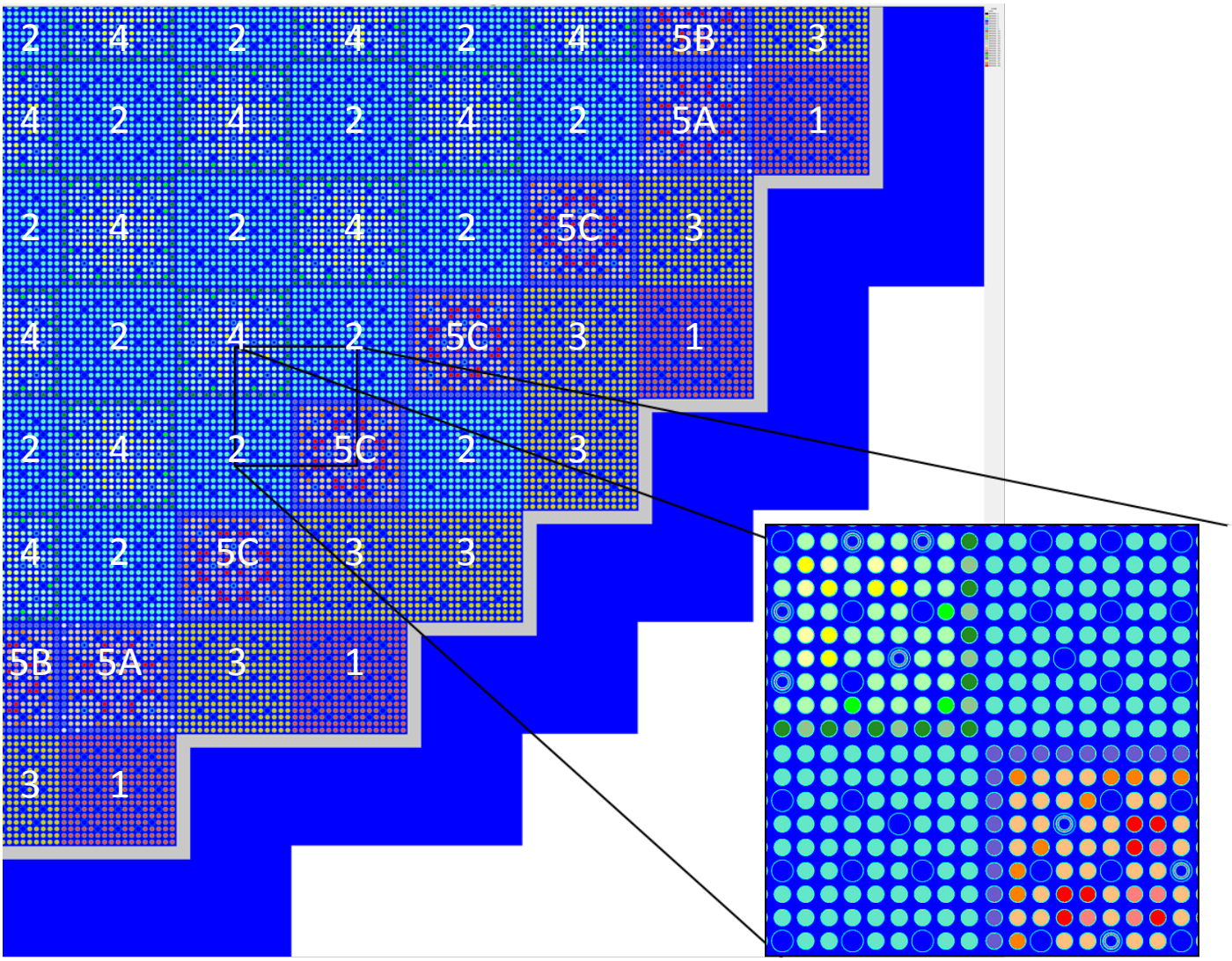

Region Group	Fraction of Total	U235 Average	IFBA Rods	WABA Rods
1	0.10	0.740	0	0
2	0.31	1.580	0	0
3	0.18	3.200	0	0
4	0.23	3.776	68	12
5A	0.05	4.376	88	4
5B	0.03	4.376	124	0
5C	0.10	4.376	124	8

Figure 6-7 AP1000 PWR 2D core: radial slice at the axial midplane
(geometry and fuel specifications shown)

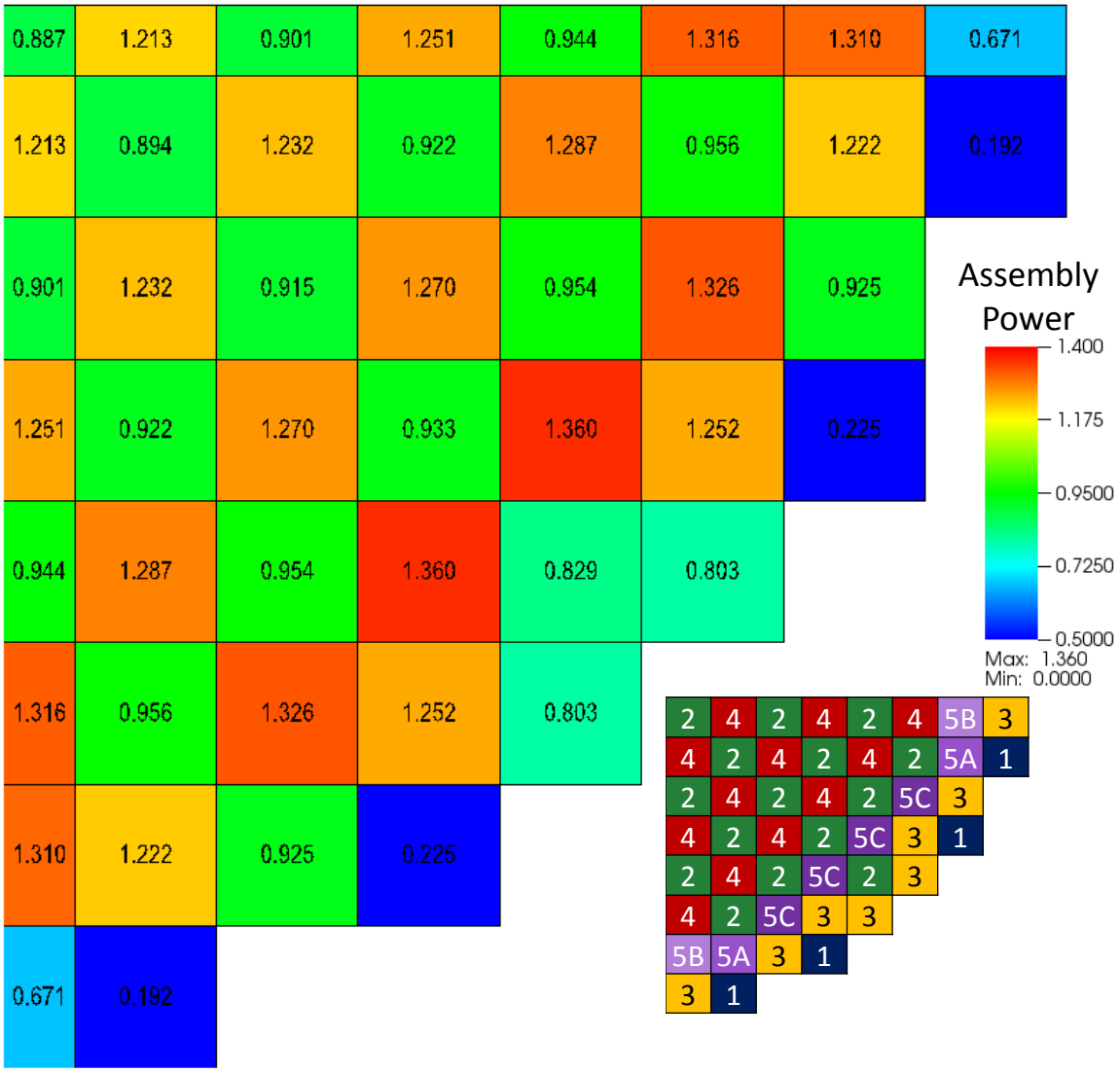

Figure 6-8 AP1000 PWR 2D core assembly power (KENO)

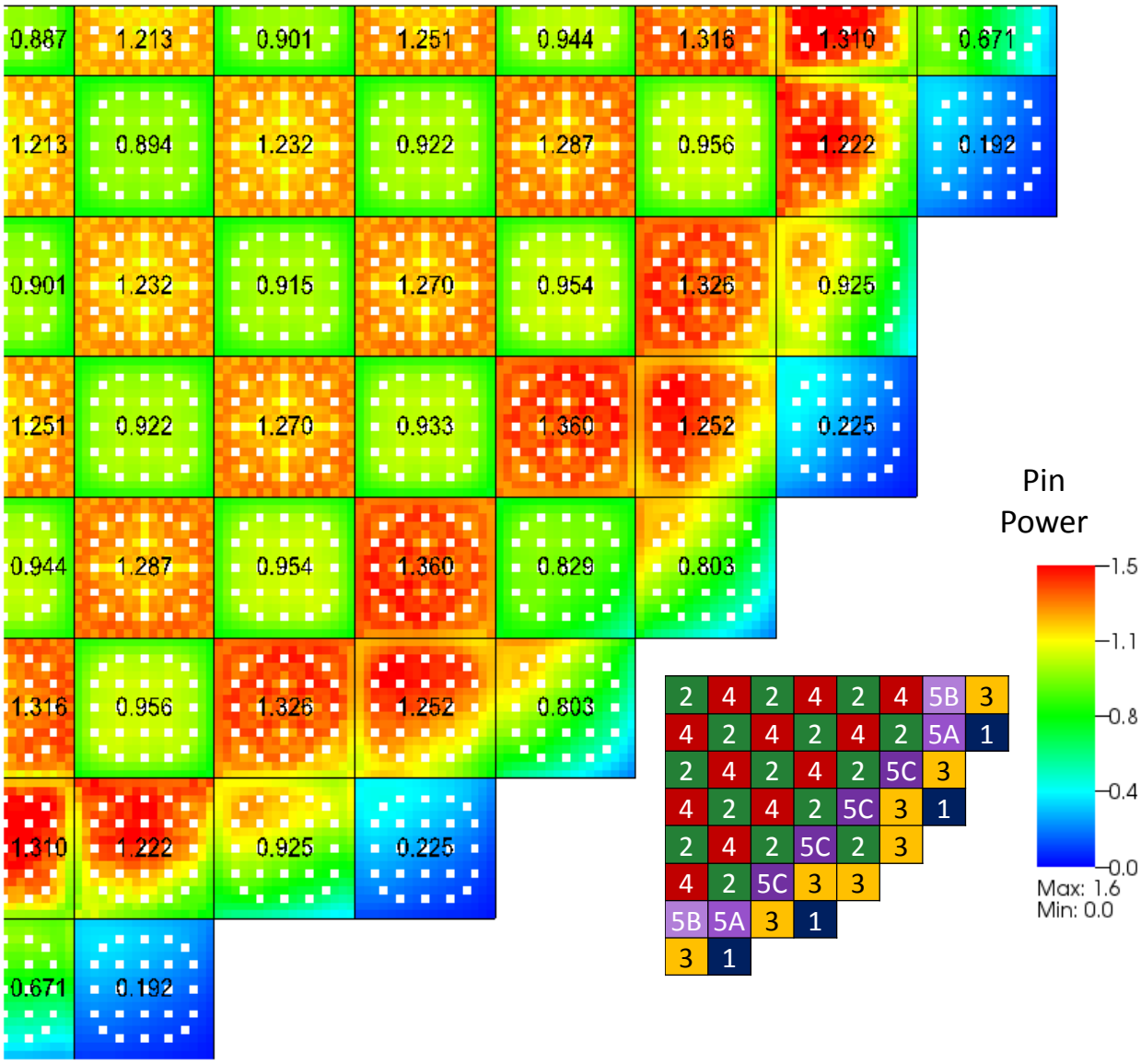

Figure 6-9 AP1000 PWR 2D core pin power (KENO)

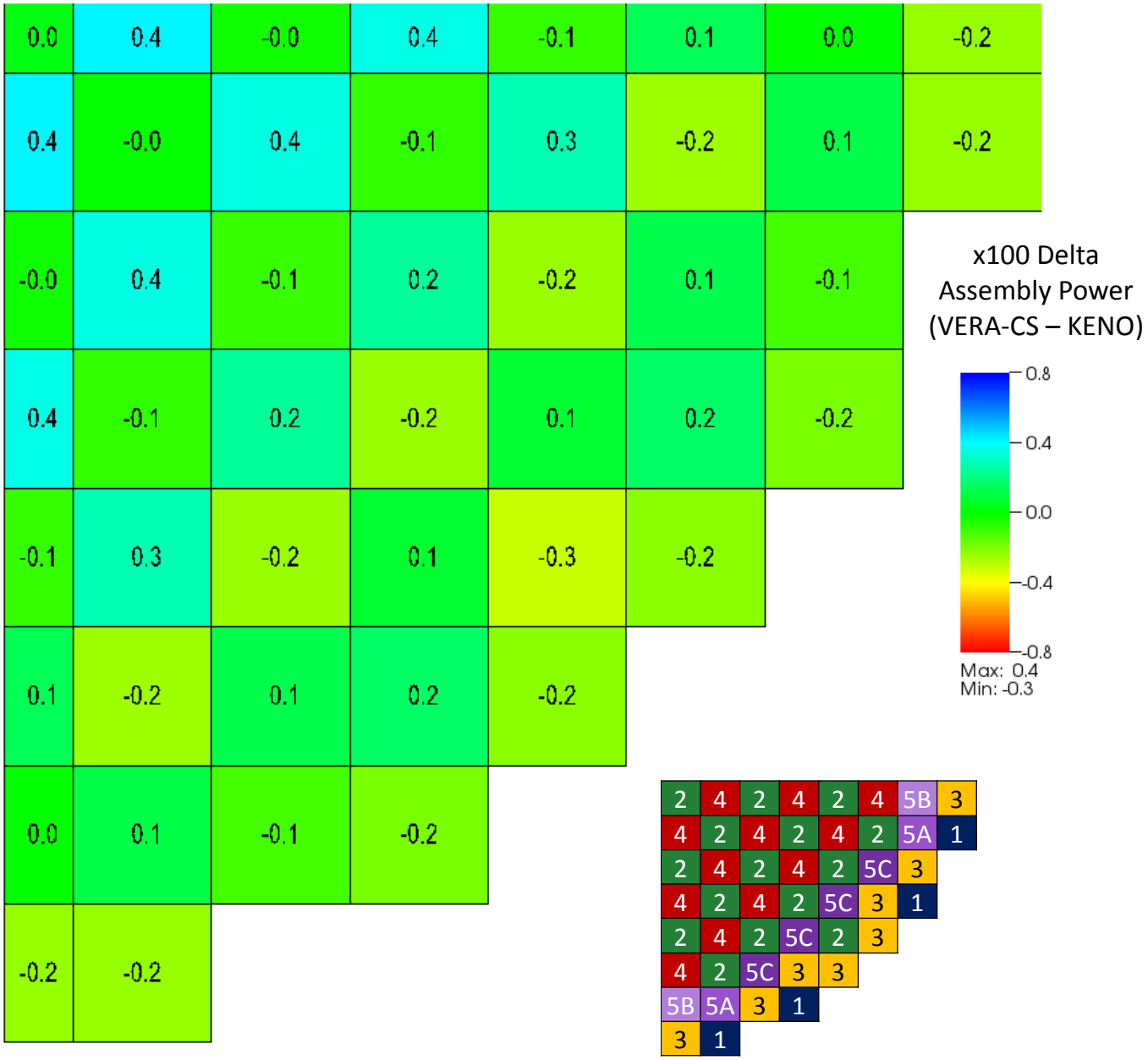

Figure 6-10 AP1000 PWR 2D core delta assembly power (VERA-CS vs. KENO)

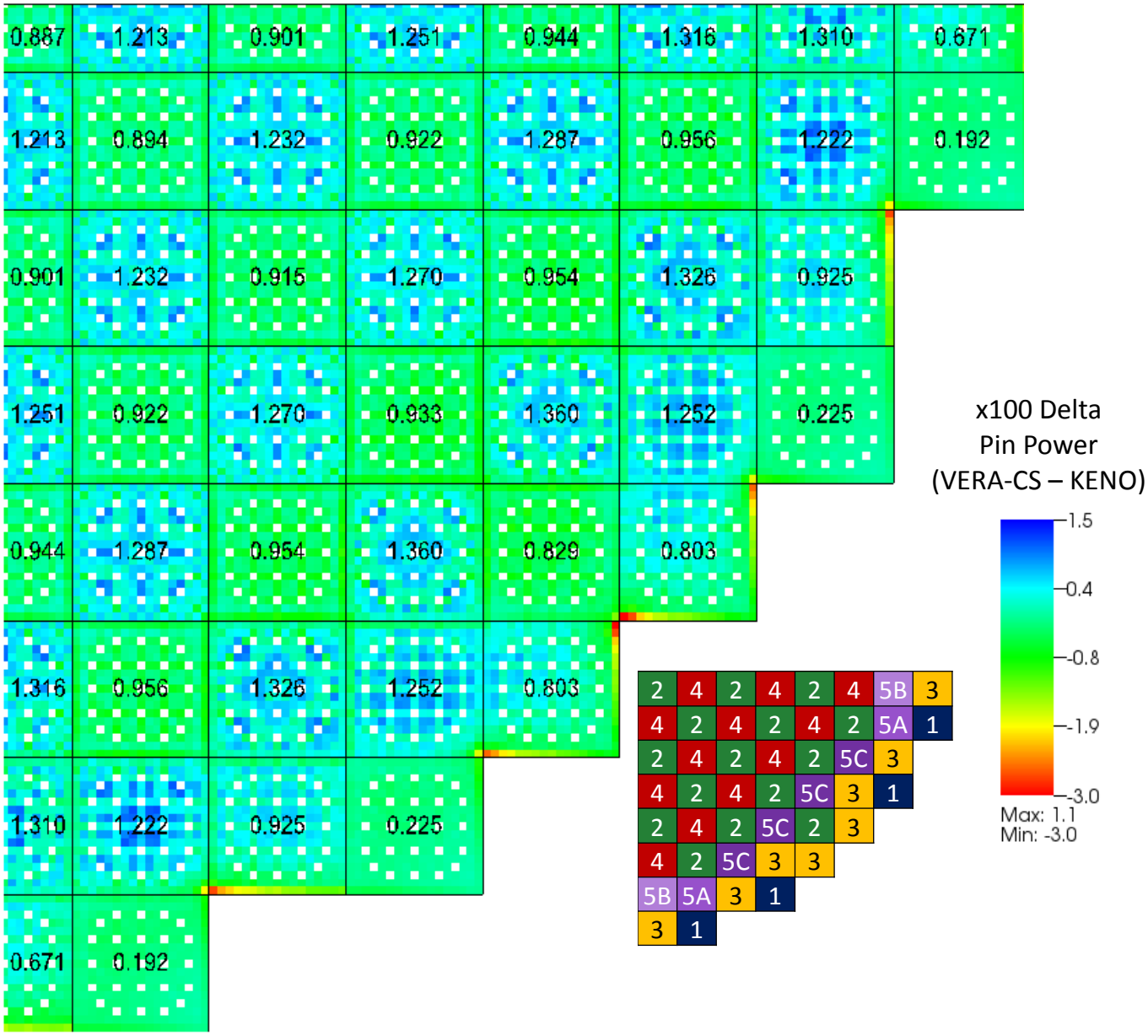

Figure 6-11 AP1000 PWR 2D core pin power comparison

(delta pin power (VERA-CS vs. KENO) – colors
assembly power (KENO)– numbers)

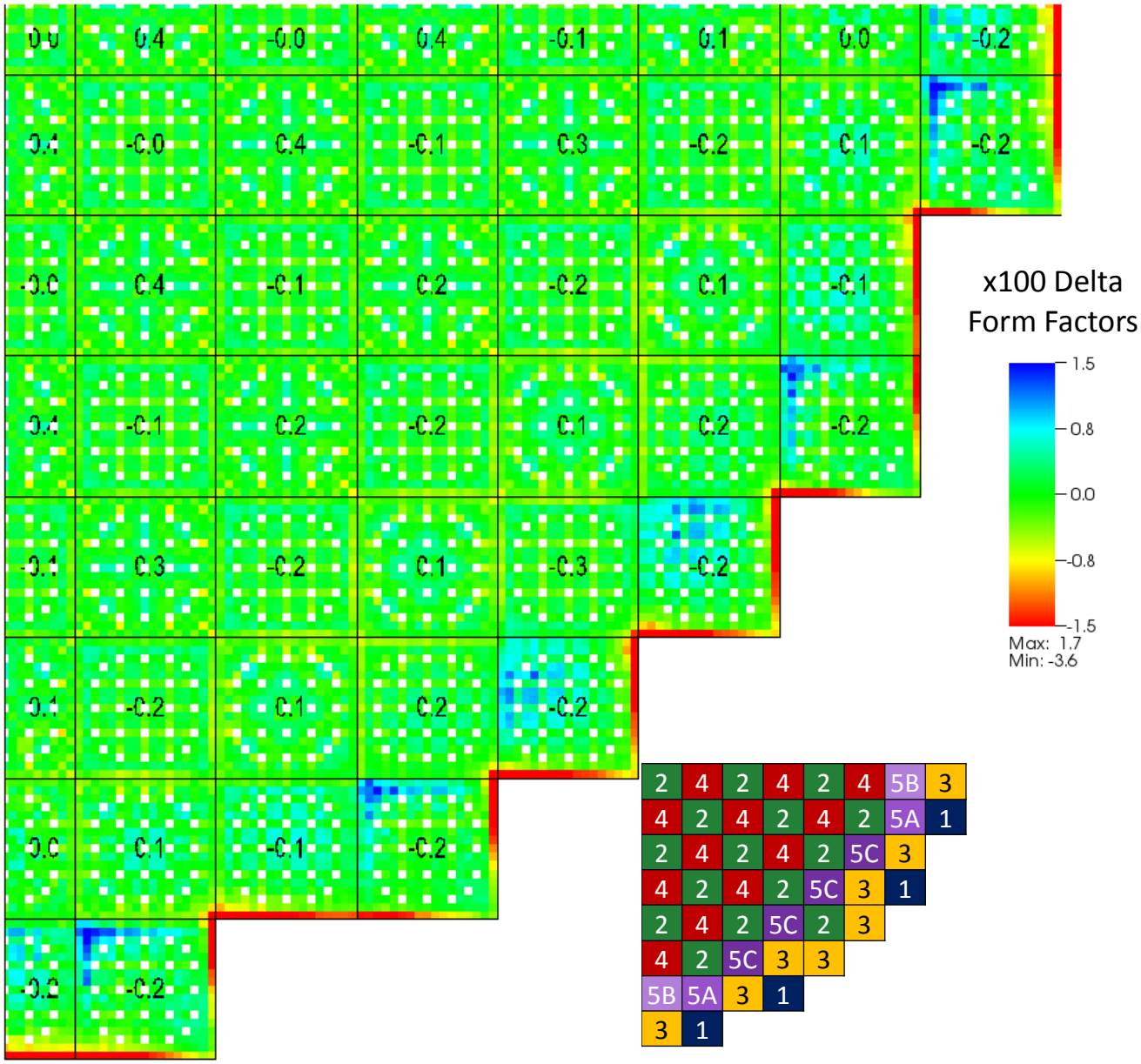

Figure 6-12 AP1000 PWR 2D core form factor comparison

(delta form factors (VERA-CS vs. KENO) - colors
delta assembly power (VERA-CS vs. KENO) – numbers)

6.4 3D Single Assembly

As the geometry of the model was being extended to 3D, the impact of introducing various axial components and heterogeneities to the fuel stack has been investigated. The impact of adding increased complexity to the **AP1000** PWR fuel stack has been assessed with a set of calculations for Reg. 3 fuel with results summarized in Table 6-4 and Figure 6-13 through Figure 6-15. More details on the KENO simulations supporting this analysis can be found in Section A.4.

First, a simulation with all the active fuel axial layers (e.g. 8" lower-enriched top and bottom blankets with 152" full-enrichment central region) but no grids and no structure above and below the active fuel has been performed ("No grids" in Table 6-4 with axial power profile given in Figure 6-13). Then, the grids present within the active fuel height, e.g. 8 mixing vane (MV) grids plus 4, shorter, flow mix grids (IFM), have been introduced ("With Grids" in Table 6-4, axial power profile in Figure 6-14). Finally, all the fuel structure above and below the fuel active height has been added to the simulation ("Entire stack in Table 6-4, axial power profile in Figure 6-15).

As the results show, there is no significant deterioration in the reactivity agreement prediction from VERA-CS vs. KENO going from 2D to 3D geometry, including addition of the grids and the top/bottom structure of the fuel stack. Remarkably, the delta eigenvalue is below 30 pcm as reported in Table 6-4.

The power distribution agreement is also overall very satisfactory, with 3D RMS <~0.5% throughout the 3D fuel assembly geometry. Deterioration in the VERA-CS power prediction in the axial levels containing spacer grids is apparent, more marked in the shorter IFM (see Figure 6-14 and Figure 6-15). This is mostly the result of differences in the transport methods and approximations underlying the SP_N formulation.

The summary results for all the fuel regions of the **AP1000** PWR first core are summarized in Table 6-5. As already noted, there is no apparent deterioration in the eigenvalue prediction from VERA-CS vs. KENO going from 2D to 3D geometries. Note that the axial asymmetries in the WABA design, which is optimized for HFP operation, cause an unphysical top-skewed power distribution for Reg. 4 and 5A/5C HZP unrodded simulations (see axial power profile comparisons for Reg. 4, 5A and 5C in Figure 6-16 through Figure 6-18, and compare with Reg. 5B in Figure 6-19, which does not have WABA). The associated power distribution comparison is thus only partially relevant, and simulations at conditions more representative of actual plant operation will need to be performed in this regard; one such simulation is reported in the next Section ("3D 3x3 Multi-Assembly"). It is however noted that the power distribution from VERA-CS, even for the very top-skewed power distribution cases, still compares very well with KENO (see percent differences in the high-power top nodes in Figure 6-16 through Figure 6-18).

In summary, the remarkable agreement in reactivity and power prediction of VERA reported for 2D geometries does not deteriorate significantly when considering the entire fuel axial stack, except for the local power at the grid spacer locations.

Table 6-4 3D assembly results (Reg. 3)

	KENO	VERA-CS					
Case	K_{eff} (+/-1 pcm)	ΔK_{eff} (pcm)	ΔAO (%)	RMS ΔP Node (%)	Max ΔP Node (%)	RMS ΔP Cell (%)	Max ΔP Cell (%)
No grids	1.00118	27	-0.13	0.14	0.20	0.25	0.79
With Grids	1.00263	21	-0.25	0.17	1.35	0.42	1.72
Entire Stack	1.00265	15	-0.40	0.48	1.50	0.52	1.95

Note: Soluble boron concentration assumed to yield approximate criticality. The "Node" power is the radially-averaged power for 49 axial layers within the 426-cm fuel active height considered for the comparison. The "Cell" power is the pin-wise power for each fuel rod in the 49 axial layers considered. The "RMS Node" is calculated based on the root mean square of the delta nodal power (VERA-KENO)×100 over all the axial layers. Max Node is the maximum absolute delta multiplied by 100 over all the axial layers. The "RMS Cell" is calculated based on the root mean square delta pin power (VERA-KENO)×100 over all the fuel rod locations and axial layers. Max Cell is the maximum absolute delta multiplied by 100 over all the fuel rod locations and axial layers.

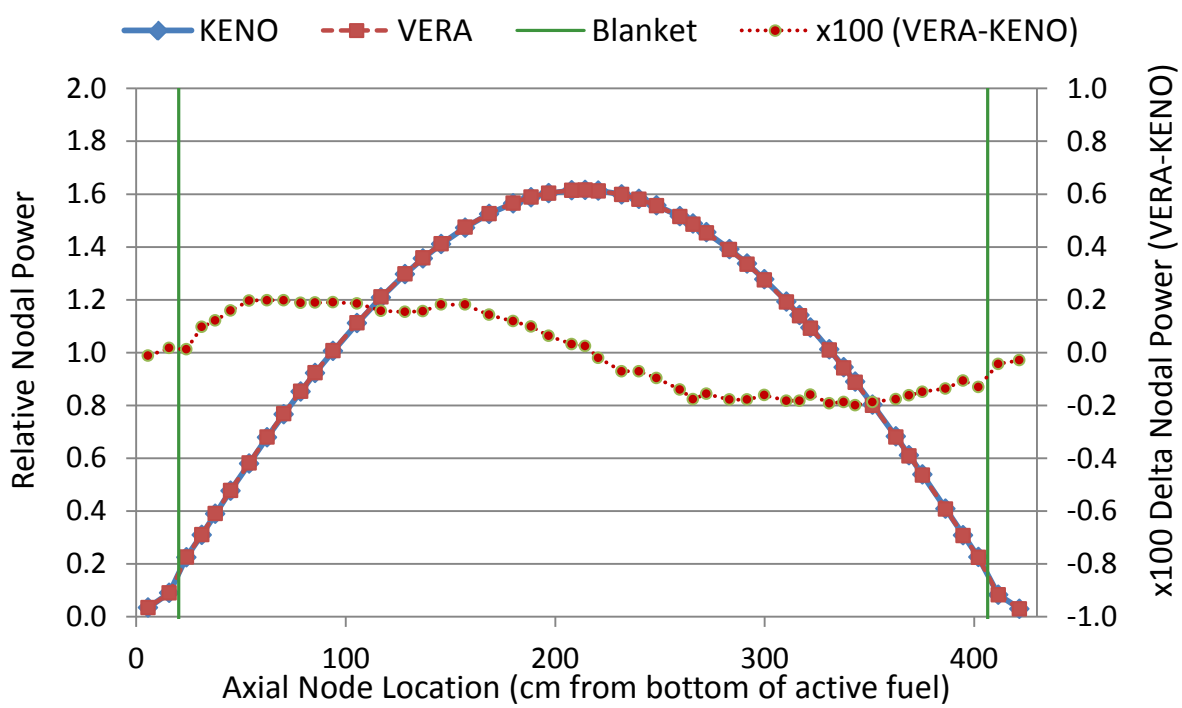

Figure 6-13 Reg. 3 assembly power distribution– no grids, void boundary conditions

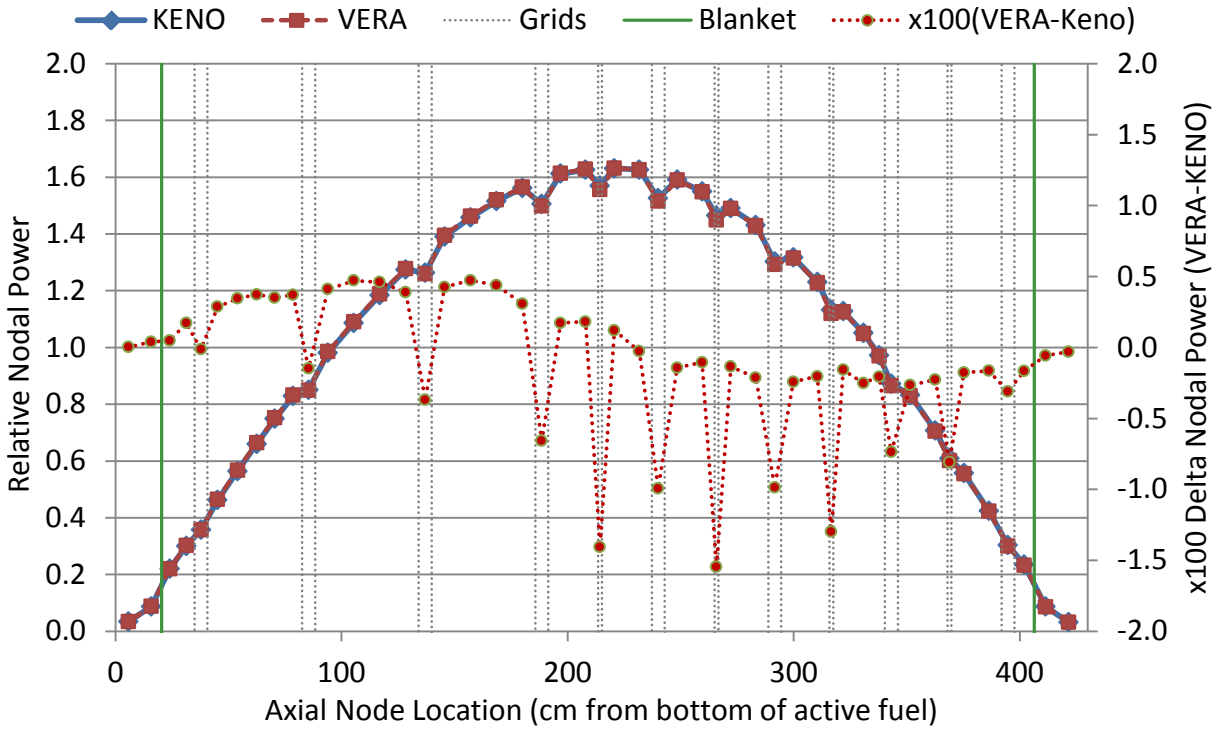

Figure 6-14 Reg. 3 assembly power distribution– w/ grids, void boundary conditions

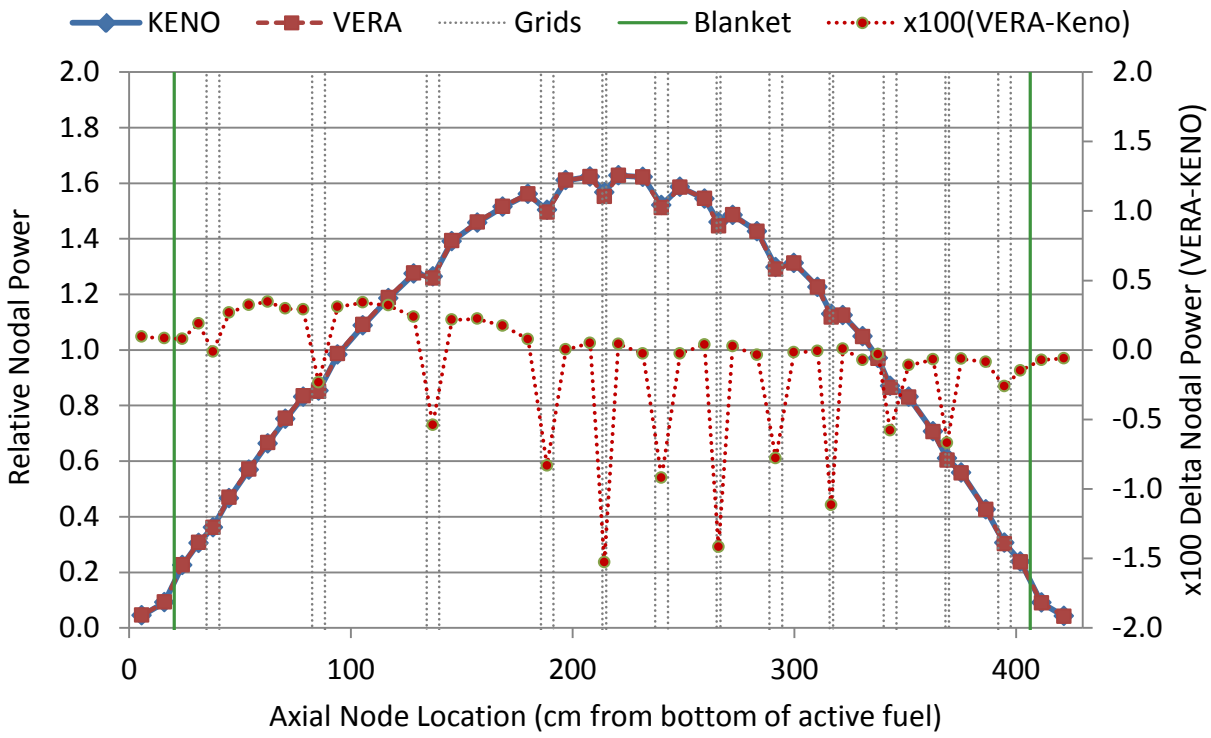

Figure 6-15 Reg. 3 assembly power distribution– entire fuel stack and structure

Table 6-5 3 D assembly summary results for all fuel regions

Reg.	K_{eff} (+/-1 pcm)	AO (%)	ΔK_{eff} (pcm)	Δ AO (%)	RMS ΔP Pin (%)	RMS ΔP Cell (%)	ΔP Hot Spot (%)
1	0.90409	-2.9	-211	-0.4	0.13	0.47	0.00
2	1.00224	-0.9	-81	-0.2	0.16	0.35	0.19
3	1.00265	1.5	52	-0.3	0.17	0.46	-0.03
4	1.00184	80.9	18	-0.5	0.20	1.29	-0.38
5A	1.00289	53.4	20	-0.8	0.22	1.13	-1.08
5B	1.00317	-0.5	-40	-0.4	0.23	0.54	0.91
5C	1.00225	93.6	-37	-0.2	0.22	1.12	0.97

Note: Soluble boron concentration to yield approximate criticality assumed for the various cases.

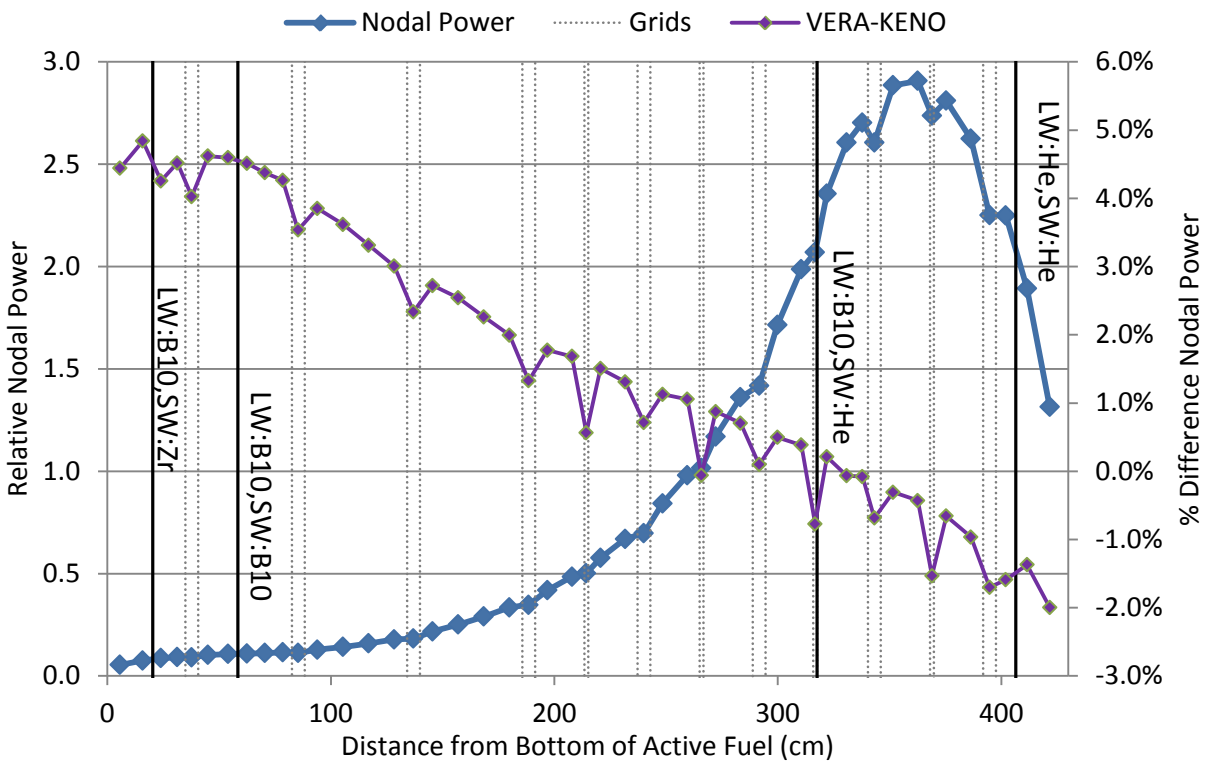

Figure 6-16 Assembly power distribution for Reg. 4 fuel stack
(68 IFBA plus 8 Long WABA and 4 Short WABA)

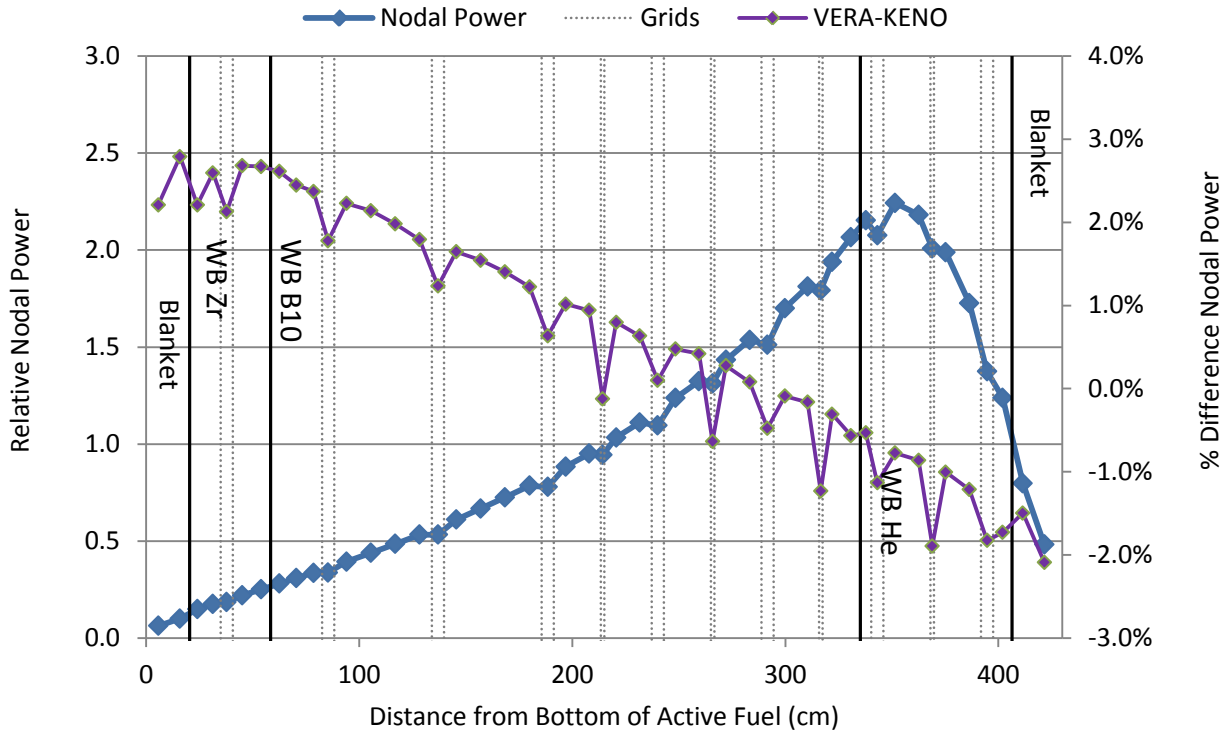

Figure 6-17 Assembly power distribution for Reg. 5A fuel stack
(124 IFBA plus 4 WABA)

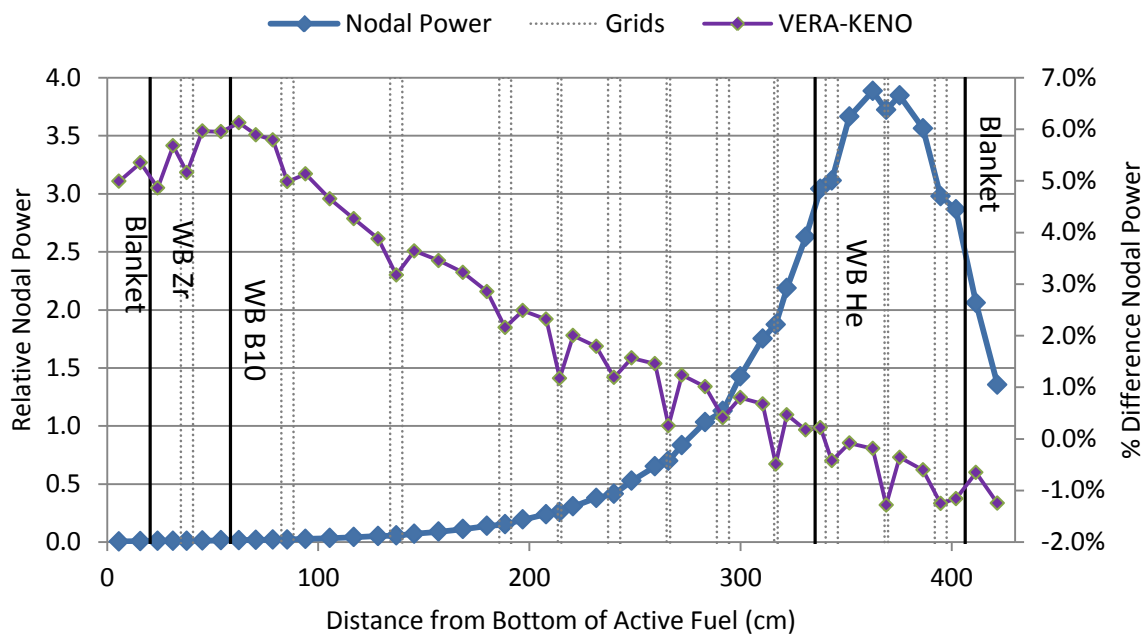

Figure 6-18 Assembly power distribution for Reg. 5C fuel stack
(124 IFBA plus 8 WABA)

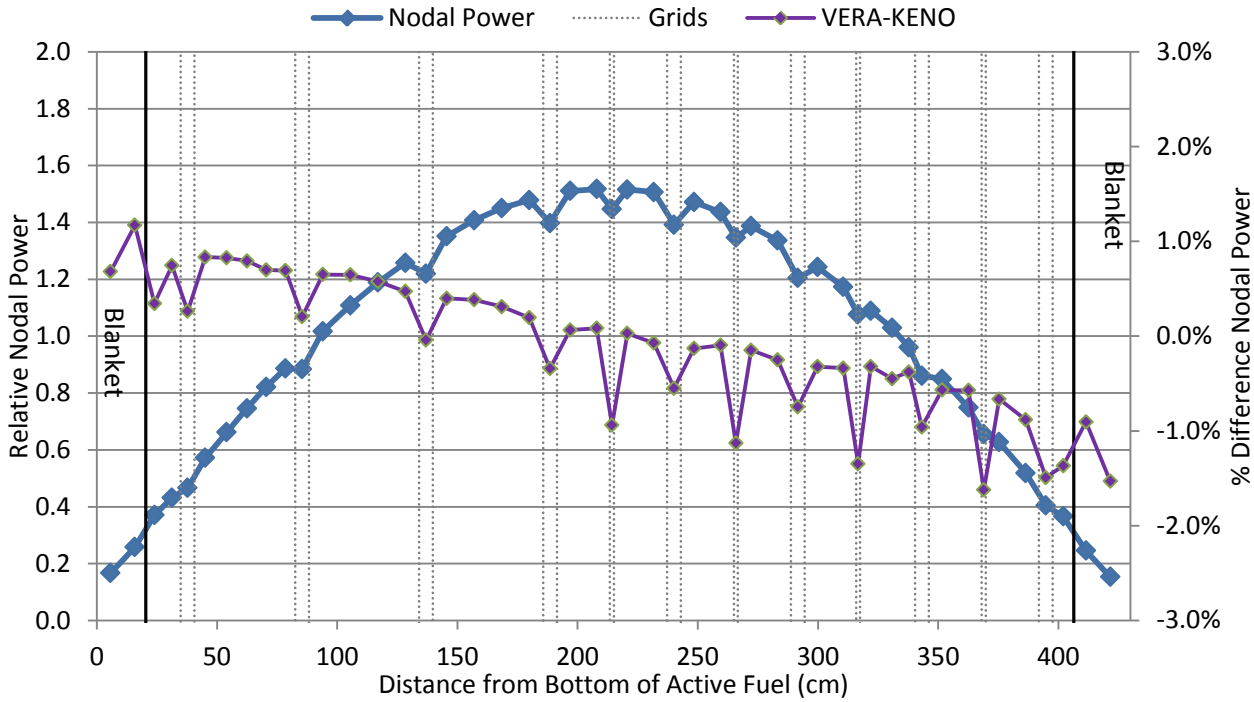

Figure 6-19 Assembly power distribution for Reg. 5B fuel stack

(124 IFBA, no WABA)

6.5 3D Multi-Assemby

The results reported in this section refer to a 3×3 multi-assembly simulation, namely the 3D counterpart of the 2D multi-lattice simulation reported in Section 6.2. The radial fuel map for this simulation is shown in Figure 6-20. A "black" Ag-In-Cd control rod bank is inserted in the top portion of the central assembly to counterbalance the effect of the part-length WABA in Reg. 4 fuel and the lack of feedbacks at HZP. In this way an approximately neutral axial offset is obtained. This simulation resembles to some extent the operation of the AO bank, which is inserted in the top of the AP1000 PWR core and keeps the AO within the prescribed limits during the reactor operation.

As for the previous simulations reported, the eigenvalue prediction from VERA-CS and KENO is in excellent agreement also for a 3D multi-assembly simulation with partial inserted control rods.

The agreement in the power distribution is also remarkable, with an RMS of less than 1% calculated on 49 axial levels and 3x3x264 fuel radial positions. Figure 6-21 shows the axial power profile together with the axial fuel and WABA transitions (vertical lines), as well as the percent difference in nodal power for VERA-CS vs. KENO. The difference in the peak node power is less than 1%, and the accuracy in the power profile predicted by VERA-CS vs. KENO is only mildly affected by the presence of a partial inserted control rod. A 3D plot of the power (KENO) and delta power (VERA-KENO) is given in Figure 6-22, together with the various fuel axial transitions and grid position in the stack. Note the power suppression in the top part of

the central assembly (Reg.2) attributed to the control rod insertion, which further skews the power to the adjacent Reg. 4 fuel and downward from the control rod (see left hand side of Figure 6-22). The discrepancy in the power prediction at the grids, IFM especially, is visible in the middle and right hand side plots of Figure 6-22. Also the larger percent difference in delta power in the bottom of the stack is noticeable, which is likely the result of a slight axial tilt in the power profile between VERA-CS and KENO (see also the trend in delta power in Figure 6-21).

In summary, despite some discrepancy in the power prediction, VERA-CS compares very well against KENO also for this challenging simulation.

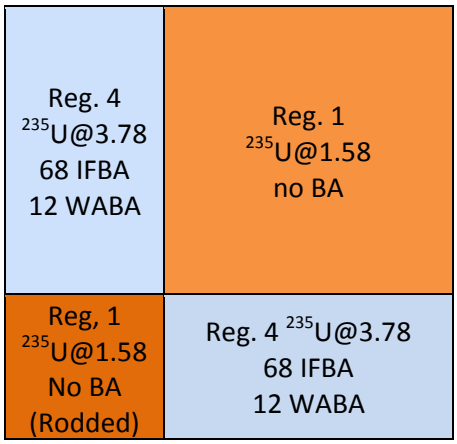

Figure 6-20 Loading Pattern for Multi-Lattice Simulations

(partial control rod Insertion in central position, Ag-In-Cd "black" bank, 1/4th geometry shown)

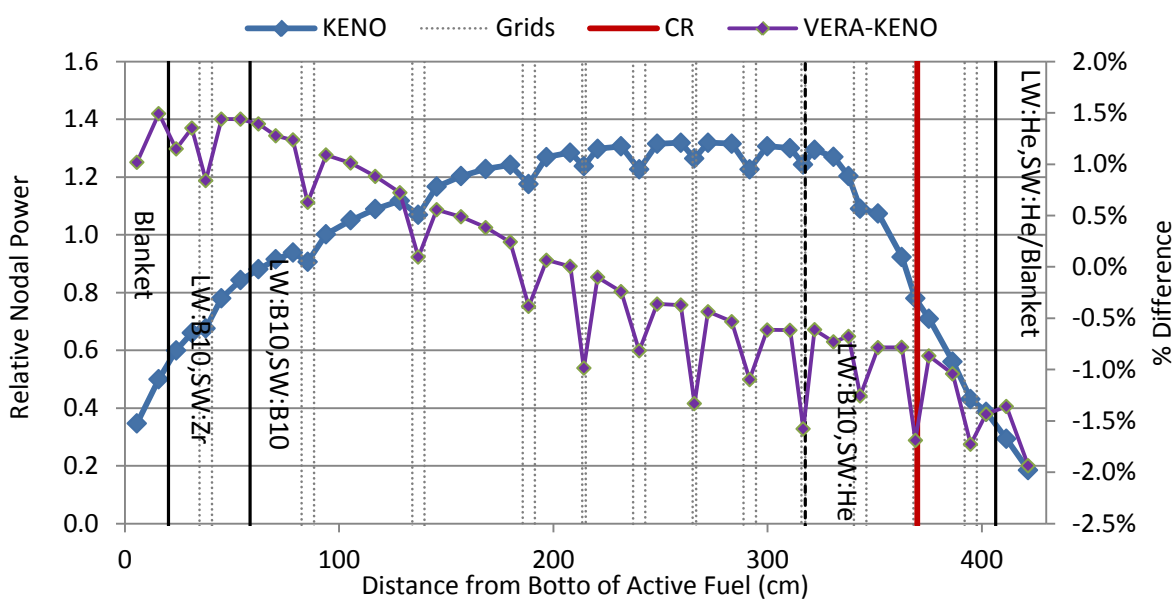

Figure 6-21 3D 3x3 assemblies axial power distribution with partial insertion of Ag-In-Cd CR

(Reg. 2 and Reg. 4 fuel, CR in Reg. 2 central assembly)

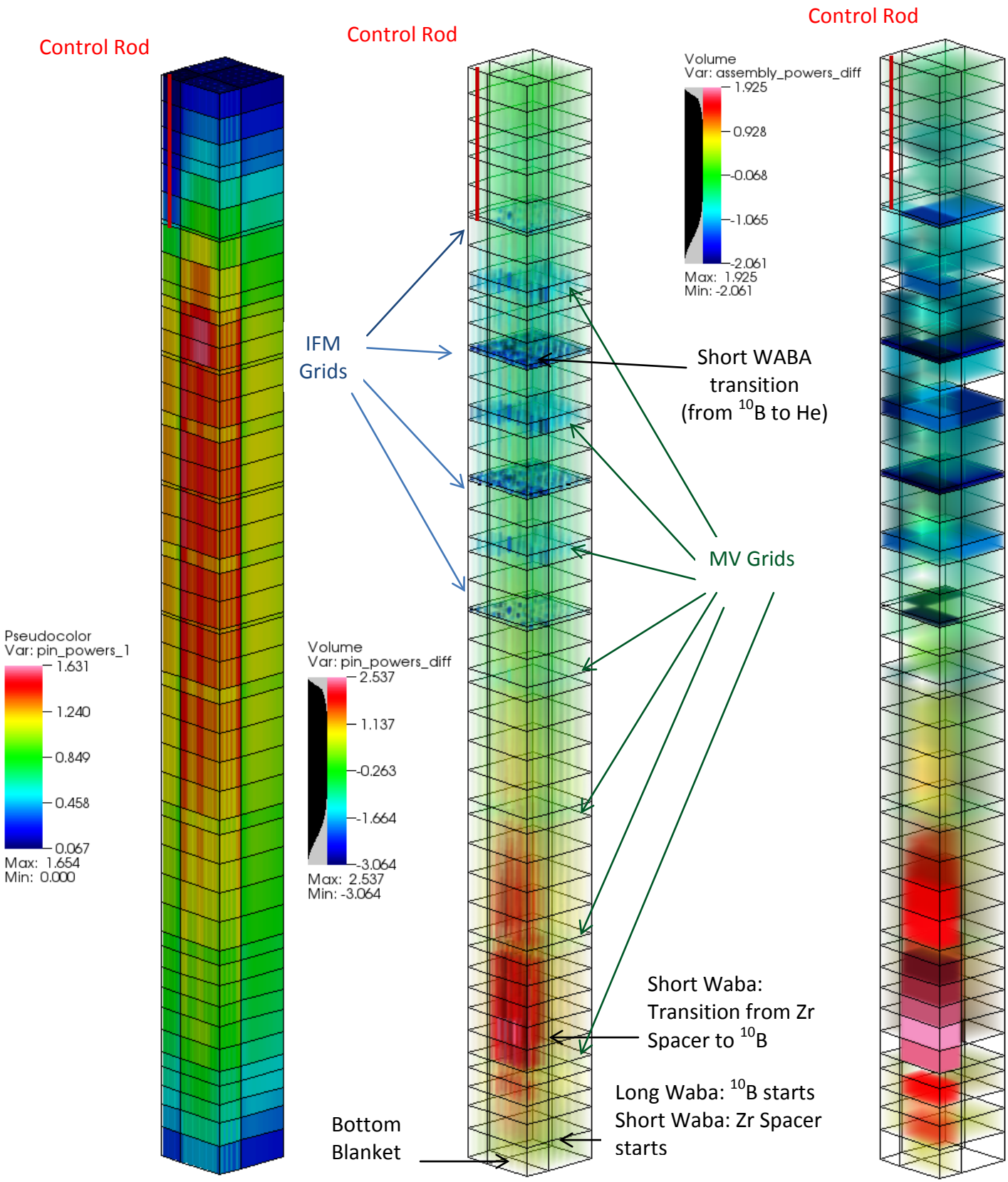

Figure 6-22 3D 3x3 power (left), delta power VERA-KENO (by cell: middle, by axial node: right)

(Reg. 2 and Reg. 4 fuel, partial inserted CR in Reg. 2 central assembly)

Table 6-6 3D 3x3 assembly summary results

KENO		VERA-CS					
K_{eff} (+/-1 pcm)	AO (%)	ΔK_{eff} (pcm)	Δ AO (%)	RMS/Max ΔP Node (%)	RMS/Max ΔP Pin (%)	RMS/Max ΔP Cell (%)	ΔP Hot Spot (%)
1.00119	2.4	-18	-0.7	0.9/2.1	0.3/0.8	0.9/3.1	-0.3

6.6 Zero Power Physics Tests

This section reports the results of the **AP1000** PWR zero power physics tests (ZPPTs). In particular, the HZP critical boron concentration for the plant startup, the rod worth for the various banks, the differential boron worth and the temperature reactivity coefficients (ITC, MTC and DTC) have been calculated with VERA-CS and KENO. Section A.6 and APPENDIX D contain more details on the KENO simulations supporting the ZPPT analysis.

The 3D quarter-core KENO model employed for these calculations is illustrated in Figure 6-24. The complexity of the core design, and in the modeling, can be appreciated from this figure. The VERA-CS **AP1000** PWR 3D core model is consistent with the KENO model, except for the reflector. Namely, a 1-in baffle stainless steel reflector has been assumed in VERA-CS. A more complex reflector geometry, closer to the actual **AP1000** PWR reflector, has been modeled in KENO due to the greater geometrical flexibility allowed by the code. The reactivity bias coming from the difference in the reflector models calculated using KENO is only 9 pcm (see APPENDIX B). Given the small magnitude of this bias, together with the fact that the impact of the different reflector model is limited primarily to the outer assemblies, it is acceptable to use the simplified reflector model adopted in VERA-CS for the calculations performed here, i.e. HZP critical boron concentration and rod worth.

The HZP All-Rods-Out critical boron concentration predicted by VERA-CS for the **AP1000** reactor start-up is 1310 ppm natural boron, a difference of only -3 ppm compared to the 1313 ppm predicted by KENO. The difference in boron worth is 0.2 pcm/ppm. These values are reported in Table 6-7. The critical boron predictions are derived from the eigenvalue predictions at the 1321 ppm tentative HZP critical soluble boron concentration assumed, using the boron worth prediction to compensate the excess reactivity calculated by each code from criticality. A reactivity bias of -120 pcm has also been applied to account for the impact of thermal expansion since both VERA and KENO models are at cold temperatures. This bias has been determined using the Westinghouse in-house core physics package. In addition, a -26 pcm reactivity bias has been applied to account for the presence of the instrumented thimbles in the AP1000 PWR core (see Section A.6). This bias has been calculated using KENO.

The Doppler, Moderator and Isothermal Temperature Coefficients, DTC, MTC and ITC, are respectively within 0.2, 0.4 and 0.6 pcm/F, with VERA predicting more negative values than KENO. These results are displayed in Table 6-8 with more details on these simulations given in

APPENDIX D. The temperature reactivity coefficient simulations is an area recommended for further investigation since the differences observed, while small, are not insignificant.

The control rod worth results from VERA-CS and KENO are reported in Table 6-9, with differences depicted in Figure 6-23. The rod worth prediction from VERA-CS is in outstanding agreement with KENO for all control banks, resulting in a delta rod worth RMS of 4 pcm (0.8%). The maximum rod worth difference is only 9 pcm, and 2.1% in terms of percentage of the rod worth. Both gray (tungsten) and black (Ag-In-Cd) banks rod worth predictions are in excellent agreement.

The HZP critical boron concentration and rod worth predicted by VERA-CS for the **AP1000** PWR first core are consistent with the predictions from the Westinghouse in-house core physics package, which reinforces the confidence in a close agreement with the measured values as the first **AP1000** reactors will come on-line.

Table 6-7 HZP Reactivity Results

	KENO	VERA	VERA-KENO
k_{eff} at 1321 ppm	**1.00066** ± 1 pcm	**1.00033**	**-33 pcm** ± 1 pcm
Boron Worth (pcm/ppm)	**-9.6 ± 0.08**	**-9.4**	**+0.2**
ΔK w/ Thermal Expansion	-120 pcm	-120 pcm	
ΔK w/ Instrumented Thimbles	-26 pcm	-26 pcm	
Startup critical boron (ppm)	**1313**	**1310**	**-3 ppm**

Table 6-8 Temperature Reactivity Coefficient Results

	KENO	VERA	VERA-KENO
Doppler Temperature Coefficient (DTC) pcm/F	-1.54 ± 0.03	-1.72	-0.18
Moderator Temperature Coefficient (MTC) pcm/F	-1.12 ± 0.04	-1.50	-0.38
Isothermal Temperature Coefficient (ITC) pcm/F	**-2.66 ± 0.05**	**-3.22**	**-0.56**

Table 6-9 AP1000 HZP Control Bank Worth Results

		KENO	VERA-CS	
Bank	**Material**	**Worth (pcm) ± 2 pcm**	**ΔWorth (pcm)**	**ΔWorth (%)**
MA	Tungsten	258	-1	-0.5
MB	Tungsten	217	-5	-2.1
MC	Tungsten	188	-2	-1.1
MD	Tungsten	234	0	0.0
M1	Ag-In-Cd	651	-4	-0.6
M2	Ag-In-Cd	887	3	0.4
AO	Ag-In-Cd	1635	-4	-0.3
S1	Ag-In-Cd	1079	0	0.0
S2	Ag-In-Cd	1096	-9	-0.8
S3	Ag-In-Cd	1124	0	0.0
S4	Ag-In-Cd	580	-3	-0.4
		RMS	**4**	**0.8**
		Max	**9**	**2.1**

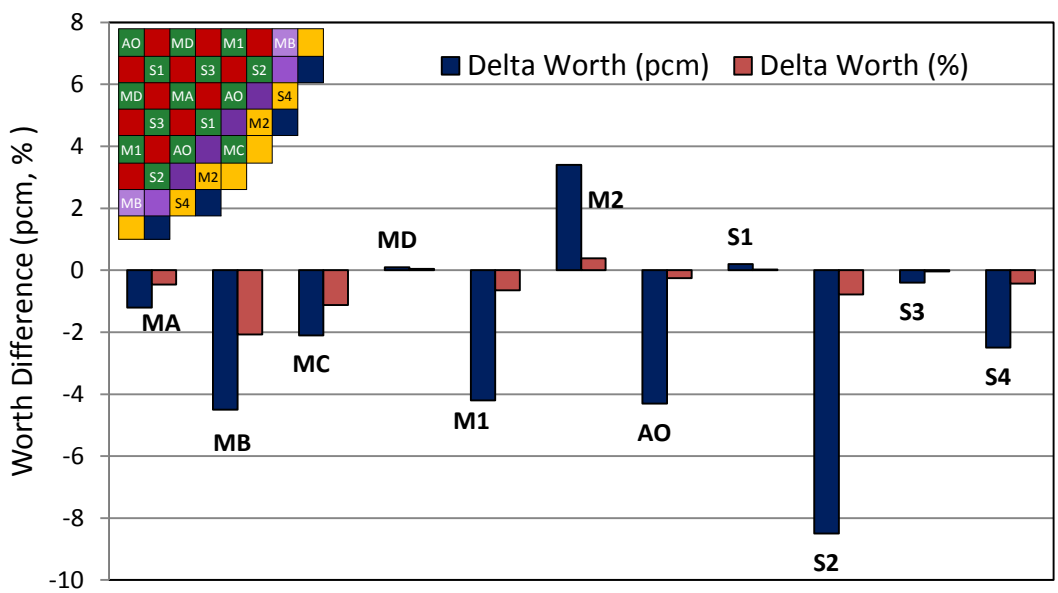

Figure 6-23 Delta in bank worth (in pcm and %) for VERA vs. KENO

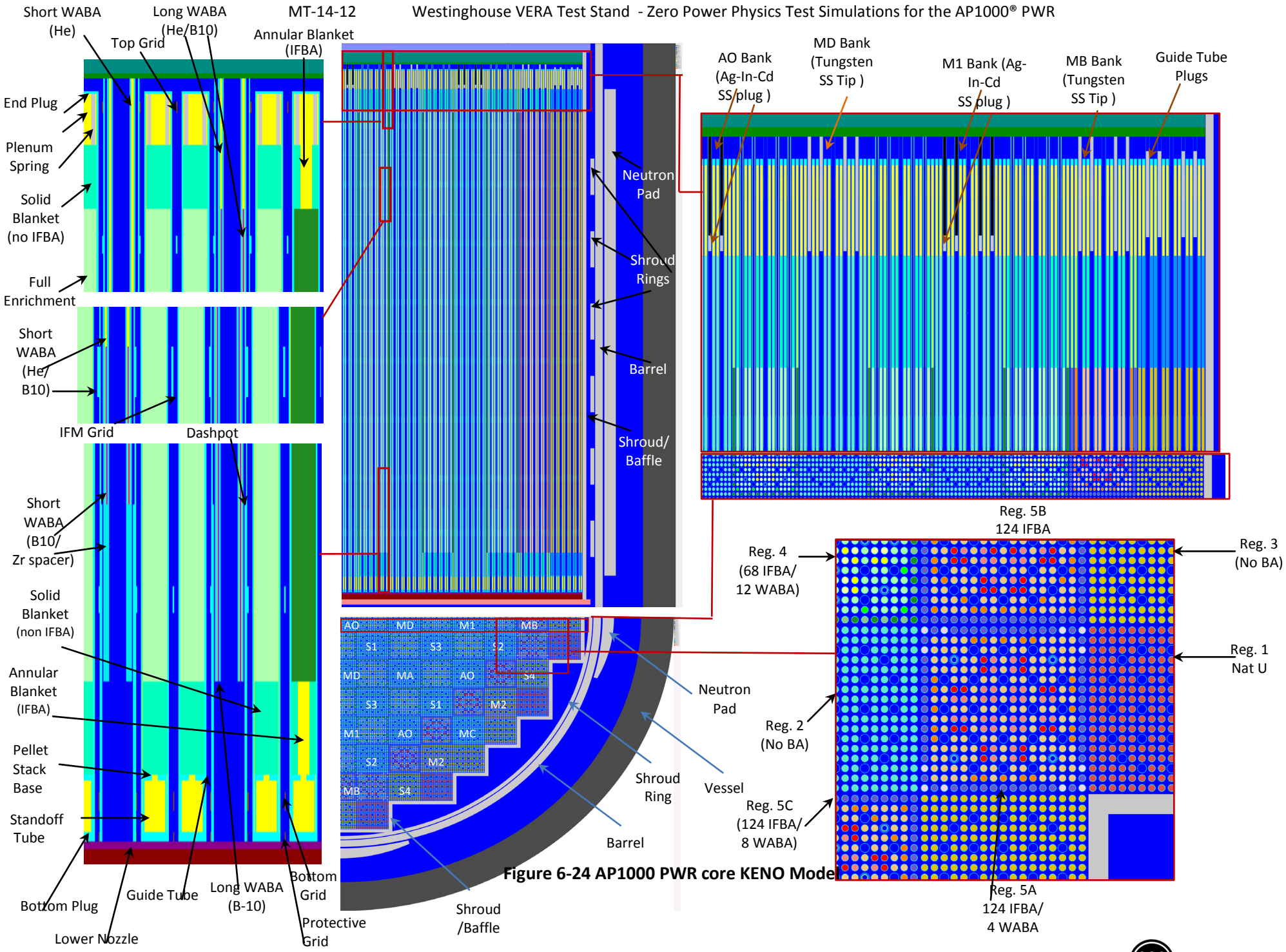

Figure 6-24 AP1000 PWR core KENO Model

7 COMPUTATIONAL REQUIREMENTS

A summary of the computer resources required for performing the VERA-CS and KENO simulations reported is given in Table 7-1. All VERA-CS calculations supporting the **AP1000** PWR core ZPPTs have been performed on the Westinghouse compute cluster. The KENO simulations have been performed on the INL's HPC Fission supercomputer.

As discussed, the VERA-CS calculations rely on the SP_N solver and namely SP_5 with P_3 scattering in 23 energy groups. Using these options result in relatively low computational resources required for 2D simulations: ~2 min on 12 cores, or ~0.4 core hours, for a 3x3 multi-lattice, ~5 min on 144 cores, or ~13 core hours, for a core radial slice with reflector. As discussed in the previous section, the results show excellent agreement in reactivity and power distribution with KENO, which obviously requires much larger computational resources (3,000 core hours for a 3x3 and nearly 50,000 core hours for the 2D core) but relies on fundamentally different and more general energy and spatial treatments.

3D simulations with VERA are significantly more computationally demanding, especially if fine axial meshes are employed, as it is required to obtain accurate 3D power distributions: a 3D assembly with fine axial mesh structure (~500 axial meshes) results in ~ 200 times the core hours of the corresponding lattice, the 3x3 assembly takes ~ 500 times the core hours of a 3x3 lattice and a 3D core with fine axial meshes (~250 axial layers) takes ~300 times the number of core hours of the 2D core simulation. Furthermore, the memory requirement for 3D simulations becomes particularly onerous: 3D core simulations with fine axial meshes require an amount of memory beyond that available on mid-size industry cluster. The computational times and memory requirements compound for coupled hot-full-power calculations; this makes core cycle depletion calculations with the current VERA-CS impossible or impractical.

On the other hand, 3D HZP eigenvalue calculations, including rod worth calculations, can rely on coarser axial mesh[f]. This approach enabled to perform ZPPT calculations with VERA using the computational resources available on the Westinghouse compute cluster, resulting in a wall-time of ~1.5 h on 320 cores. The resulting VERA predictions are in excellent agreement with counterpart Monte Carlo calculations, requiring ~50 times the number of core-hours employed by VERA. However, the computational time required by VERA to perform this "single state point" calculation, which does not require criticality search iterations or thermal-hydraulic feedback, is indicative of the impracticality of its use for coupled depletion calculations.

[f] The SP_N calculations presented in this report employed a 2x2 radial mesh per pin with 73 axial meshes used for the ZPPT core calculations, resulting in total 6.0 million computational cells. In 23 energy groups, with 3 degrees of freedom per space-energy location for the SP_5 (see Section 5.1.1), the resulting total number of degrees of freedom for the AP1000 ZPPT cases is over 400 million and the number of nonzero entries in the matrix representing the SP_5 operator exceeds 32 billion. The ~500 core-hours required for these calculations breaks down in ~10% for cross sections generation by XSProc, ~30% for setup operations such as matrix and preconditioner construction, and ~60% was spent in the SP_N eigenvalue calculation. If a fine axial mesh structure with ~270 axial cells is used, then the total number of degrees of freedom is 1.6 billions, with over 100 billion of nonzero entries in the matrix representing the SP_5 operator.

These concerns are confirmed by the runtime performance of ~20hr on ~20,000 cores for 3D core coupled calculation (without depletion) reported in Ref. 47. In order to perform calculations on ~1,000 cores with ~1hr runtime per depletion step (which would translate in a cycle depletion of a couple of days per reload: still impractical for daily reload activities, but acceptable to obtain high-fidelity reference solutions), a ~400 reduction in computational resources is required with respect to those currently utilized by VERA-CS.

It should be noted that the SP_5P_3 solver with 23-energy groups is not the only option available in VERA-CS, and use of a lower SP_N order and/or fewer number of groups to reduce the computation resources is certainly possible. While these options can be further developed and possibly employed in the future for cycle depletion calculations with coupling, the resulting impact on accuracy should be ascertained. At the time of this work the SP_5P_3 option with 23 energy groups appeared the most reliable option for this work and has thus been employed.

Table 7-1 Computer resources used for VERA-CS and KENO AP1000 simulations

	KENO					VERA-CS SP_5P_3 23g				
	Particles (x10^9)	Pin Unc. %	Cores #	Wall Time	Core* hours	Cores #	Cells #	Core* hours	Wall Time	Memory
2D Lattice	1.1	0.02	312	~3.5h	1K	12	324	0.2	~1 min	<96 GB
3x3 Lattice	3	0.04	300	~10h	3K	12	3K	0.4	~2 min	<96 GB
2D Core	25	0.06	300	~6d	43K	144	86K	13	~5 min	<512 GB
3D Assembly	17.5	0.08	240	~3d	17K	64	0.2M	32	30 min	<512 GB
3D 3x3 Assembly	25	~0.1	180	~6d	26K	144	1.5M	96	40 min	<1.2 TB
3D Core (Eigenvalue)	25	0.38	180	6.5d	28K	320	6M	0.5K	100 min	<4 TB
3D Core * (Pin Power)	50	Pow >1 1% Pow <1 4%	180	10.5d	45K	4,096	24M	2.3K	34 min	<32TB

* VERA calculation performed on Titan OLCF since the computational resources required exceed those available on the Westinghouse's VERA compute cluster.

8 USABILITY OF VERA-CS

VERA-CS models are set up through VERAIN, the VERA common input. This has been found intuitive and efficient to model commercial PWR cores with square lattice fuel assemblies. While there are some limitations in the current modeling capabilities, there appears to be no inherent barriers preventing future extension of the current features. The fact that through VERAIN it has been possible to set up the first core of the **AP1000** PWR, which is a fairly complicated design with several advanced features (see Figure 4-1 through Figure 4-8), is an important point of merit for VERA. The IFBA fuel coating is treated with good efficiency with the 1D cross section homogenization procedure prior to the SP_N calculation. Part length WABA inserts are modeled properly. The fuel stack modeling capabilities are in general fairly comprehensive, including the neutronically relevant structure above and below the active fuel.

The VERA "one-step" simulation approach, among other things, favors compactness and flexibility in the input structure. One example is the input structure for the inserts (i.e., WABA, control rods), which are set-up independently from the fuel assembly where they are inserted. Westinghouse has successfully modeled another commercial PWR (a 2-loop core), in addition to the **AP1000** PWR core, using VERA. The resulting modeling effort was quite modest, amounting to a few hours.

In general, the average core designer will find setting up simulations for VERA a relatively easy effort, especially if provided with representative sample input decks.

The main limitations in the current VERA modeling capabilities noted as part of this work are:

- no automatic thermal expansion of fuel and structure from cold to hot conditions
- reflector model limited to a "jagged" (e.g. baffle-like) structure surrounded by water
- no provision for direct assignment of material number densities to a given cell

Thermal expansion is an important phenomenon which impacts reactivity and power distribution[g]. The reactivity bias for the lack of thermal expansion has been calculated here using Westinghouse in-house codes, but a systematic treatment going forward is needed for VERA. The power distribution comparisons presented for VERA vs. KENO are appropriate since both codes adopt a consistent assumption, i.e. cold dimensions; on the other hand, this is not realistic when comparing to measurements, and inappropriate for comparison to typical industrial simulators modeling thermal expansion.

The reflector modeling capability, currently limited to an axially-uniform baffle surrounded by water, leads to some inaccuracies for reflectors with additional or different structure and higher degree axial heterogeneity, as is the case for the **AP1000** PWR. While the impact on reactivity may be minor, the impact on power distribution, especially for the outermost

[g] For instance, the inter-assembly gap typically becomes narrower as a result of thermal expansion, which has a significant impact on the pin power of the peripheral pins of an assembly, especially the corner pin.

peripheral assemblies and pins, can be significant. This is discussed in more detail in APPENDIX B. Notably, for smaller cores, proper reflector modeling capabilities are likely more important.

Materials are specified in VERA with the aid of an HDF5 material composition file, which is essentially a library that is linked through an input card and contains a list of elements (e.g. Zr, B, etc.) and typical mixtures (e.g. Zircaloy, Pyrex etc.) used in LWR cores, together with their isotopic composition and atomic mass. The HDF5 material composition file can also be edited and customized, for instance an **AP1000** PWR-specific file was created to include materials such as Zirlo and IFBA. This is convenient as it allows the user to specify the materials for the various elements (e.g. fuel cladding, inserts etc.) by assigning the material type in the input (e.g. "Zirlo" or "WABA") thus keeping the user input file simple and concise. One drawback is that the HDF5 file is not easy to modify using typical HD5 file editing tools, and an easier way for users to create and/or modify this file would be an asset.

Based on the user's material type specification and using the HDF5 material composition file linked, VERA automatically calculates number densities for the neutronic calculation. This is convenient for typical engineering analysis, and a similar process is used in typical core simulators. However, there is currently no provision in VERA to directly input number densities for a given structure, which is preferable when number densities are pre-assigned or pre-calculated (e.g. benchmarks). For instance for this analysis, number densities generated using Westinghouse in-house codes had been pre-calculated, but could not be directly assigned in VERA as desired to ensure consistency among the models. As a workaround, the HDF5 material composition file had to be manually modified in conjunction with adjusting the material density in the input to approximate the desired isotopic number density, which resulted in a time consuming and error prone activity. It is thus recommended that a provision to directly input number densities be implemented in VERA.

Other limitations in VERA-CS modeling capabilities that might arise as fuel geometries are extended to other arrays than typical square-pitch fuel assemblies have not been encountered here, but should be kept in mind for other potential industrial applications.

In terms of execution, VERA-CS simulations are run via a short shell script launched from the terminal window. This is not unlike other core simulators, including industrial ones. Westinghouse has not found this process particularly challenging, or a priority for improvement.

At the end of a VERA simulation, the resulting eigenvalue and pin power distribution are available in an HDF5 file, while the only ASCII output provided with the SP_N solver is a short log file providing summary information on the execution.

The HDF5 file generated by VERA can be post-processed to extract the relevant information. CASL has developed scripts for the HDF5 file post-processing that can be used to generate "SILO" files for visualization of results and model information with the VisIt visualization tool (Ref. 14). Other utilities have been developed for code to code power distribution comparisons

which can also be used for visualization with VisIt. These scripts have been used for this work and in general were found convenient to use, though additional efforts to systematize this process should be invested in the future.

Furthermore, an ASCII output file with the information characterizing the simulation performed, including the results obtained, and visualization of the model used in the simulation should be provided alongside VERA's execution for immediate interrogation by the user. Verification from the user of the model input to VERA-CS beforehand is particularly important to avoid performing computationally burdensome calculations using the wrong model, beside for QA reasons.

VERA-CS execution through the SP_N solver was found very robust and stable. There have been no instances to report where a calculation failed to converge, or converged to an unphysical result. This is a very positive behavior indicating the maturity of the solver used and the high quality of the software implementation.

There have been instances of failed executions due to lack of enough memory to perform the calculation attempted. For the user determining the amount of needed memory is currently a "trial and error" process. In general, the memory requirements for 3D core calculations are impractical for execution of VERA-CS on a mid-size (~1,000 cores) cluster, as already reported in Section 7.

The user manuals currently supporting VERA-CS are inadequate if not absent. Efforts should be made to systematically document the options available and the methods employed for the various components, especially considering the needs and potential support requests of a wider user community. It should be remarked that for the Westinghouse Test Stand CASL developers have always been available for providing support to the code build, execution, and post-processing.

Some improvements could be made in the code-specific input section of the manual, especially given the current lack of detailed information explaining the various calculation options available for the codes. In this area the importance of providing appropriate defaults as well as specific examples cannot be overemphasized.

It should also be pointed out that there is a significant validation effort entailed in using VERA-CS, especially at this stage of the development as confidence in its prediction capabilities is being built. In particular, for this work, the validation of the VERA-CS results with independent KENO Monte Carlo simulations has been fundamental to enhance the confidence in the results obtained, even more so due to the absence of measurements for the simulations performed.[h]

[h] It is worthwhile noting that CASL is developing its own Monte Carlo capability with the SHIFT code, which might facilitate future validation efforts due to massively parallel execution capabilities and reliance on the practicality of the VERA common input for model setup. The application of SHIFT to the **AP1000 PWR core** simulations is ongoing and will be documented in the future.

In summary, at the current state, VERA-CS has been found convenient to use by the average engineer after an initial, reasonably short, learning period and with support from CASL to overcome contingent issues. Improvements in terms of features, documentation, build process, and I/O (listed in decreasing order of priority, as perceived by the authors) could certainly be made but due to ongoing developments within constrained resources, these improvements should not be considered urgent as they have not been an impediment to performing simulations for the Test Stand. Priority should be given to implement thermal expansion and improve the reflector modeling capabilities to enable realistic hot-full-power simulations.

As a final remark on VERA's usability, a substantial reduction of the computational resources (memory, compute cores and wall-time) is the paramount next step to allow industrial use of VERA-CS. Practical capabilities for cycle depletion with coupling are uttermost priorities for industrial application of VERA-CS.

9 CONCLUSIONS

Westinghouse has successfully performed simulations of the zero power physics tests for its state-of-the-art **AP1000** PWR using VERA-CS. The **AP1000** reactor features an advanced first core with radial and axial heterogeneities, IFBA and WABA burnable absorbers, enrichments from natural U to 4.8 w/o ^{235}U, and a combination of light tungsten control banks and heavy, Ag-In-Cd control banks to perform the MSHIM advanced operational strategy.

All VERA simulations reported have been performed by Westinghouse personnel on a VERA build installed on a dedicated Westinghouse compute cluster. A positive resolution of some initial challenges in building VERA has been attained thanks to a dedicated effort from CASL and Westinghouse personnel. This has resulted in a streamlined process developed for building VERA on external platforms which has been documented and is now available for future deployments. The VERA build at Westinghouse is fully operational, and it has been successfully updated and ported to different computer systems.

In performing the Test Stand simulations, Westinghouse has observed an impressive agreement between VERA and KENO, used to provide the reference numerical results, for its **AP1000** PWR first core.

In particular, the **AP1000** PWR HZP critical boron concentration predicted by VERA for the start-up core is within 3 ppm of the KENO prediction. The RMS in the delta rod worth prediction is 4 pcm, with a maximum difference of 9 pcm, across the eleven control banks of the **AP1000** PWR. The delta in differential boron worth is 0.2 pcm/ppm. The deltas in Doppler, Moderator and Isothermal Temperature Coefficients, DTC, MTC and ITC, are respectively less than 0.2, 0.4 and 0.6 pcm/F.

The results of the ZPPT simulations from VERA are consistent with Westinghouse predictions using in-house core physics tools and licensed methods. This reinforces the confidence in the Westinghouse prediction for the start-up tests, as several **AP1000** units will soon begin operation, and provides a clear example of application of CASL technology that has proved beneficial to the nuclear industry.

VERA is in notable agreement with KENO also in terms of power distribution prediction. Throughout simulations including radial core slices and 3D multi-assembly with partially inserted control rod banks, the delta power RMS for VERA vs. KENO has kept well below 1%, with the delta power at the hot spot also consistently below 1%. The high-quality benchmark scenarios generated alongside this activity can be utilized for code comparison and methods development at the industry, and constitute another valuable asset of the Test Stand.

In terms of practicality of use, the VERA input system, VERAIN, has been found to provide a practical, effective and reasonably comprehensive interface to set up simulations of commercial PWR cores. With VERAIN, it has been possible to implement a core model of the complexity of the **AP1000** PWR core in a convenient ASCII format using a common input deck.

Areas of improvement concern features development, I&O, post-processing and user's manual, with specific recommendations given in Section 8. None of these issues are an impediment to perform Test-Stand type of simulations but should be addressed before wider release of VERA to the industrial community.

Code execution has been found robust and stable, indicative of the high quality of the solvers used and the software implementation.

The major concern at the current state regards the computational performance. Cycle depletion calculations on industry mid-size clusters with VERA-CS are impractical due to excessive wall-time and memory requirements. Due to the uttermost relevance of these calculations to the industrial community, it is now of the highest priority for CASL to tackle and attain a substantial reduction in the computational burden of VERA, without deteriorating the excellent prediction capabilities observed through this activity.

As a final consideration, the Westinghouse Test Stand has been a markedly positive experience providing tangible reciprocal value to the organizations involved. The advanced simulation application selected proved pertinent and engaging, showing the potential benefits, and current limitations, of using higher-fidelity core physics tool to obtain reliable reference solutions for challenging simulation scenarios.

The enthusiasm and dedication offered by the many people involved, from Westinghouse as well as CASL, is acknowledged as a testimony of their dedication and engagement, and has been a key contributor to the success of the Westinghouse Test Stand.

10 ACKNOWLEDGEMENTS

The authors would like to acknowledge the following individuals for their contribution to the Test Stand activities.

From Westinghouse: Sumit Ray, Director, Methods & Technology for the unwavering support, Jeff Secker, Fellow Engineer in Methods and Technology, for consulting and oversight; David Salazar, Sr. Engineer in New Reactor Technology, for advice on the **AP1000** PWR core modeling; the Westinghouse PWR Methods group (Mohamed Ouisloumen and Larry Mayhue, Fellow engineers, Baocheng Zhang, Boyan Ivanov and Harish Huria, Principal Engineers) for all their advice and support to the simulations performed; Keith Drudy, Manager of New Reactor technology for supporting this work; Bob Fetterman, Fellow Engineer of New Reactor Technology for consulting on the **AP1000** PWR core design; Larry Hampshire and Joseph Walsh, Principal Engineers of Engineering Computing Systems for supporting the VERA build on, and configuration of, the Westinghouse VERA computer cluster; Greg Fischer, Sr. Engineer of Radiation Engineering & Analysis for the support on the VERA build and execution of the VERA simulations.

From CASL: Rose Montgomery (TVA), Doug Burns (INL) and Steve Hess (EPRI) for their support to the Test Stands, John Turner (ORNL) for support to the VERA deployment, Roscoe Bartlett (ORNL) for the invaluable help provided for the VERA build on the Westinghouse computer, Mark Baird (ORNL) for supporting the VERA build and enabling KENO builds and updates on INL Fission computer cluster, Jess Gehin (ORNL) for support and advice, Tom Evans (ORNL) and the Insilico developers, and namely Steve Hamilton (ORNL) for his insights on the cross section homogenization for $SP_{N,}$ Ben Collins (UM) and the MPACT developers.

The authors wish to thank Aaron Graham, UM and intern at Westinghouse during the summer of 2013, for the support in setting up the initial Test Stand simulations.

Finally, Westinghouse is grateful to the KENO-VI development and CE data teams at ORNL, including Kursat Bekar and Cihangir Celik, for their availability and support in providing the validation basis for the **AP1000 PWR core** VERA results.

11 REFERENCES

1. M. Hone et al., **AP1000** Reference Report, Westinghouse Electric Company, March 2012 WCAP-17524-NP
2. T.M. Evans et al., 2010. Denovo: A New Three-Dimensional Parallel Discrete Ordinates Code in SCALE. *Nuclear Technology*, 171, pp.171–200.
3. SCALE: A Comprehensive Modeling and Simulation Suite for Nuclear Safety Analysis and Design, ORNL/TM-2005/39, Version 6.1, June 2011. Available from Radiation Safety Information Computational Center at Oak Ridge National Laboratory as CCC-785.
4. A.T. Godfrey, et al. "Operational Reactor Model Demonstration with VERA: Watts Bar Unit 1 Cycle 1", Revision 1 August 1 2013 CASL-U-2013-0105-001
5. A.T. Godfrey, et al. "Analysis of Two-Dimensional Lattice Physics Verification Problems with MPACT", Dec. 21 2013, CASL-U-2012-0172-000
6. The HDF5 Group, May 14, 2013. http://www.hdfgroup.org/HDF5/
7. HDFView, February 12, 2013. http://www.hdfgroup.org/hdf-java-html/hdfview/
8. D.F. Hollenbach, L.M. Petrie, and N.F. Landers, "KENO-VI: A General Quadratic Version of the KENO Program," Vol. II, Sect. F17 of SCALE: A Modular Code System for Performing Standardized Computer Analysis for Licensing Evaluation, NUREG/CR-0200, Rev. 7 (ORNL/NUREG/CR/CSD-2R7), 3 vols., April 2004. Available from the Radiation Safety Information Computational Center at Oak Ridge National Laboratory as CCC-545.
9. A.T. Godfrey, "VERA Core Physics Benchmark Progression Problem Specifications", Revision 2, CASL-U-2012-0131-002, CASL, March 29, 2013.
10. X-5 Monte Carlo Team, MCNP—A general Monte Carlo N-Particle Transport Code, Version 5, vol. 1, LA-UR-03-1987, 2003. http://mcnp.lanl.gov/ http://rsicc.ornl.gov
11. M.E. Dunn and N.M. Greene, "AMPX-2000: A Cross section Processing System for Generating Nuclear Data for Criticality Safety Applications," Trans. Am. Nucl. Soc. 86, 118–119 (2002).
12. Watts Bar Nuclear Plant, Tennessee Valley Authority, May 2013. http://www.tva.com/power/nuclear/wattsbar.htm
13. Watts Bar Unit 2 Final Safety Analysis Report (FSAR), Amendment 93, Section 4, ML091400651, April 30, 2009. http://adamswebsearch2.nrc.gov/idmws/ViewDocByAccession.asp?AccessionNumber=ML091400651
14. VisIt Visualization Tool, LLNL, March 25, 2013. https://wci.llnl.gov/codes/visit
15. B. Zhang, E. Müller, D. Sato, C. Hah, L. Mayhue, and J. Casal, "NEXUS – A New Nuclear Data System for Light Water Core Analysis", ICAPP'05, Seoul, Korea, 2005.
16. L. Mayhue, B. Zhang, D. Sato, and D.C. Jung, "PWR Core Modeling using the NEXUS Once-Through Cross Section Model", PHYSOR-2006, ANS Topical Meeting on Reactor Physics, Vancouver, Canada, September 10-14, 2006.
17. D.C. Jung, L. Mayhue, S. W. Park, Y. S. Jung, and C.K. Lee, "The Qualification of the NEXUS Once-Through Cross section System for OPR1000 Core", Transactions of the Korean Nuclear Society, Spring Meeting, Jeju, Korea, May 10-11, 2007.

18. L. Mayhue, R. Milanova, H. Huria, B. Zhang, E. Müller, F. Franceschini, M. Ouisloumen, P. Forslund Guimaraes, "Qualification of the NEXUS/ANC Nuclear Design System for PWR Analyses", PHYSOR-2008, Interlaken, Switzerland, September, 2008
19. B. Zhang, et. Al., "Qualification of the NEXUS Nuclear Data Methodology", WCAP-16045-NP-A, Addendum 1, November, 2005.
20. T. Morita, et al., "Application of MSHIM Core Control Strategy for Westinghouse AP1000 Nuclear Power Plant", GENES4/ANP2003, September 2003.
21. K. Drudy, etc., Robustness of the MSHIM Operation and Control Strategy in the **AP1000** Design, 17th International Conference on Nuclear Engineering (ICONE 17), July 12-16, 2009, Brussels, Belgium.
22. M. Ouisloumen, et al., "The New Westinghouse Assembly Lattice Code, ANS International Meeting on Mathematical Methods for Nuclear Applications, Salt Lake City, Utah, USA (2001)
23. M. Ouisloumen et al.,"Qualification of the Two-Dimensional Transport Code PARAGON', WCAP-16045-NP-A, August, 2004.
24. H. C. Huria and M. Ouisloumen, "Integral Data Testing for Thermal Spectrum Critical Experiments using ENDF/B-VII.0", Advances in Nuclear Fuel Management IV, Hilton Head Island, South Carolina, USA, April,2009.
25. H.C. Huria, V. N. Kucukboyaci, and M. Ouisloumen, "ENDF/B-VII.0 Based Library for PARAGON" PHYSOR 2010 – Advances in Reactor Physics to Power the Nuclear Renaissance, Pittsburgh, Pennsylvania, USA, May 9-14, 2010.
26. V. N. Kucukboyaci, H. C. Huria, and M. Ouisloumen, "PARAGON Library with 4.0eV Upscattering Cut-Off", PHYSOR 2010 – Advances in Reactor Physics to Power the Nuclear Renaissance, Pittsburgh, Pennsylvania, USA, May 9-14, 2010.
27. B. Zhang, F. Franceschini, E. Müller and P.G. Forslund, "Development of New Pin Power Recovery Methodology," International Conference on Mathematics, Computational Methods & Reactor Physics (M&C 2009), Saratoga Springs, New York, May 3~7, 2009.
28. B. Zhang, F. Franceschini, et al., "Westinghouse New Pin Power Methodology to Meet the Challenges of **AP1000** and Advanced PWR Fuel Assembly Design", Topfuel 2011 Int. Conf., Sept. 11-14 2011, Chengdu, China
29. B. Zhang, B. Ivanov et al., "Development of 3D Pseudo Pin-by-Pin Calculation Methodology in ANC", *PHYSOR 2012 – Advances in Reactor Physics,* Knoxville, Tennessee, USA, April 15-20, 2012, on CD-ROM, American Nuclear Society, LaGrange Park, IL (2012)
30. F. Franceschini, B. Zhang, et al., "Pin Power Redistribution due to Control Rod Depletion within the Westinghouse NEXUS System", American Nuclear Society Trans., Vol. 10, 720-722 (2009)
31. F. Franceschini, B. Zhang, et al., "Development of a Control Rod Depletion Methodology for the Westinghouse NEXUS System", *Progress of Nuclear Energy*, in press, available on-line at http://www.sciencedirect.com/science/article/pii/S0149197012001424
32. Y.S. Liu et al, "Pin Power Prediction in the Westinghouse Advanced Nodal Code", Trans. Am. Nuclear Soc., 53, 246, 1986.
33. Y.S. Liu, et al., "ANC: A Westinghouse Advanced Nodal Computer Code". WCAP-10966-A, Westinghouse Electric Company, Sep. 1986

34. Teuchos: The Trilinos Tools Library, SNL, May 24, 2007, http://trilinos.sandia.gov/packages/teuchos/
35. Milestone completion Report, L3:RTM.SUP.P5.02, "Generation of Multigroup Nuclear Data libraries for CASL", CASL, September 28, 2012.
36. M.E. Dunn and N.M. Greene, "AMPX-2000: A Cross section Processing System for Generating Nuclear Data for Criticality Safety Applications," *Trans. Am. Nucl. Soc*. **86**, 118–119 (2002).
37. B. Kochunas, et. al, "Overview of the Development and Design of MPACT," Proceedings M&C 2013, Sun Valley, ID, May 5-9, 2013.
38. Y. Liu, et. al, "Resonance Self-Shielding Methodology in MPACT, Proceedings M&C 2013, Sun Valley, ID, May 5-9, 2013.
39. B.S. Collins, "Assessment of the 2D MOC Solver in MPACT, Proceedings M&C 2013, Sun Valley, ID, May 5-9, 2013.
40. A.T. Godfrey, F. Franceschini, et. al, "Analysis of Two Dimensional Lattice Physics Verification Problems with MPACT", CASL-U-2012-0172-000, CASL, December 21, 2012.
41. B. Kelley and E. Larsen, "2D/1D Approximation to the Neutron Transport Equation: Theory," Proceedings M&C 2013, Sun Valley, ID, May 5-9, 2013.
42. B. Kelley, B.S. Collins, and E. Larsen, "2D/1D Approximation to the Neutron Transport Equation: Numerical Results," Proceedings M&C 2013, Sun Valley, ID, May 5-9, 2013.
43. M. L. Williams and K. S. Kim, "The Embedded Self-Shielding Method," PHYSOR 2012 Advances in Reactor Physics Linking Research, Industry, and Education, Knoxville, Tenn., April 15-20, 2012, on CD-ROM, American Nuclear Society, LaGrange Park, Ill. (2012)
44. E.W. Larsen, J.E. Morel, & J.M. McGhee, 1996. Asymptotic Derivation of the Multigroup P1 and Simplified PN Equations with Anisotropic Scattering. Nuclear Science and Engineering, 123, pp.328–342.
45. Watts Bar Nuclear Plant, Unit 1, Initial Startup Report to the Unites States Nuclear Regulatory Commission, Tennessee Valley Authority, NRC Docket No. 50-390, May 1996.
46. U. Decher, et al., "ENDF/B-VI Performance in PWR Applications", Trans. Am. Nucl. Soc.,73,417, 1995.
47. S. Palmtag, "Demonstration of Neutronics Coupled to Thermal-Hydraulics for a Full-Core Problem using VERA", CASL-U-2013-0196-000, December 30, 2013

APPENDIX A CE KENO-VI SIMULATIONS

The following gives more details on the KENO simulations supporting the reference results documented in Section 6. In particular, the 2D lattices and multi-lattice, 2D Core, 3D assembly and multi-assembly and 3D core KENO models for the **AP1000** PWR core and main simulation parameters are described.

A.1 2D Lattices[i]

CE KENO-VI models were created for every unique fuel lattice characterizing the **AP1000** PWR startup core (a total of 20 lattices). Additionally several controlled lattices and some at higher fuel temperatures were generated but these are not included in this report. The lattice models were generated with quarter symmetry and reflecting boundary conditions. Table A-1 provides some representative information on the lattice models. A depiction of the KENO model for a sample lattice, specifically Reg. 5A with 88 IFBA and 4 WABA, is shown in Figure A-1.

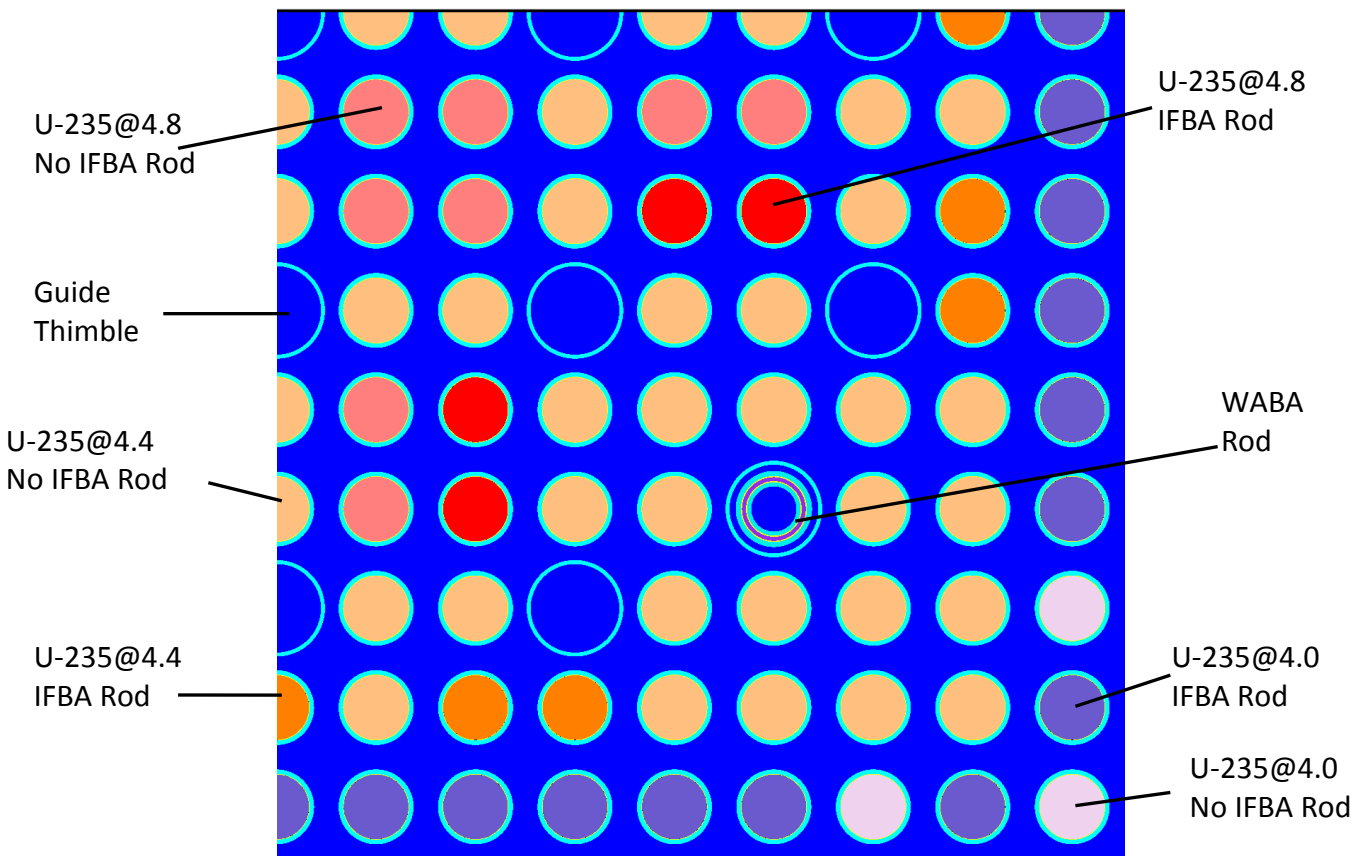

Figure A-1 Example 2D Lattice Model for KENO-VI (Reg. 5A)
(see Figure 4-3)

[i] Results discussed in Section 6.1

Table A-1 Representative 2D Lattice Monte Carlo Parameters

Total # Particles	1e9
# Particles / Generation	1e6
# Generations	1100
# Skipped Generations	100
# Cores	312
Memory / Core	2.7 GB
Runtime	3.5 hours
Eigenvalue Uncertainty	< ± 3 pcm
Average Pin Power Uncertainty	± 0.025%
Maximum Pin Power Uncertainty	± 0.030%

A.2 2D Multi-Lattice[j]

Multi-lattice simulations representing the center nine assemblies (3x3) in the **AP1000** PWR core at the axial midplane have been performed. The central location was either uncontrolled or controlled with standard (Ag-In-Cd) or gray (tungsten) control rods. These cases represent challenging scenarios due to the presence of control rod and the interaction between fuel rods of neighboring lattices, which have significantly different enrichment and may experience marked power gradients. Like the single lattices, advantage is taken for quarter and octant symmetry. A depiction of the KENO model for a controlled multi-lattice is shown in Figure A-2, with representative parameters of the KENO simulation given in Table A-2.

Table A-2 Representative 2D 3x3 Multi-Lattice Monte Carlo Parameters

Total # Particles	3.2e9
# Particles / Generation	2e6
# Generations	1600
# Skipped Generations	200
# Cores	300
Memory / Core	3.2 GB
Runtime	11 hours
Eigenvalue Uncertainty	< ± 2 pcm
Average Pin Power Uncertainty	± 0.04%
Maximum Pin Power Uncertainty	± 0.09%

[j] Results discussed in Section 6.2

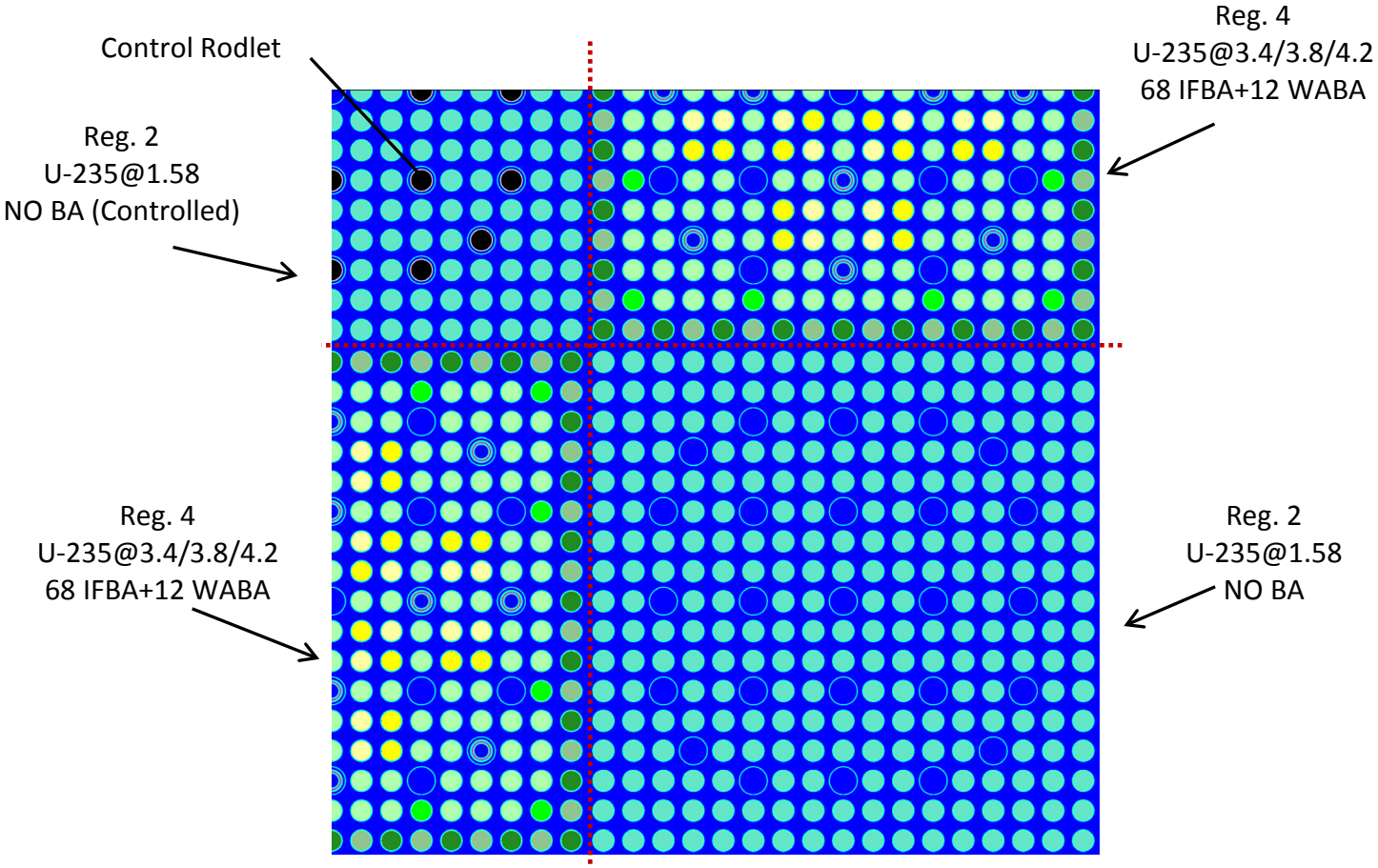

Figure A-2 2D Multi-Lattice Model for KENO-VI
(Controlled, Reg. 2 & 4 - see Figure 4-2 and Figure 6-3)

A.3 2D Core[k]

The KENO 2D core models provide realistic radial power distributions with adequate uncertainty for pin power distribution comparison with VERA-CS solution. The fuel region for the 2D core model reproduces a radial slice of the **AP1000** PWR core at the axial mid-plane. Several versions of the 2D core were executed to determine the significance of several radial reflector treatments, as described in APPENDIX B. For consistent comparison to VERA-CS, a 1-inch baffle model is used, as shown in Figure A-3. Table A-3 summarizes the representative parameters of the KENO simulation.

[k] Results discussed in Section 6.3

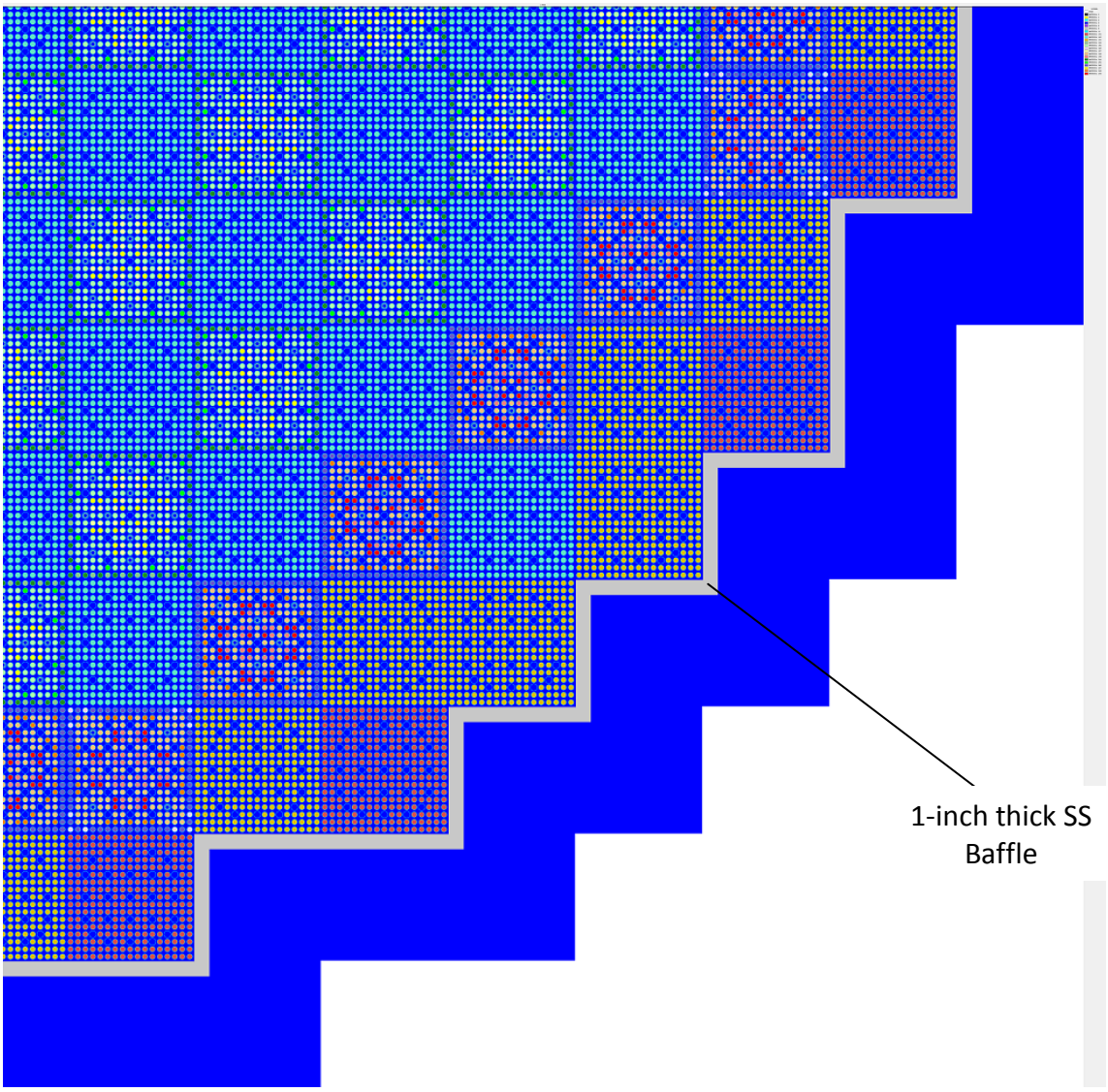

Figure A-3 KENO 2D Core Model
(quarter symmetry)

Table A-3 2D Core Monte Carlo Parameters

Total # Particles	25e9
# Particles / Generation	5e6
# Generations	5000
# Skipped Generations	500
# Cores	300
Memory / Core	5.3 GB
Runtime	6 days
Eigenvalue Uncertainty	< ± 0.5 pcm
Average Pin Power Uncertainty	± 0.06%
Maximum Pin Power Uncertainty (by Power)	Power < 1.0: ± 0.28% Power > 1.0: ± 0.08%

A.4 3D Single Assembly[I]

KENO models for each of the seven assembly types (five regions with three poison configurations in the fifth region) characterizing the **AP1000** PWR startup core were created. These simulations provide the reference solutions for 3D power distribution comparisons against VERA-CS, including the impact of axial leakage, axial blankets, and spacer grids. The fuel stack region above and below the active fuel is fairly detailed in the KENO models, as discussed in Section 5.3. Outside of the fuel rod region, the nozzles and core plates are homogenized with the coolant. Vacuum boundary conditions are assumed outside the core plates. This detailed fuel stack model provides an excellent numerical reference solution for comparison to deterministic codes that typically rely on simplified geometrical model outside of the active fuel. Furthermore, the 3D effects of the grids are appropriately taken into account by KENO with the semi-explicit spacer grid models, thereby also providing a valuable reference for comparison to deterministic approaches. The semi-explicit spacer grid KENO model adopted has been discussed in Section 5.3; an example is shown in Figure 5-1.

The coolant conditions and boron concentrations for the single assemblies were provided by Westinghouse using in-house core methods to predict near-critical conditions. This reduces the significance of the critical buckling correction when comparing results to typical core simulators. The natural assembly is sub-critical even without soluble boron, which has thus been assumed in this case. Control rods have not been modeled in the single assembly calculations, but thimble plugs have been included in the top portion of the unused guide tubes as appropriate.

The axial meshing used for the fission reaction rate tallies was consistent between KENO and VERA. Namely, a 49-level mesh structure (in the fuel) was chosen based on actual material

[I] Results discussed in Section 6.4

boundaries, e.g. axial blankets, grid spacers, dashpot, WABA, and fully inserted control rod elevations. A maximum mesh size of 4.5-inch was allowed between material boundaries. Each spacer grid is encompassed by a dedicated mesh. The tally mesh is fixed for all 3D problems to ensure consistency between simulation results.

Note that three variations of Reg. 3 assembly (3.2% - no IFBA) were created, with and without the spacer grids and without the regions outside of the fuel stack to perform this sensitivity study have been reported in Table 6-4.

Figure A-4 depicts the KENO model for one of the seven assemblies modeled, and specifically Reg. 4 fuel stack, featuring 68 IFBA rods with 8 “long” WABA inserts and 4 “short” WABA inserts (see Figure 4-2 and Figure 4-7). Table A-4 summarizes the representative parameters of 3D assembly KENO simulations.

Table A-4 Representative 3D Single Assembly Monte Carlo Parameters

Total # Particles	17.5e9
# Particles / Generation	5e6
# Generations	3500
# Skipped Generations	500
# Cores	240
Memory / Core	5.3 GB
Runtime	3 days
Eigenvalue Uncertainty	< ± 0.7 pcm
Average Pin Power Uncertainty	± 0.05%
Maximum Pin Power Uncertainty (by Power)	Power < 1.0: ± 0.21% Power > 1.0: ± 0.12%

Figure A-4 3D Assembly Model for KENO-VI - Region 4
(not shown to scale – axial slice at y=0; quarter symmetry)

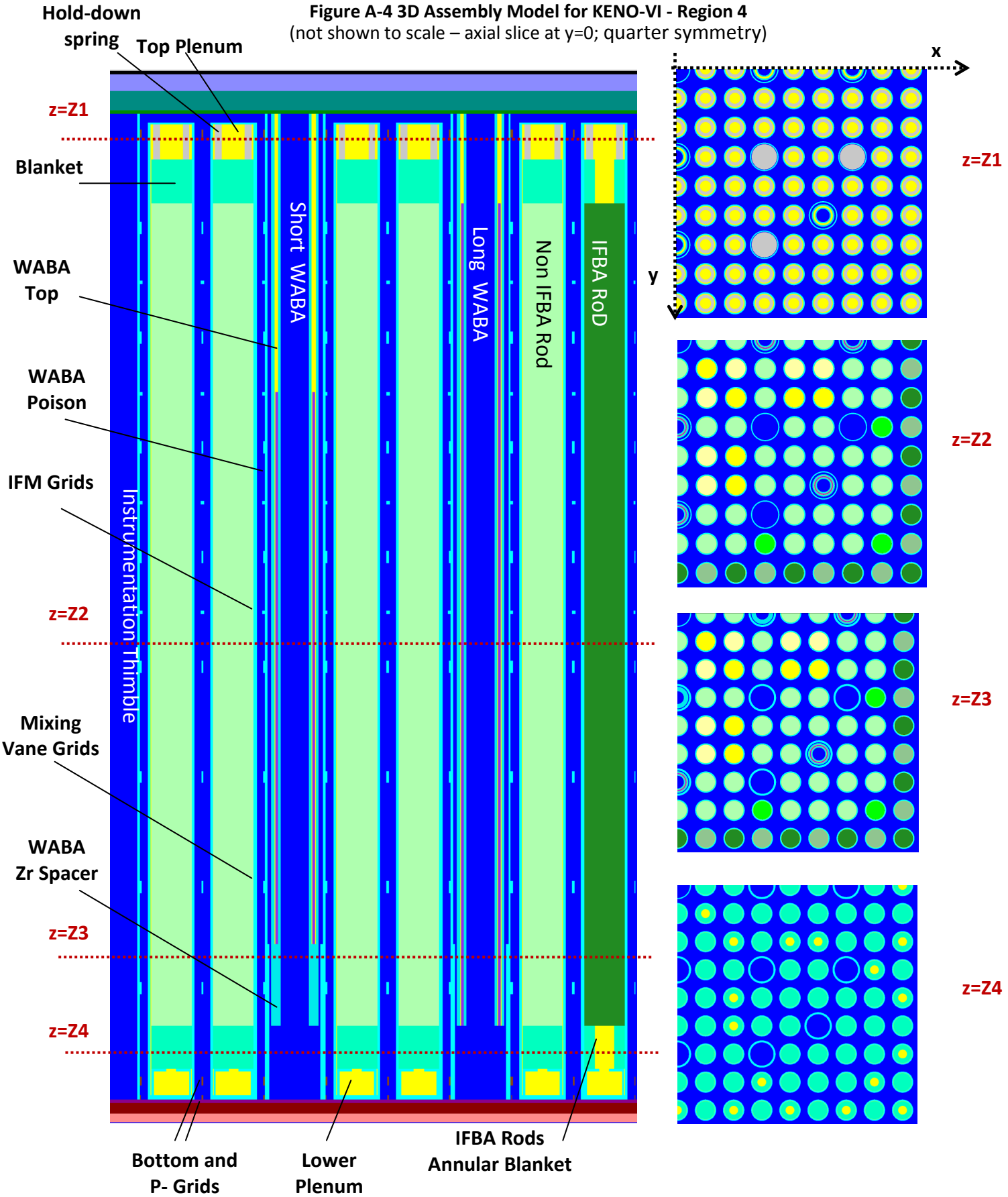

A.5 3D 3x3 Multi-Assembly with Control Rod[m]

The KENO 3D 3x3 multi-assembly model depicted in Figure A-5 allows simulation of the center nine assemblies of the **AP1000** PWR core. The axial geometry is the same as the corresponding 3D assembly cases (Reg. 2 and Reg. 4) and the radial geometry is consistent with the 2D multi-lattice case in Section A.2. Quarter symmetry is utilized.

This model allows capturing the interactions of the different pins at the assembly interfaces, as for the corresponding 2D multi-lattice case. Moreover, the three-dimensional impact of spacer grids, WABA rods and especially control rod insertion are captured.

The Ag-In-Cd AO control rod bank is partially inserted into the center assembly in such a way to generate a neutral axial offset. This is similar in functionality and placement to the AO bank during normal operation. The soluble boron in the coolant has been adjusted to obtain approximate criticality. The thimble plugs and the tips of the S1 control bank, which is placed on the adjacent assembly on the 3x3 diagonal (see Figure 4-8), are also modeled. These are located, axially, in the fuel rod top plenum region.

The extent of this model is approaching the limits for obtaining 3D KENO power distribution with adequate statistics for comparison to deterministic codes. Due to these challenges, only one KENO 3D 3x3 assembly case has been executed. The main Monte-Carlo parameters for this simulation are given in Table A-5.

Table A-5 3D 3x3 Multi-Assembly Monte Carlo Parameters

Total # Particles	50e9
# Particles / Generation	5e6
# Generations	10,000
# Skipped Generations	500
# Cores	240
Memory / Core	5.3 GB
Runtime	9.1 days
Eigenvalue Uncertainty	< ± 0.3 pcm
Average Pin Power Uncertainty	± 0.07%
Maximum Pin Power Uncertainty (by Power)	Power < 1.0: ± 0.31% Power > 1.0: ± 0.20%

[m] Results discussed in Section 6.5

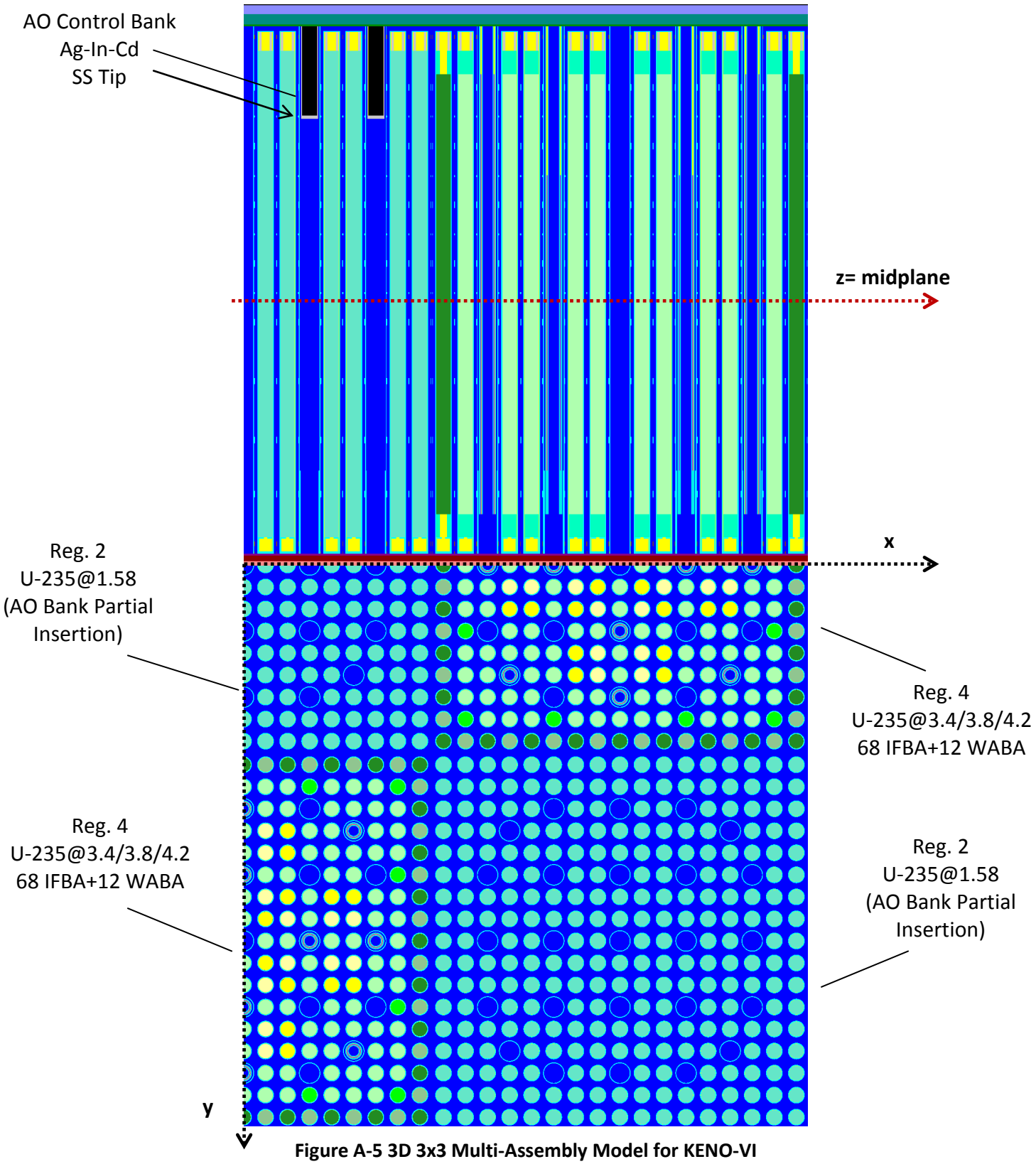

Figure A-5 3D 3x3 Multi-Assembly Model for KENO-VI

(not shown to scale – radial slice at core mid-plane – axial slice at y=0)

A.6 3D Quarter Core Zero Power Physics Tests[n]

The KENO models supporting the **AP1000** PWR core ZPPTs simulations are depicted in Figure 6-24. The reflector model employed is highlighted in Figure A-6 and Figure A-7. The KENO reflector model employed for the 3D ZPPT simulations is a more accurate 3D representation of the **AP1000** PWR reflector compared to the VERA-CS model, which consists of an axially uniform
1-inch thick baffle surrounded by water[o]. The impact of the various additional reflector components (e.g. shroud rings, neutron pads, etc.) on eigenvalue and power distribution is discussed in the sensitivity studies reported in APPENDIX B and APPENDIX C[p].

Isothermal conditions at 565K with a soluble boron concentration of 1321 ppm (natural boron with ^{10}B isotopic abundance of 19.9 at%) have been assumed for the startup, consistent with the values reported in Ref. 1. The KENO models supporting the ZPPT simulations have been executed on the INL supercomputer Fission, with more details on the simulations performed given below. Note that each case is a 3D core Monte Carlo simulation.

1. **All-Rods-Out Criticality (2 Cases)**
    a. Reference All-Rods-Out Geometry, no instrumentation
    b. Same as 1a with in-core instrumentation thimbles inserted to calculate instrumentation reactivity worth
    c. Same as 1a with simplified reflector for sensitivity analysis

2. **Control Bank Reactivity Worth (11 Cases)**
    a. Same as 1a but with each of the eleven control rod banks fully inserted

3. **Differential Boron Reactivity Worth (1 Case)**
    a. Same as 1a but with reduced soluble boron concentration to establish boron reactivity worth

4. **Temperature Reactivity Coefficient (14)**
    a. Same as 1a with various fuel and moderator temperatures and moderator densities to calculate ITC, MTC and DTC (see APPENDIX D)

5. **MSHIM-type Control Rod Pattern**
    a. Same as 1a with control banks AO inserted at 226 steps, MA fully inserted and MB at 88 steps withdrawn
    b. Same as 1a but with simplified reflector for sensitivity analysis

---

[n] Results discussed in Section 6.6

[o] Note that a consistent, 1-inch thick baffle reflector, is used in the KENO model supporting 2D core power distribution comparisons vs. VERA, as shown in Figure A-3

[p] These KENO sensitivity studies also allowed to determine an eigenvalue bias to apply to the VERA ZPPT results to compensate for the approximate reflector model employed

The **AP1000** PWR core ZPPT KENO simulations above required a total of nearly 235,000 CPU-hours to be executed, or approximately 40 days of wall-time with an average of 250 cores usage. This entailed a significant human effort, beside computer's usage, with the intent of establishing a solid numerical reference for this work.

Most of these cases have been simulated with a number of particles adequate to establish reliable eigenvalue results. A higher number of particles have been employed in selected cases to reduce the coarse-mesh power distribution statistical uncertainty to enable meaningful comparison to deterministic codes at selected locations (e.g. assembly power, high-power fuel rods)[q]. Representative Monte-Carlo parameters employed for these calculations are reported in Table A-6.

The KENO ZPPT results are summarized in Table A-7, including various adjustments described in the footnotes. The KENO ZPPT results are also reported in Table 6-7 and Table 6-9 in the "Results" Section of this report.

Table A-6 Representative 3D Core Monte Carlo Parameters

Parameter	Eigenvalue Only	Eigenvalue & Power
Total # Particles	5e9	50e9
# Particles / Generation	5e6	5e6
# Generations	1000	10000
# Skipped Generations	250	500
# Cores	180	180
Memory / Core	10.7 GB	10.7 GB
Runtime	28 hours	10.3 days
Eigenvalue Uncertainty	< ± 1.5 pcm	< ± 0.4 pcm
Average Pin Power Uncertainty	± 0.97%	± 0.27%
Maximum Pin Power Uncertainty (by Power)	Power < 1.0: ± 14.29% Power > 1.0: ± 3.12%	Power < 1.0: ± 3.39% Power > 1.0: ± 0.86%

[q] Obtaining fine-mesh low-uncertainty 3D core power distribution with the current KENO is impractical.

Table A-7 CE KENO-VI ZPPT Results for First AP1000 Startup

Physics Parameter	Result
Criticality	
Eigenvalue @ 1321 ppmB†	0.99920 ± 0.00001
Critical Boron (ppm)†	1313 ± 1
Control Bank Worths	
MA (Grey)	258 ± 2
MB (Grey)	217 ± 2
MC (Grey)	188 ± 2
MD (Grey)	234 ± 2
M1 (Black)	651 ± 2
M2 (Black)	887 ± 2
AO (Black)	1635 ± 2
S1 (Black)	1079 ± 2
S2 (Black)	1096 ± 2
S3 (Black)	1124 ± 2
S4 (Black)	580 ± 2
Differential Boron Worth (pcm/ppm)	-9.56 ± 0.08
Temperature Reactivity Coefficients	
MTC (pcm/F)	-1.12 ± 0.04‡
DTC (pcm/F)	-1.54 ± 0.03‡
ITC (pcm/F)	-2.66 ± 0.05‡

†Criticality results are corrected for the following items:

1. -120 pcm for thermal expansion, provided by Westinghouse
2. -26 pcm to account for the presence of the in-core instrumentation thimbles calculated by KENO. The uncertainty in this value is approximately 2 pcm.
3. -18 pcm calculated by KENO to compensate for the fact that the S(α,β) cross section for the H-1 isotope present in the CE data libraries used are at 550K instead of the 565 HZP temperature . This bias has been calculated separately as part of the ITC calculations documented in APPENDIX D. The uncertainty in this value is approximately 2 pcm.

‡The temperature coefficient uncertainties are estimated by propagation of KENO eigenvalue uncertainties through the coefficient calculation using an independent Monte Carlo sampling procedure.

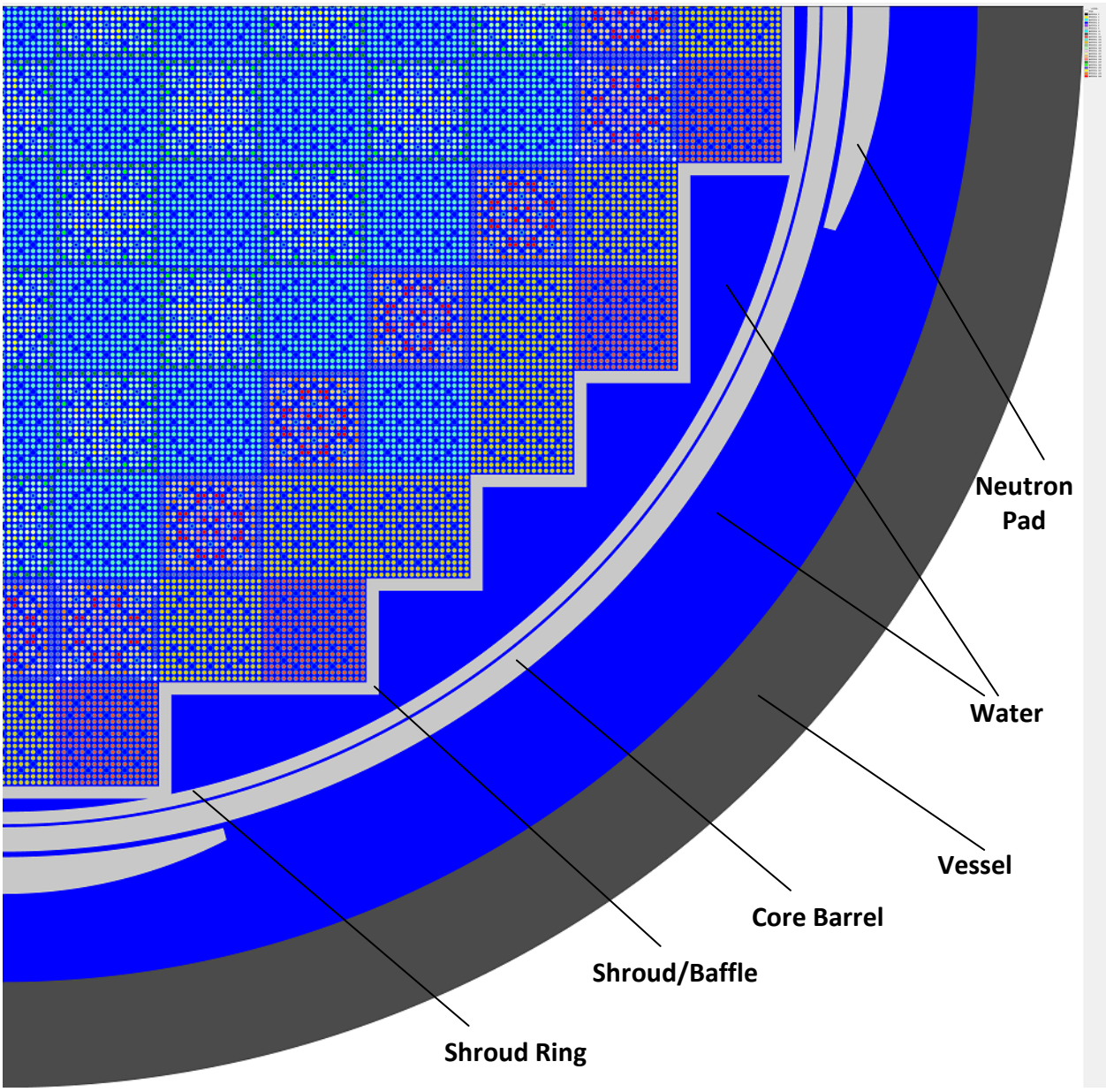

Figure A-6 KENO ZPPT Core Model (1 of 2)
(quarter core, radial view)

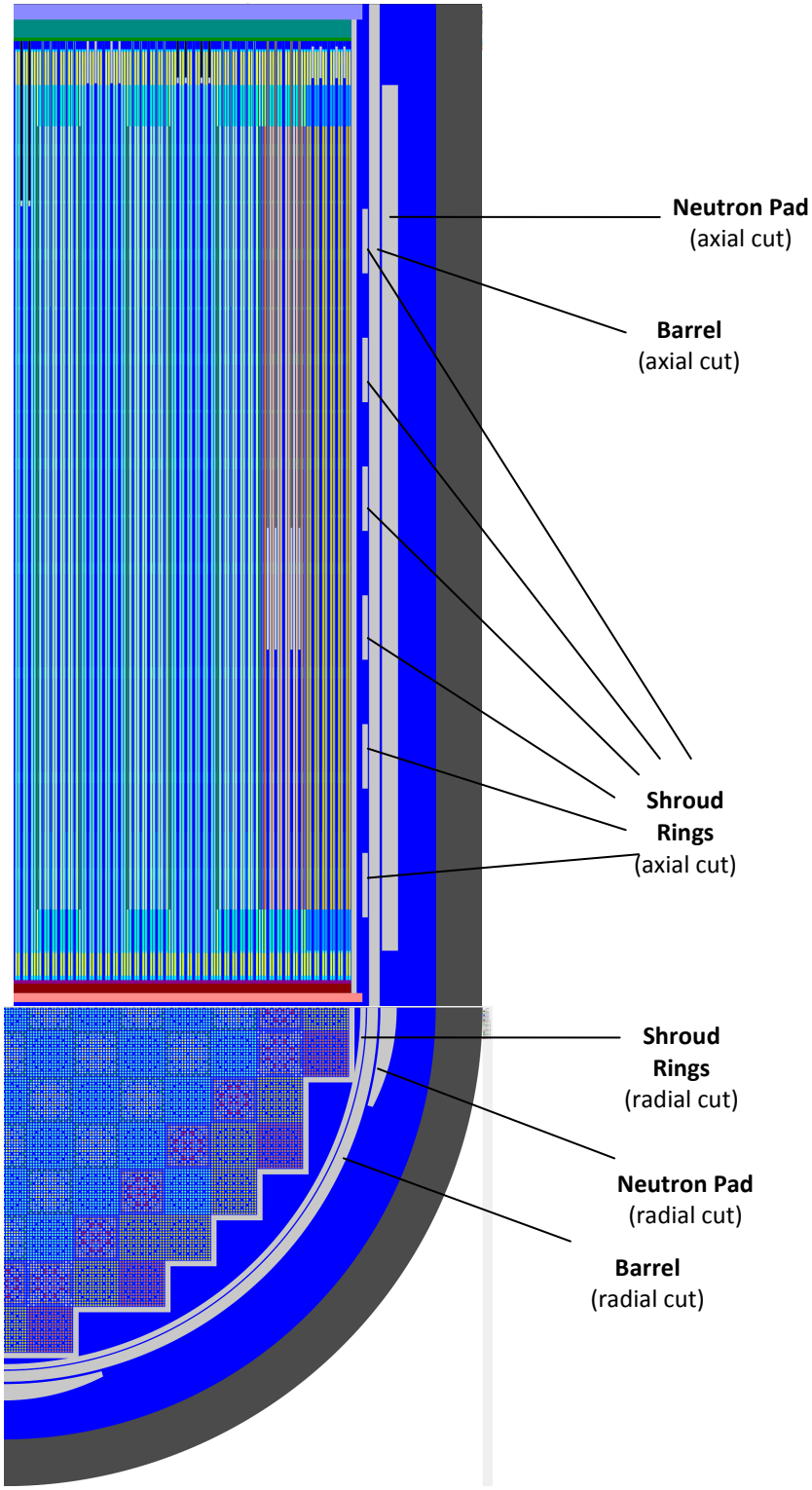

Figure A-7 KENO ZPPT Core Model (2 of 2)
(axial view and radial views, quarter core)

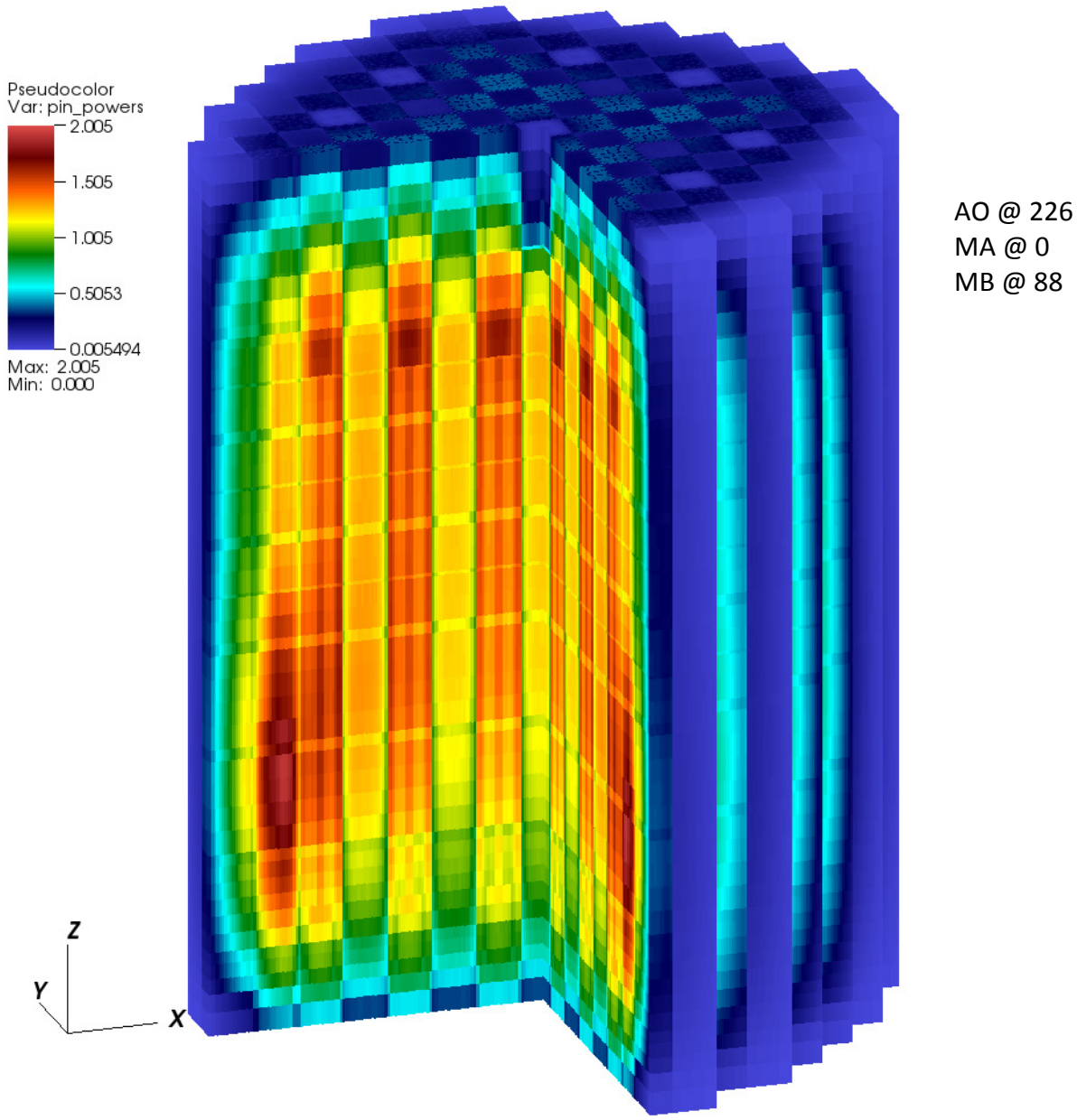

Figure A-8 Visualization of 3D Fission Distribution from KENO-VI

APPENDIX B RADIAL REFLECTOR SENSITIVITY STUDY

A sensitivity analysis on the reflector model has been carried out taking advantage of KENO general geometry modeling capabilities. In particular, 2D KENO core simulations relying on same fuel region but increasingly complex radial reflector structure have been performed to assess the impact of various reflector components on the eigenvalue and power distribution. These simulations are described below and shown in Figure B-1.

The reflector model currently featured in VERA-CS is represented by "Case 2", while "Case 3" and "Case 4" emulate the **AP1000** PWR reflector at axial planes without and with shroud rings. The results from these simulations helps establish reactivity biases for core calculations with the current VERA-CS reflector model. Case 2 is also the proper model to undertake consistent power distribution comparisons with the corresponding VERA-CS model reported in Section 6.3.

Case 1: No baffle is present; an assembly pitch thickness of moderator surrounds the jagged core boundary, followed by void and vacuum (non-reentrant) boundaries.

Case 2: 1-inch baffle model; a 1-inch thick solid stainless steel baffle is added to Case #1. This model is consistent with the VERA-CS reflector modeling capability, and it has thus been used as basis to establish biases and sensitivities.

Case 3: Full reflector model; the core barrel, neutron pads, and vessel are added to Case #2. A vacuum boundary is placed outside the cylindrical vessel. This model represents the reflector structure for axial regions without a shroud ring (see also Figure A-7, Figure 4-9 and Figure 4-10).

Case 4: Shroud ring model; a shroud ring, inside the core barrel, is added to Case #3. This model represents the reflector in the axial regions featuring shroud rings (see also Figure A-7, Figure 4-9 and Figure 4-10). The results can be used to quantify the radial effects of the shroud rings on the local peripheral pin power distribution.

Each of these models was executed with CE KENO-VI using quarter symmetry and Monte-Carlo parameters as reported in Table A-3. The effects of the various reflector components are summarized in Table B-1.

The impact on pin power of each reflector component is illustrated in Figure B-2 through Figure B-4. For each case, two images are provided. The top image gives the distribution of absolute pin power differences, in percent. The bottom image gives the distribution of pin power relative differences (absolute divided by pin power), in percent. For the latter, the scales are divided into two ranges, the first for fuel rods above a relative power of 0.8 (color scale), and the second for pins below 0.8 (gray scale). This subdivision helps discriminating low-power lower-importance locations from locations of higher power and importance. The minimum and maximum relative differences for each distribution are shown in the respective legends.

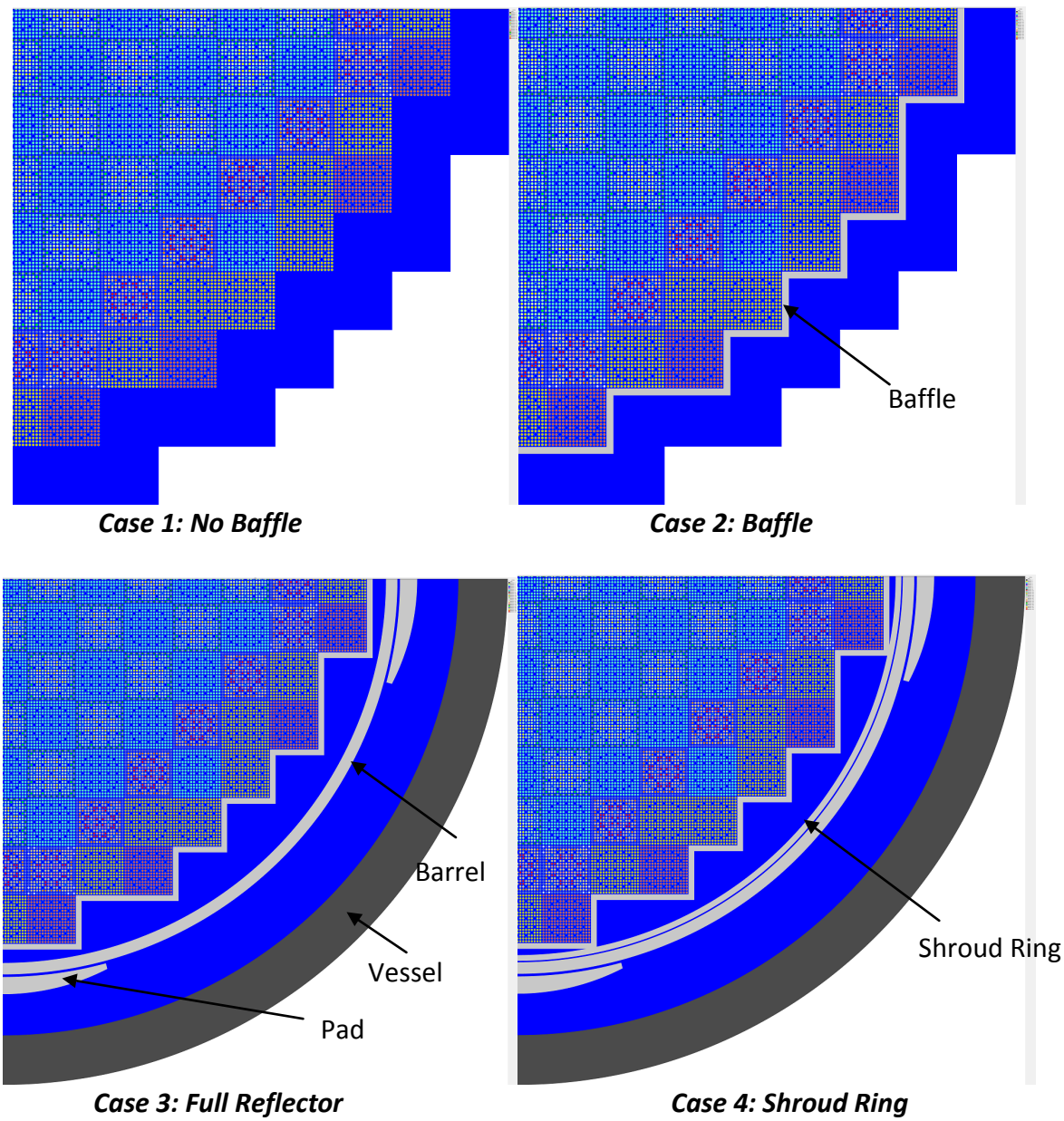

Case 1: No Baffle ***Case 2: Baffle***

Case 3: Full Reflector ***Case 4: Shroud Ring***

Figure B-1 KENO 2D Core Radial Reflector Models

While the estimated uncertainty in the pin power calculation varies depending on the fuel rod location and power, and average pin power uncertainty of ~0.06%, and a maximum pin power uncertainty of ~0.3% (occurring on the outermost fuel rod in the natural uranium assemblies) has been estimated for this set of calculations.

The comparison of Case 2 (1-inch baffle plus water) with Case 1 (all water) is given for illustrative purpose; it shows that trading water for steel immediately outside of the core reduces thermalized neutrons backscattering into the core. This especially impacts the peripheral rods of 3.2 w/o ^{235}U assemblies, given the higher thermal fission cross-section compared to natural U assemblies, and even more so around the 45 degree symmetry line, where there is a higher likelihood of neutrons crossing from one assembly to the other after

being thermalized (Figure B-2, top image). On the other hand, the presence of a baffle stainless steel improves fast neutron backscattering into the core, which is shown in Figure B-2, bottom image. The net effect of these compensating effects on reactivity is a ~35 pcm reduction in reactivity for the 1-inch baffle reflector compared to a hypothetical "all water" reflector. Introducing additional steel (Case 3 and Case 4) further improves fast neutrons backscattering, but the net effect is still a slight reactivity reduction (~25 pcm) compared to an "all water" reflector (see top row of in Table B-1).

Comparison of the more refined Case 3 and Case 4 reflector models with the simpler Case 2 baffle reflector implemented in VERA-CS indicates a very small reactivity bias (~<-10 pcm) fostered by the latter, compared to the more faithful representations of the **AP1000** PWR reflector of Case 3 and 4. While the impact on reactivity is small and virtually negligible, at least for static (no depletion) calculations, the impact on the power distribution, especially following the introduction of the shroud ring (Case 4) is not insignificant. This is explained by the shroud ring placement, intermediate between the water region after the baffle and the barrel, not too close to the core to significantly detract from neutron thermalization backscattering but not too far to only marginally improve fast neutron backscattering. The resulting impact on the power distribution is visible in Figure B-4; this amounts to a ~0.6% RMS in absolute delta assembly power between Case 4 and Case 2, with a ~2.5% maximum delta assembly power, occurring in the low power assembly on the "flat" portion of the core periphery. While still modest, the magnitude of these differences suggest that a more general reflector model in VERA-CS, potentially including a provision for modeling radial structural rings in addition to the current baffle reflector region, would be opportune.

Table B-1 Incremental Differences in 2D Core Models From Case to Case

Parameter†	Case 2-1: Baffle vs. No Baffle	Case 3-2: Full w/o Ring vs. Baffle	Case 4-2: Full w/ Ring vs. Baffle	Case 4-3: Shroud Ring
Change in Eigenvalue (pcm)	-34 ± 1	3 ± 1	9 ± 1	7 ± 1
Pin Power RMS (%) (absolute/relative)	3.45 / 6.73	0.19 / 0.51	0.59 / 1.47	0.42 / 0.96
Peak Pin Power Difference (%) (absolute/relative)	41.7 / 56.3	1.11 / 4.99	3.29 / 10.23	2.38 / 6.33
Assembly Power RMS (%) (absolute/relative)	1.34 / 1.95	0.17 / 0.31	0.57 / 0.99	0.40 / 0.68
Peak Assembly Power Difference (%) (absolute/relative)	4.63 / 5.46	0.74 / 1.10	2.44 / 3.64	1.70 / 2.51

† Absolute pin power difference (Case_B – Case_A)x100 and relative pin power difference (Case_B – Case_A)/Case_Ax100 are both provided since the dominating effects are typically from peripheral low-power pins.

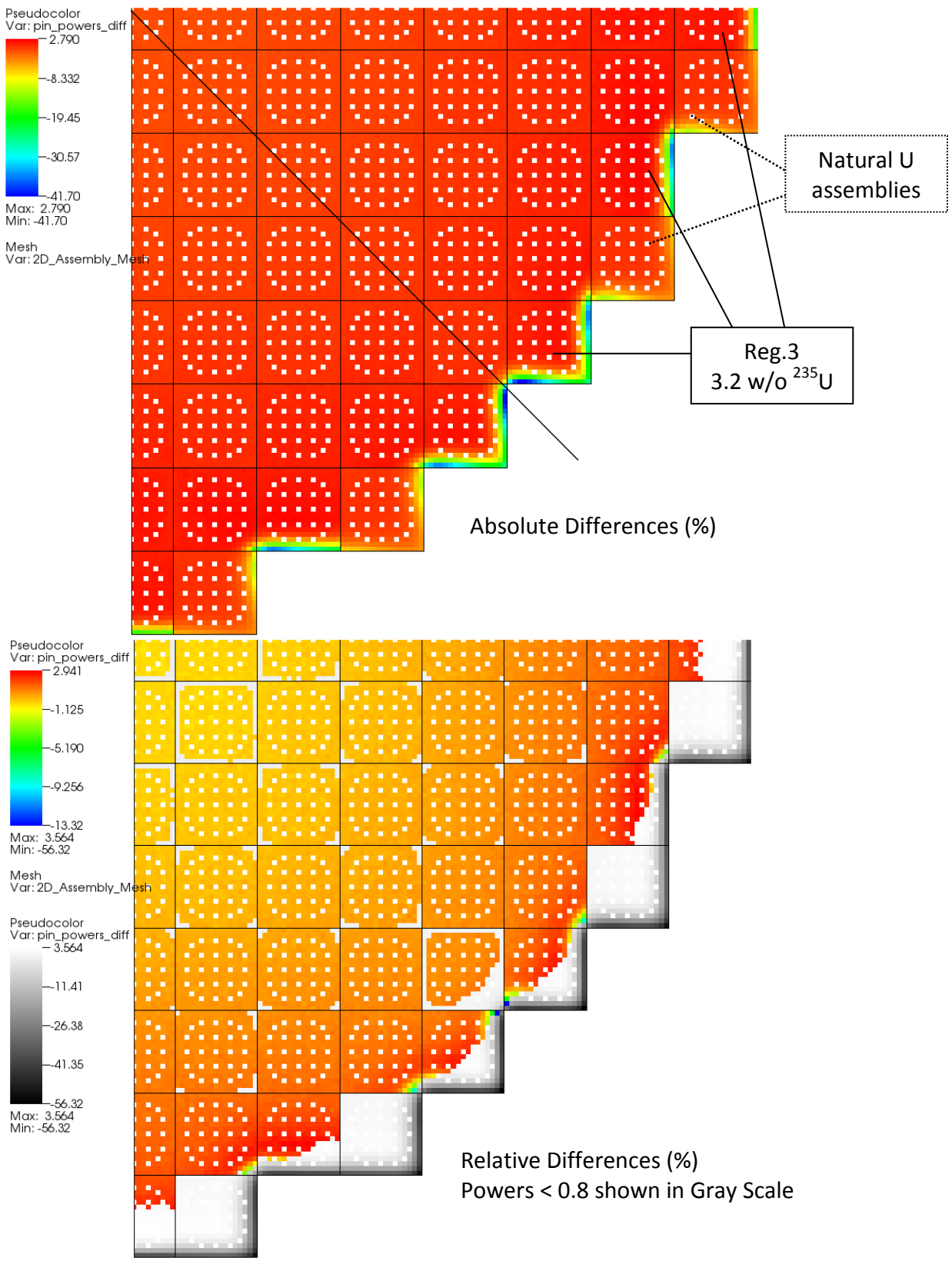

Figure B-2 Radial Pin Power Effects of the Baffle

(Case 2 vs. Case 1)

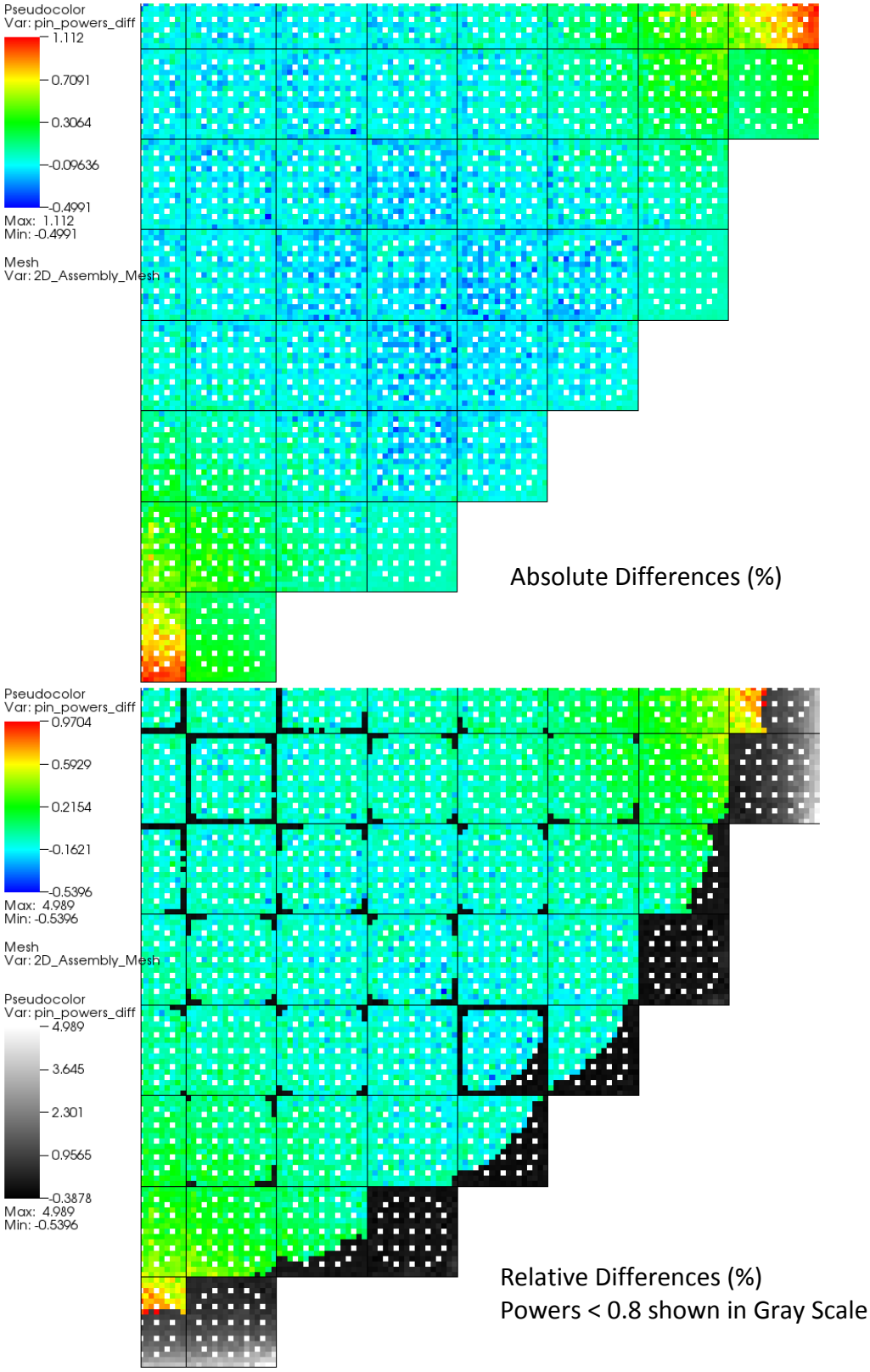

Figure B-3 Radial Pin Power Effects of the Core Barrel, Pads, and Vessel

(Case 3 vs. Case 2)

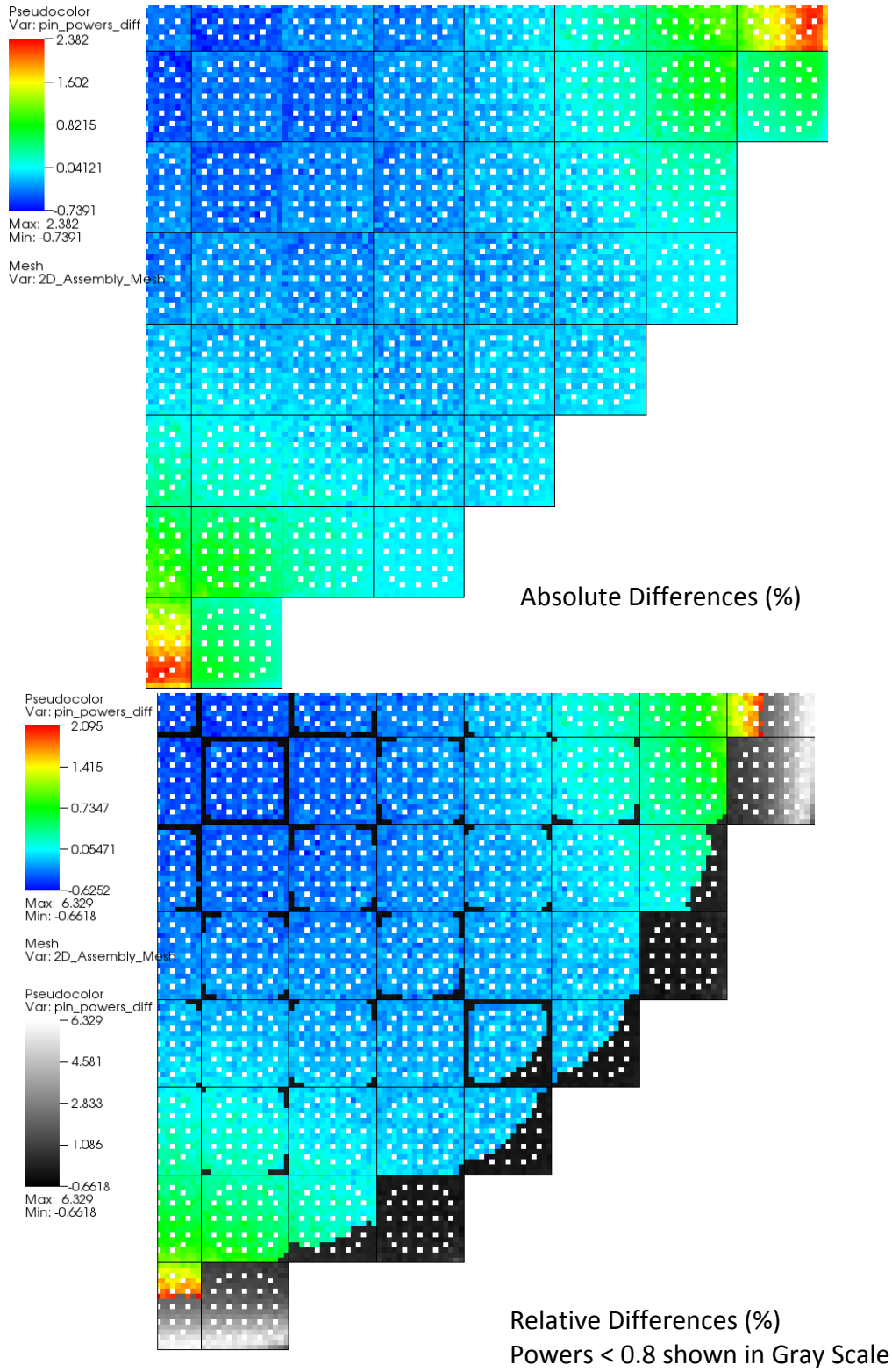

Figure B-4 Radial Pin Power Effects of Shroud Ring

(Case 4 vs. Case 3)

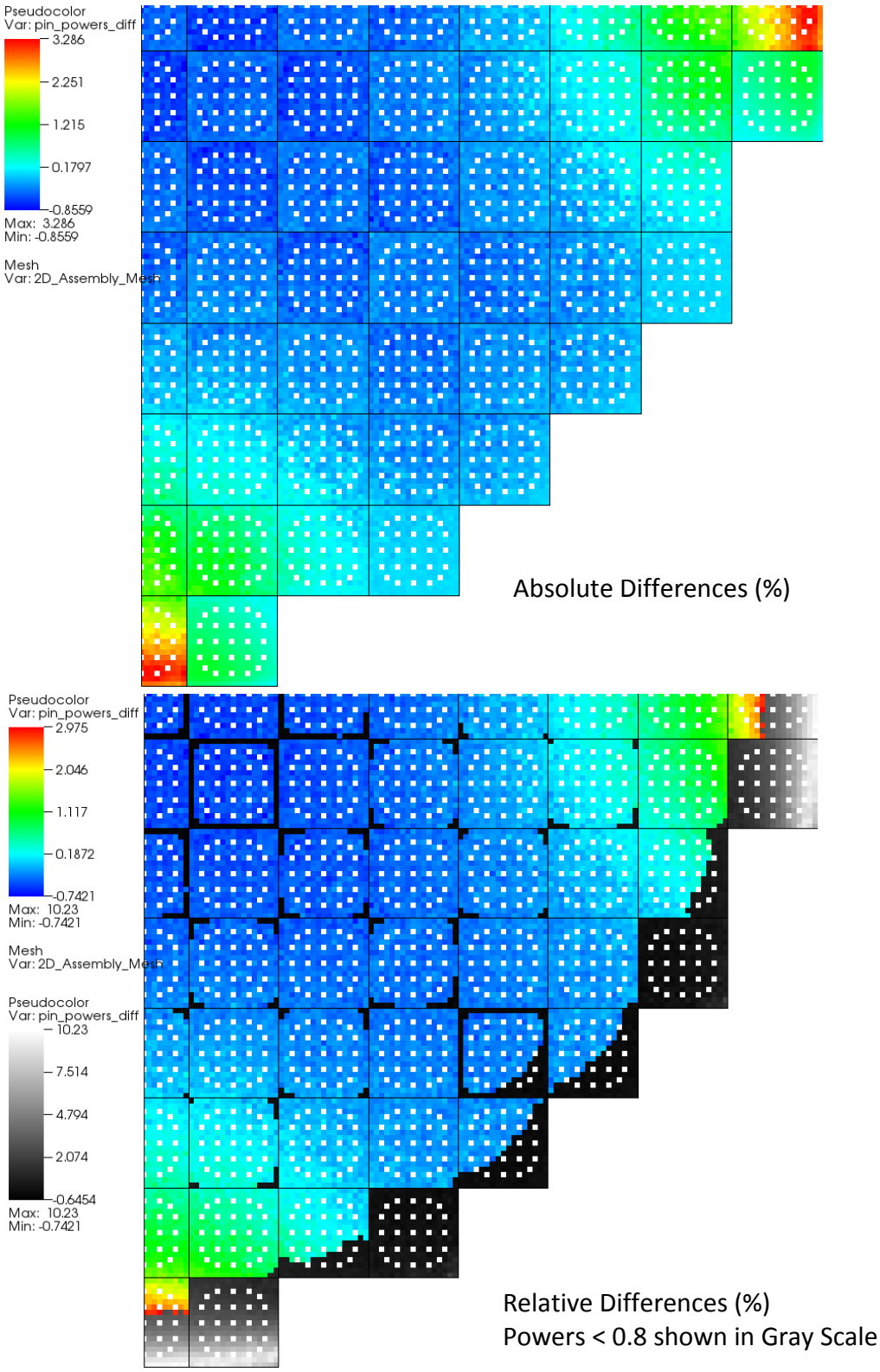

Figure B-5 Radial Pin Power Effects of the Core Barrel, Pads, Vessel, and Shroud Ring

(Case 4 vs. Case 2)

APPENDIX C AXIAL REFLECTOR SENSITIVITY STUDY

The **AP1000** PWR core support structure utilizes six shroud rings approximately equally spaced axially and slightly offset toward the bottom of the core. The height of each ring is roughly equal to the space between rings. These rings can be observed in the axial cut of the KENO model shown in Figure C-1 ("Explicit" ring KENO model on the left of Figure C-1), with reference to Figure 4-10 for the shroud isometric view.

The axial heterogeneity introduced by these rings leads to a bias with respect to the axially uniform reflector model currently supported by VERA[r]. A sensitivity study was thus performed using KENO to quantify the error of modeling the rings as axially homogeneous, by smearing the explicit reflector into a uniform ring which preserves the structural material of the explicit reflector model. The results of this study can inform on the errors associated with an axially uniform reflector implementation[s].

For this study, the 3D KENO results for the explicit and smeared reflector models have been compared in detail. The reference case is the explicit rings model. This has been used in the ZPPT simulations presented in the "Results" Section of this document. The comparison case is the smeared reflector model in which the six shroud rings are smeared into an axially uniform cylinder with same radii as the original rings but extending for the entire active fuel region. Note that the structural material of the explicit model is preserved in the smeared model by artificially reducing the density of the reflector material, approximately in half given the roughly twofold increase in volume of the smeared model. These models are depicted in Figure C-1.

The Monte-Carlo parameters for these KENO simulations are shown in Table C-1. A large number of particles are employed to reduce the statistical uncertainty on the power distribution. While the pin power uncertainty is relative high, the uncertainty in the assembly powers and average axial power shape are adequate for making coarse-mesh comparisons between the smeared and explicit model. Note that the core configuration modeled has several control banks inserted to produce a near-neutral axial offset, thus facilitating axial power shape comparisons. Namely the AO bank is partially inserted in the top of the core, the MA bank is fully inserted and the MB bank is partially inserted in the top of the core.

[r] This is in addition to the bias caused by the current limitation in VERA of modeling only a baffle-type reflector structure radially, which has been discussed in APPENDIX B.
[s] Typical industrial core simulators are also limited to an axially uniform reflector model.

Table C-1 3D Shroud Ring Analysis Monte Carlo Parameters

Total # Particles	25e9
# Particles / Generation	5e6
# Generations	5000
# Skipped Generations	500
# Cores	180
Memory / Core	10.7 GB
Runtime	6.5 days
Eigenvalue Uncertainty	< ± 0.5 pcm
Average Pin Power Uncertainty	± 0.39%
Maximum Pin Power Uncertainty (by Power)	Power < 1.0: ± 4.66% Power > 1.0: ± 1.25%
Max Assembly Power Uncertainty	± 0.14%

The eigenvalues and delta assembly powers for the smeared vs. explicit model are summarized below, and depicted in Figure C-1 through Figure C-3. Specifically, the absolute delta power in % is compared: $(P_{sm}-P_{ex})*100$, with a positive difference indicating an increase in power when using the smeared vs. the explicit model.

- The core reactivity is essentially equivalent for the two models, within the eigenvalue uncertainty of the calculations (0.3 ± 0.7 pcm).
- The axial offset difference is -0.15%. The RMS difference in axial power (integrated on the radial planes) is 0.2%; the maximum % difference in axial power is 0.4%.
- The maximum axially-integrated assembly power difference is 0.2%. See Figure C-3.
- The 3D assembly power RMS difference is 0.2%, with a maximum % difference of 0.7%. The largest differences occur in the peripheral assemblies in proximity of the shroud rings in the explicit model, as expected. See Figure C-4.
- While generally the impact on assembly power does not propagate significantly towards the inner higher-power assemblies, this is not true for the top shroud ring, where the MB peripheral control rod bank is partially inserted, and the bottom of the core without shroud ring in the explicit model, which could be due to power rebalancing effects in conjunction with the effect of the control banks. The impact of statistical noise on the comparison should also not be excluded.

In summary, these studies indicate that an axially heterogeneous reflector modeling capability in VERA-CS is not urgent but should be considered as part of future improvements especially for non-standard reflector models and advanced reactor operation (with insertion of control banks during operation).

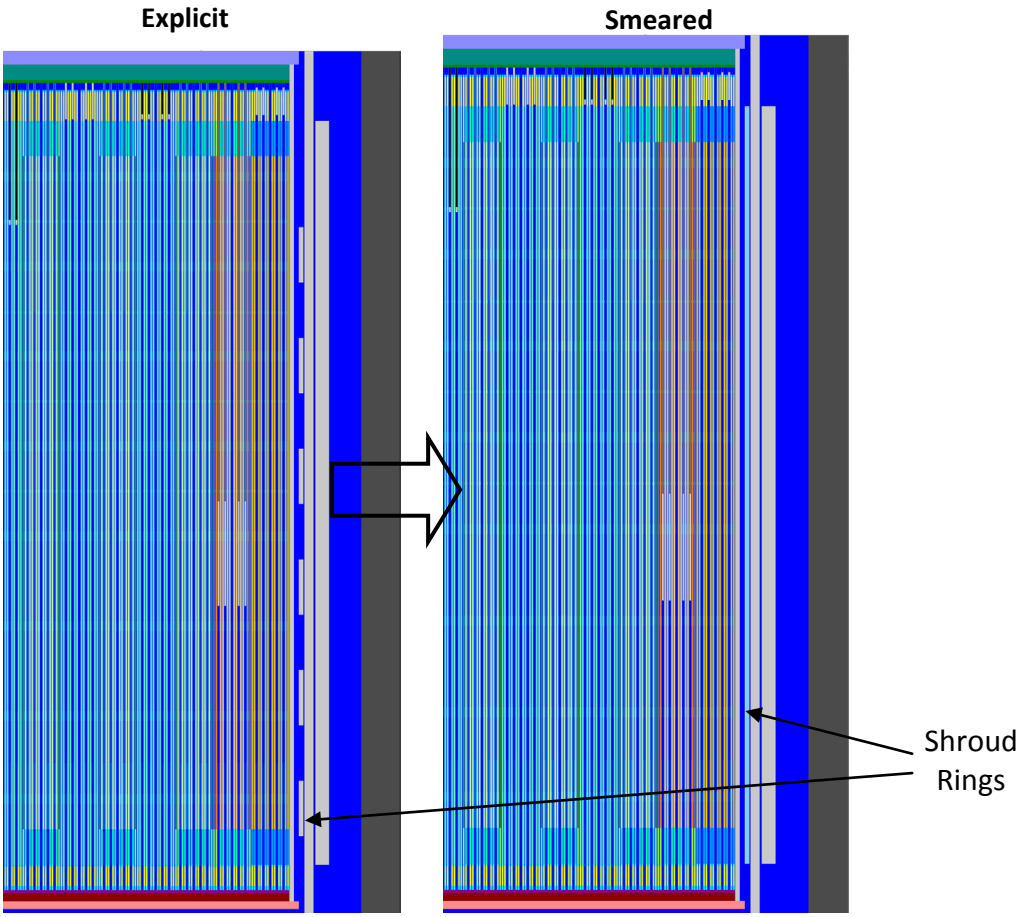

Figure C-1 Axially Smeared Shroud Ring Model

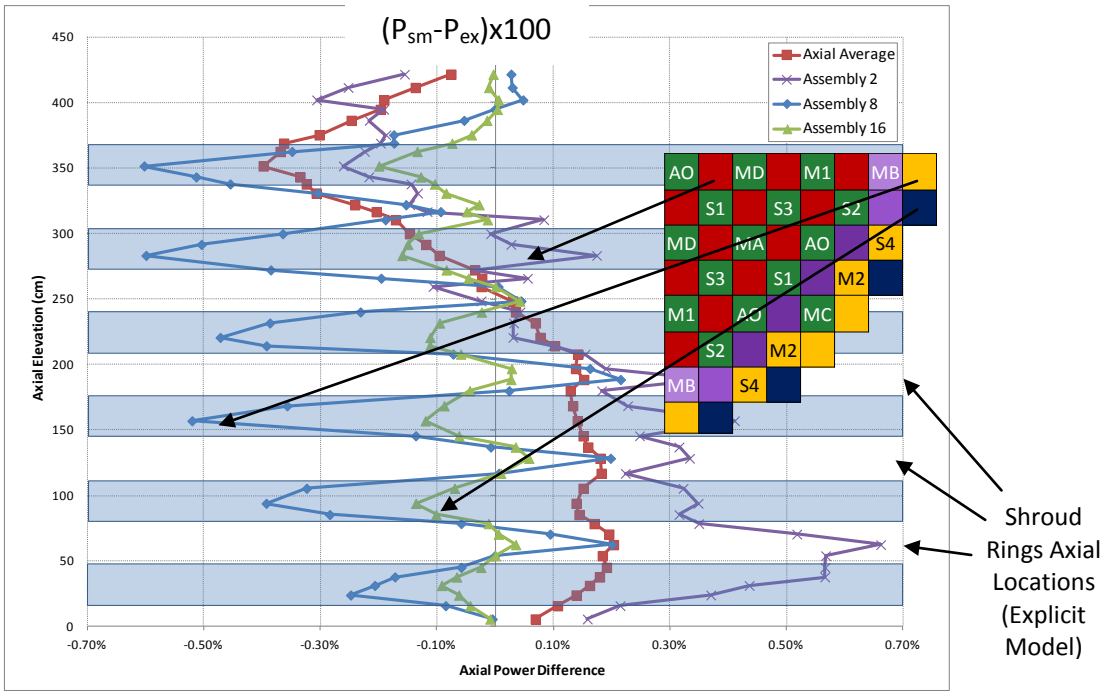

Figure C-2 Axial Power Differences between Explicit and Smeared Shroud Ring Models

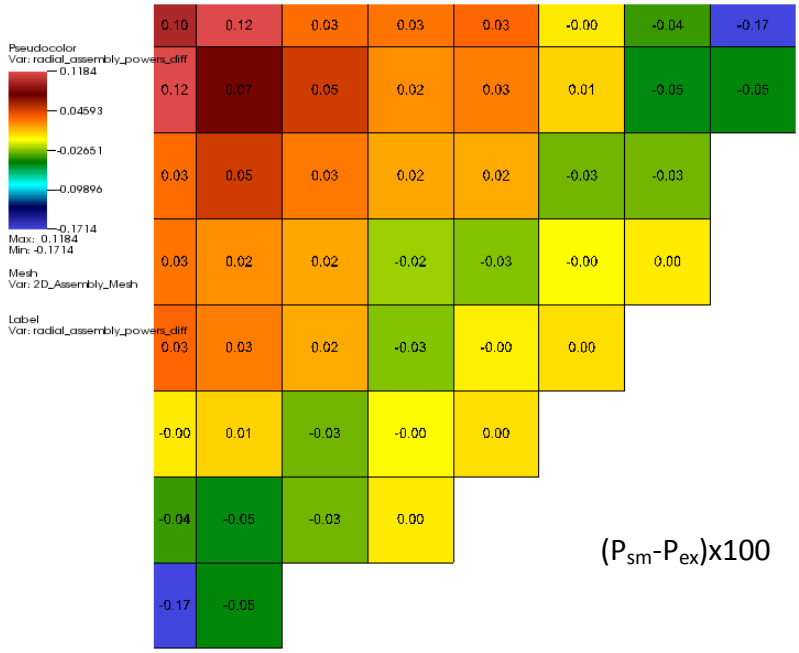

Figure C-3 Radial Power Differences between Explicit and Smeared Shroud Ring Models

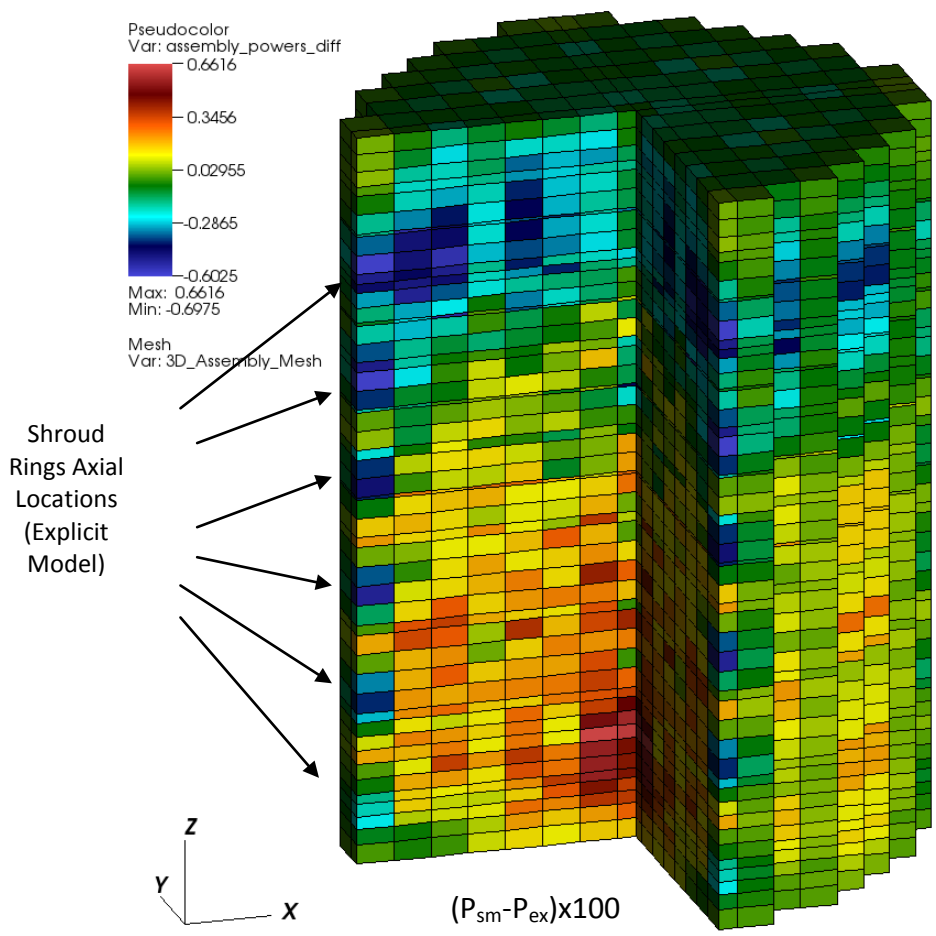

Figure C-4 3D Power Differences between Explicit and Smeared Shroud Ring Models

APPENDIX D KENO ISOTHERMAL TEMPERATURE COEFFICIENT

The HZP ARO isothermal temperature coefficient (ITC) has been estimated for the **AP1000** PWR core using the detailed CE KENO-VI model described in Section 5.3. However, due to the direct approach to using the continuous energy cross section data, KENO cannot easily implement the cross section perturbation approach which is typically employed in industry codes for these types of calculations. Furthermore, the stochastic nature of the Monte Carlo method can result in substantial errors for calculations based on small reactivity changes, if the estimated uncertainty in reactivity represents a significant fraction of the actual reactivity change.

Two main limitations in the current KENO version complicate its use for this type of calculation. First, no temperature interpolation or Doppler broadening is performed[t]. The AMPX data is provided and used directly in the transport calculation. Libraries exist at 565K (the HZP temperature) and 600K, but intermediate temperatures needed for the temperature perturbations (4F to 5K) are not available; in addition, the reactivity trends between 565K and 600K are not necessarily indicative of the trend from small temperature changes.

The second current limitation regards the availability and current use of S(α,β) continuous energy neutron scattering data for the H-1 isotope. The current ENDF/B-VII.0 data includes this data only at 550K and 600K (and other 50K increments), and KENO performs no interpolation, but rather applies the value available in the library at the nearest temperature input in the model. In addition, KENO does not permit different temperatures in isotopes belonging to the same composition (e.g. H-1 and O-16). For these reasons, it is not possible to perform a small moderator temperature perturbation at 565K and, as will be shown, this effect can be significant.

In order to overcome these limitations, the following methodology was utilized for this analysis:

- A new development KENO version has been provided by the ORNL SCALE team which permitted setting the temperature of individual isotopes (mainly H-1) uniquely from other isotopes and compositions. This has been accomplished by manipulation of the cross section data files.
- New Doppler-broadened CE libraries have been created and provided by the ORNL SCALE team at temperatures between 550K and 580K, at 5K increments (six additional libraries). These libraries were generated with AMPX consistent with the methods employed to generate the 565K and 600K library. Note that the S(α,β) data for these libraries remained at either 550K or 600K, depending on which was closest to the library temperature.
- The ITC calculation has been split in three individual simulations, and the results later combined. These three simulations are described below: a Moderator Temperature-Only Coefficient, a Moderator Density Coefficient (MDC) and a Doppler Temperature Coefficient (DTC).

[t] Research into on-the-fly Doppler broadening is ongoing at ORNL and this capability will be available soon.

- Rather than directly using the reactivity delta from single state-point calculations at few perturbed temperatures, that can be sensitive to non-physical variation from the Monte Carlo stochastic process, results have been generated for all temperatures between 550K and 580K. These reactivity points have then been fit with a polynomial, and the slope of the curve at the 565K ITC temperature has been used as representative of the relevant reactivity coefficient (e.g. MTC, MDC and DTC). This method ensures that the reactivity coefficient calculation relies on a smoothly varying reactivity trend vs. temperature.
- The uncertainty in the above procedure is estimated using a separate Monte Carlo sampling procedure. The uncertainties of each of the input KENO eigenvalues were propagated to the final coefficients by sampling each data point from a normal distribution based on the calculated KENO mean and sigma, and fitting the calculated data as described in the previous item. 100,000 ITC values were calculated in this manner, each based on sixteen independently sampled eigenvalues. The final uncertainty in the calculated ITC was estimated as the standard deviation of this population of 100,000 ITC values.

The KENO cases used for these calculations relied on 5e9 particles (1000 generations with 5e6 particles per generation, skipping the first 250 generations). Each calculation took approximately 29 hours on 180 cores. The results of counterpart simulations performed using VERA are also plotted in the following sections. It will be shown that the trends with temperature for each of the reactivity coefficient components are similar for KENO and VERA, except some differences noted in the Moderator Density Coefficient predictions. This consistent behavior provides good confidence in the overall appropriateness of the methodology adopted and the results obtained for these calculations.

1. Moderator Temperature-Only Coefficient

The worth of the **AP1000** PWR moderator temperature was calculated by perturbing the H-1 temperature from 550K to 600K. As mentioned, due to the lack of temperature interpolation on the scattering data, these are the only temperatures for which KENO calculations are possible. Thus, these simulations capture essentially the reactivity worth of the change in S(α,β) data over a 50K temperature interval from 550K to 600K. The trend is assumed to be linear, and calculations performed at 500K have confirmed this. The results are shown in Table D-1 and plotted in Figure D-1. Figure D-1 shows also the trend in eigenvalue obtained from VERA for counterpart simulations perturbing the moderator temperature, which is in very good agreement with KENO: -0.73 pcm/F for VERA vs. -0.66 ± 0.02 pcm/F for KENO. It should be noted that this not a typical MTC calculation, where both density and temperature are perturbed simultaneously. The impact of the density variation is assessed separately.

Note also that the KENO result implies that all KENO core eigenvalues calculated at 565K should be adjusted by **-18 pcm** for the lack of temperature dependence in the S(α,β) scattering data treatment. The KENO results reported in Section 6 incorporate this adjustment.

Table D-1 Moderator Temperature-Only Reactivity Coefficient

Temperature (K)	Eigenvalue
550	1.000840 ± 0.000014
600	1.000242 ± 0.000014
Coefficient	**-0.66 ± 0.02 pcm/F**

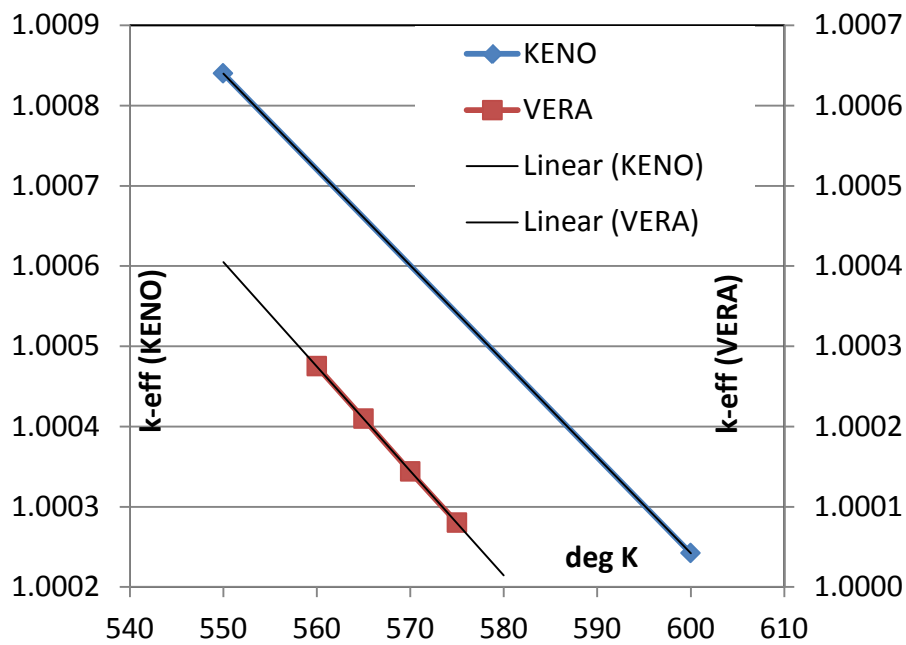

Figure D-1 KENO and VERA Reactivity vs. Moderator Temperature

2. Moderator Density Coefficient (MDC)

The KENO moderator density calculations were performed at 565K for all materials except for H-1, which used the nearest temperature of 550K, and the corresponding water density at each temperature between 550K and 580K, in 5K increments. The results are provided in Table D-2 and Figure D-2. Figure D-2 shows also the trend in eigenvalue from counterpart simulations performed with VERA. The MDC was calculated by evaluating the derivative of the parabolic fit at 565K, amounting to -0.45 ± 0.03 pcm/F for KENO and -0.77 pcm/F for VERA. The discrepancy in the MDC prediction accounts for the majority of the difference observed in the MTC and ITC predictions in KENO and VERA.

Combining the moderator density and temperature components, the effective Moderator Temperature Coefficient (MTC) for the **AP1000** PWR core is predicted to be **-1.12 ± 0.04 pcm/F for KENO vs. -1.50 pcm/F for VERA**.

Table D-2 Moderator Density Reactivity Coefficient

Temperature (K)	Density (g/cc)	Eigenvalue
550	0.76972	1.000850 ± 0.000016
555	0.76106	1.000845 ± 0.000016
560	0.75207	1.000855 ± 0.000013
565	0.74271	1.000840 ± 0.000014
570	0.73294	1.000770 ± 0.000012
575	0.72269	1.000716 ± 0.000012
580	0.71190	1.000583 ± 0.000013
Coefficient	**-0.45 ± 0.03 pcm/F**	

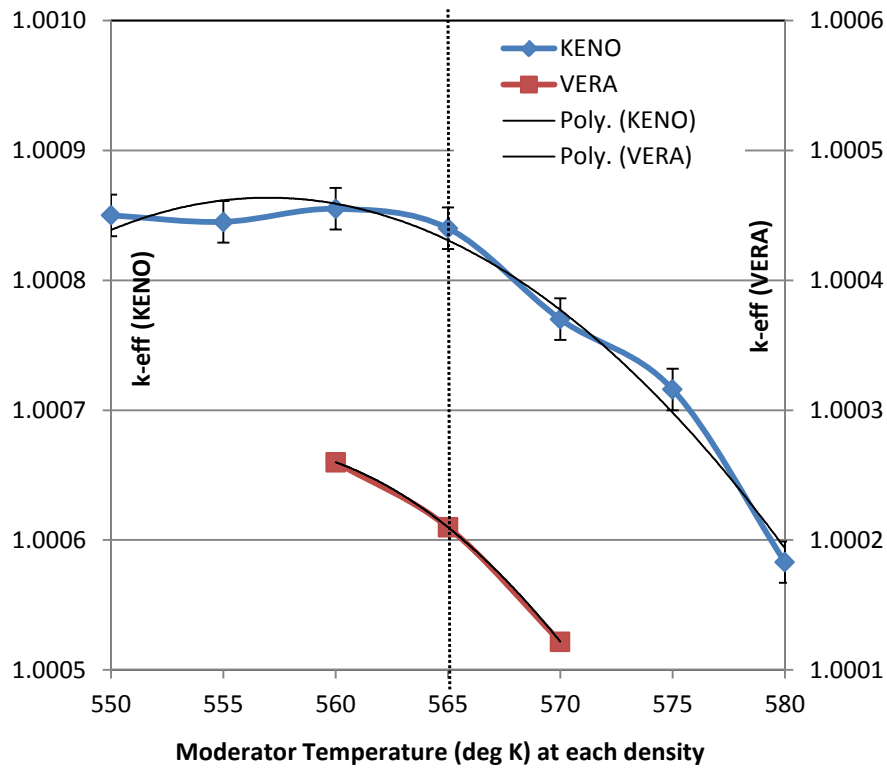

Figure D-2 KENO Reactivity vs. Moderator Density

3. Doppler Temperature Coefficient (DTC)

The KENO DTC is estimated using the Doppler-broadened libraries provided by the SCALE development team at 5K temperature increments. The temperature of all materials and isotopes other than H-1 is perturbed along with the fuel temperature. Calculations have been

performed showing very small reactivity worth from the temperature of these other material; less than the estimated eigenvalue uncertainty. For these KENO simulations, the H-1 temperature is fixed at 550K and the moderator density is held at the 565K value. The results are provided in Table D-3 and Figure D-3 . Figure D-3 shows also the trend in eigenvalue from counterpart simulations performed with VERA. The **DTC** was calculated by evaluating the derivative of the linear fit at 565K, which is **-1.58 ± 0.03 pcm/F for KENO** vs. **-1.72 pcm/F for VERA.**

Table D-3 Doppler Temperature Reactivity Coefficient

Temperature (K)	Eigenvalue
550	1.001409 ± 0.000013
555	1.001243 ± 0.000013
560	1.001132 ± 0.000013
565	1.000964 ± 0.000013
570	1.000847 ± 0.000012
575	1.000726 ± 0.000012
580	1.000554 ± 0.000013
Coefficient	**-1.54 ± 0.03 pcm/F**

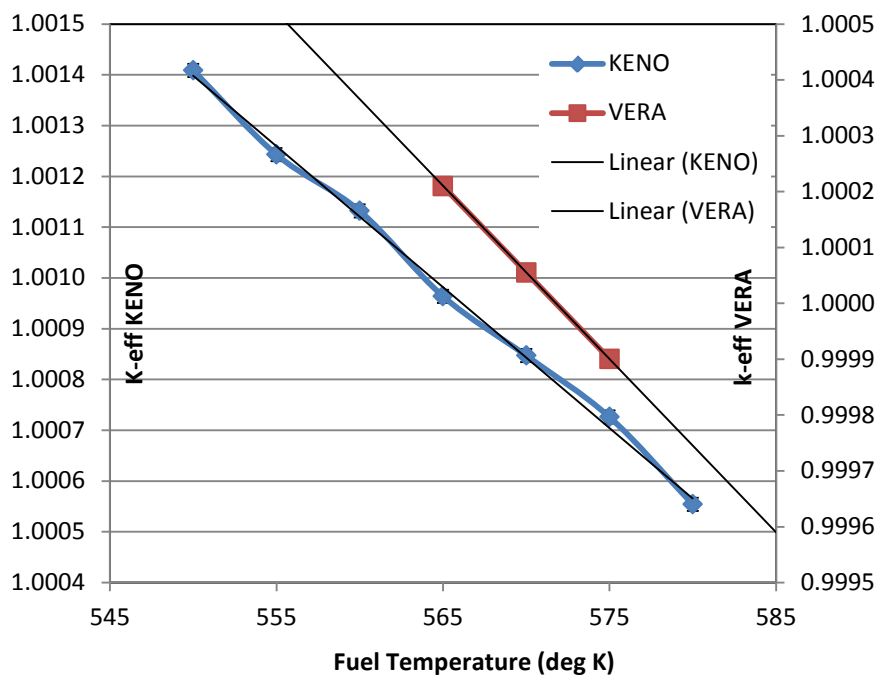

Figure D-3 KENO Reactivity vs. Fuel Temperature

Combining the moderator temperature and fuel temperature components, the Isothermal Temperature Coefficient (ITC) for the **AP1000 PWR core** is predicted to be **-2.66 ± 0.05 pcm/F**

from KENO and **-3.22 pcm/F from VERA**. The reported KENO uncertainty is an estimate, as previously discussed, and is below the measurement uncertainty for the ITC.

APPENDIX E KENO VERIFICATION AGAINST MCNP

CE KENO-VI has been extensively utilized as the numeric reference solution for the **AP1000** PWR configurations discussed in this report. In order to demonstrate confidence in the KENO data and methods, comparisons of the eigenvalue and pin power (normalized fission rate) distributions for the 2D 17x17 PWR lattices described in Ref. 9 obtained with KENO and the Monte-Carlo particle transport code MCNP5 are provided. These comparisons are shown in the table below, and indicate an outstanding agreement in eigenvalue and power distribution between KENO and MCNP5.

MCNP5 is a general-purpose Monte Carlo N–Particle code that can be used for neutron, photon, electron, or coupled neutron/photon/electron transport, including the capability to calculate eigenvalues for critical systems (Ref. 10). The ENDF/B-VII.0 continuous energy data libraries at 600K were used in this analysis.

Table E-1 2D 17x17 Lattice Comparisons between KENO and MCNP

Case	Lattice Description	MCNP k-inf	KENO Difference (pcm)	KENO Pin Power RMS (%)	KENO Pin Power Max (%)
2A	565K	1.18189	38	0.040	0.096
2B	600K	1.18303	40	0.050	0.148
2C	900K	1.17378	4	0.059	0.138
2D	1200K	1.16598	-39	0.064	0.185
2E	12 Pyrex	1.06915	49	0.061	0.192
2F	24 Pyrex	0.97529	65	0.057	0.154
2G	24 AIC	0.84682	90	0.061	0.177
2H	24 B4C	0.78723	99	0.077	0.233
2I	Instrument Thimble	1.17959	39	0.069	0.189
2J	Instrument + 24 Pyrex	0.97456	66	0.068	0.172
2K	Zoned + 24 Pyrex	1.01952	54	0.057	0.180
2L	80 IFBA	1.01844	38	0.061	0.149
2M	128 IFBA	0.93841	39	0.069	0.183
2N	104 IFBA + 20 WABA	0.86901	58	0.060	0.138
2O	12 Gadolinia	1.04735	35	0.061	0.171
2P	24 Gadolinia	0.92692	44	0.075	0.205
	Average		**45**	**0.062%**	**0.172%**

For MCNP, 1e8 particle histories were used with 2000 cycles and 50,000 particles per cycle (and 100 skipped cycles), resulting in eigenvalue uncertainties less than 7 pcm and individual pin power uncertainties less than 0.1%.

The KENO version employed for this comparison is the same as that discussed in Section 5.3. It is a pre-release version of SCALE 6.2 Beta. The KENO calculations rely on 1e9 particle histories, with 2750 cycles and 400,000 particles per generation, and 250 skipped cycles. The resulting uncertainties are <3 pcm and <0.06% individual pin power.

APPENDIX F VERA INSTALLATION GUIDE

The VERA Installation Guide is a living document compiled to guide future (and current) system administrators through the process of system preparation to receive VERA and its components. This includes setting up the system security/permissions, network connections, and file system. It also includes retrieving VERA, building prerequisites and the calculation tools, performing unit tests, and ultimately deploying VERA for end-users.

The guide is a ReStructured Text (.rst) file which is a simple markup-based ASCII file format that can be converted into any of several more-readable formats such as PDF or HTML. Because of the length and level of detail of the guide, it will not be reproduced here, but rather representative samples will be shown to demonstrate the working and final forms of the guide.

Note that when VERA is retrieved from the repository, a copy of the guide is provided in triplicate (as .rst, .pdf, and .html files) in the documentation area. This provides those working with the guide a means to both follow the guide more easily and to record deviations and/or suggested changes to be passed back to the maintainers of VERA and its distribution systems.

```
Documentation For Installed VERA Components
-------------------------------------------

Once installed, information on how to access the installed VERA components
along wi

  <insta
    READ

Appendix
========

Set Up R
--------

In order
outside
login1.o
the 3-ch
machine
Git and

In one's

  ~/.ssh

which co

  host t
  Hostna
  User <
  LocalF
  LocalF

  Host c
  HostKe
  Hostna
  Port 2
  User <

  Host u
```

```
For a given compiler set, TPLs can be installed for different configurations,
such as debug (dbg), optimized (opt), or other variations
(e.g. dbg-checkedstl).  The standard TPL install, and the one used in this
guide as

  TPL_IN

All of t

* VERA_D
* VERA_D
* TPL_IN

to deter
building.

Initial
=======

Before a
setup is
performe
VERA Dev
componen

Requesti
--------

Before o
one must
and be g
to the C
to get s
list of

System C
--------

Before w
```

```
=========================
 VERA Installation Guide
=========================

:Author: Roscoe A. Bartlett (bartlettra@ornl.gov)
:Author: Mark Baird (bairdml@ornl.gov)
:Author: Joel A. Kulesza (kuleszj@westinghouse.com)

.. sectnum::

.. contents::


Introduction
============

This guide describes the structure and setup of the standard VERA development
environment (VERA Dev Env) and standard Third Party Libraries (TPLs) that need
to be in place before installing many of the VERA simulation components.  It
describes everything from the initial setup on a new machine to the final
builds and testing of VERA components.  The goal of this document is to
describe how to create the directories and contents outlined in `Standard VERA
Dev Env Directory Structure`_, which once finished, allows one to clone the
VERA git source repositories and build any of the necessary VERA components on a
given system.

WARNING: This guide only describes the installation of the VERA Dev Env and
TPLs and does not contain specific information about specific VERA simulation
components.  That information is found in other sources.  Please consult with
a CASL representative about what VERA components are available to install from
source and what capabilities they provide.  Mention of other VERA repositories
in only used as examples and may not even be up to date.


Standard VERA Dev Env Directory Structure
=========================================

The standard directory structure for the installation of the VERA Development
Environment (VERA Dev Env) is given below::

  ${VERA_DEV_ENV_BASE}/
    common_tools/
      cmake-2.8.5/
```

Figure F-1 Example of VERA Installation Guide ReStructured Text File

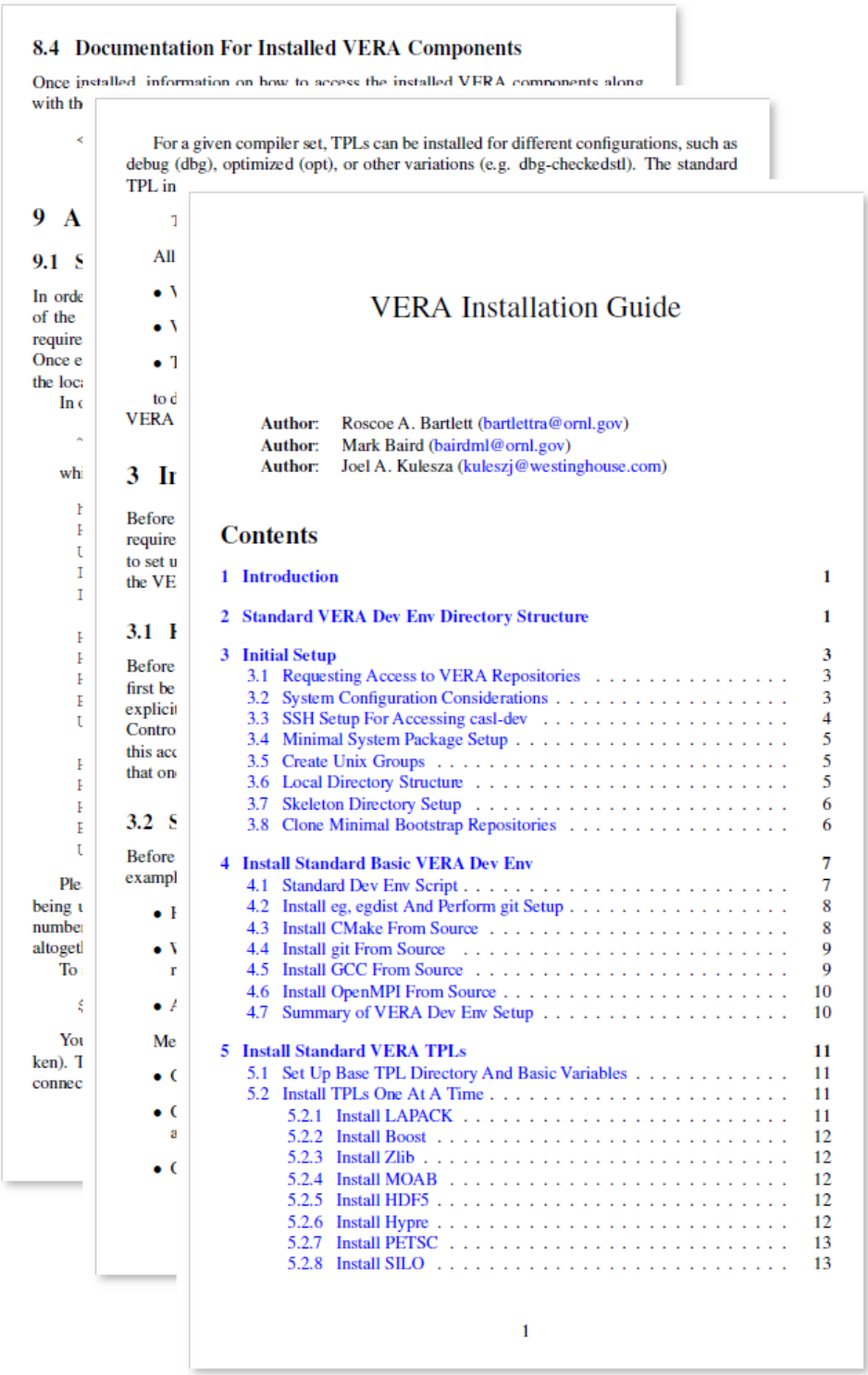

8.4 Documentation For Installed VERA Components

For a given compiler set, TPLs can be installed for different configurations, such as debug (dbg), optimized (opt), or other variations (e.g. dbg-checkedstl). The standard TPL in

VERA Installation Guide

Author: Roscoe A. Bartlett (bartlettra@ornl.gov)
Author: Mark Baird (bairdml@ornl.gov)
Author: Joel A. Kulesza (kuleszj@westinghouse.com)

Contents

1 Introduction 1
2 Standard VERA Dev Env Directory Structure 1
3 Initial Setup 3
3.1 Requesting Access to VERA Repositories 3
3.2 System Configuration Considerations 3
3.3 SSH Setup For Accessing casl-dev 4
3.4 Minimal System Package Setup 5
3.5 Create Unix Groups 5
3.6 Local Directory Structure 5
3.7 Skeleton Directory Setup 6
3.8 Clone Minimal Bootstrap Repositories 6
4 Install Standard Basic VERA Dev Env 7
4.1 Standard Dev Env Script 7
4.2 Install eg, egdist And Perform git Setup 8
4.3 Install CMake From Source 8
4.4 Install git From Source 9
4.5 Install GCC From Source 9
4.6 Install OpenMPI From Source 10
4.7 Summary of VERA Dev Env Setup 10
5 Install Standard VERA TPLs 11
5.1 Set Up Base TPL Directory And Basic Variables 11
5.2 Install TPLs One At A Time 11
5.2.1 Install LAPACK 11
5.2.2 Install Boost 12
5.2.3 Install Zlib 12
5.2.4 Install MOAB 12
5.2.5 Install HDF5 12
5.2.6 Install Hypre 12
5.2.7 Install PETSC 13
5.2.8 Install SILO 13

1

Figure F-2 Example of VERA Installation Guide PDF File

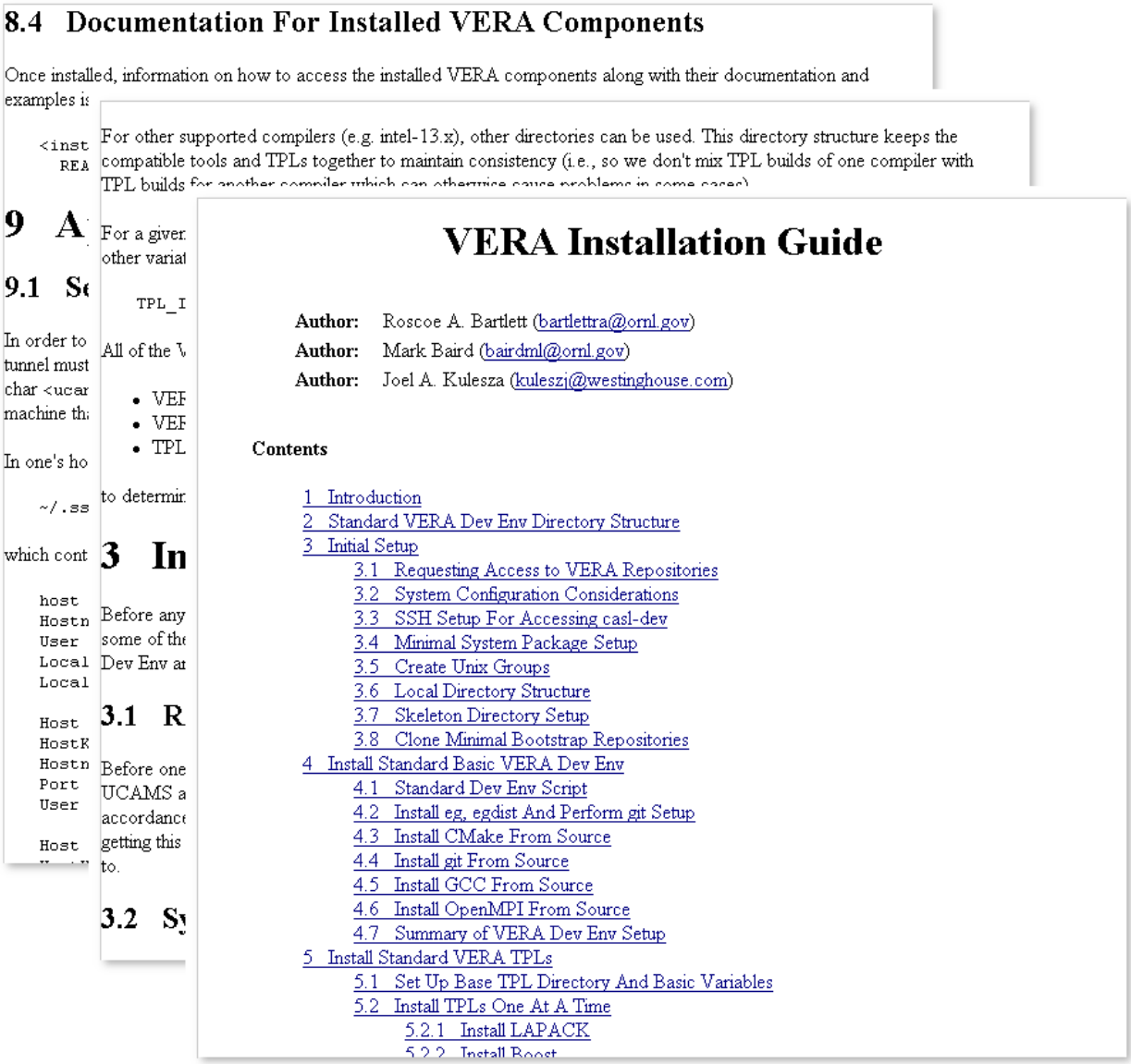

8.4 Documentation For Installed VERA Components

Once installed, information on how to access the installed VERA components along with their documentation and examples is

For other supported compilers (e.g. intel-13.x), other directories can be used. This directory structure keeps the compatible tools and TPLs together to maintain consistency (i.e., so we don't mix TPL builds of one compiler with TPL builds

VERA Installation Guide

Author: Roscoe A. Bartlett (bartlettra@ornl.gov)
Author: Mark Baird (bairdml@ornl.gov)
Author: Joel A. Kulesza (kuleszj@westinghouse.com)

Contents

1 Introduction
2 Standard VERA Dev Env Directory Structure
3 Initial Setup
3.1 Requesting Access to VERA Repositories
3.2 System Configuration Considerations
3.3 SSH Setup For Accessing casl-dev
3.4 Minimal System Package Setup
3.5 Create Unix Groups
3.6 Local Directory Structure
3.7 Skeleton Directory Setup
3.8 Clone Minimal Bootstrap Repositories
4 Install Standard Basic VERA Dev Env
4.1 Standard Dev Env Script
4.2 Install eg, egdist And Perform git Setup
4.3 Install CMake From Source
4.4 Install git From Source
4.5 Install GCC From Source
4.6 Install OpenMPI From Source
4.7 Summary of VERA Dev Env Setup
5 Install Standard VERA TPLs
5.1 Set Up Base TPL Directory And Basic Variables
5.2 Install TPLs One At A Time
5.2.1 Install LAPACK

Figure F-3 Example of VERA Installation Guide HTML File

APPENDIX G VERA AP1000 PWR INPUT

A sample **AP1000** PWR 3D core VERAIN input deck is given below.

```
[CASEID]
  title 'AP1000 PWR: ARO'
[STATE]
  power     0.0              ! %
  tinlet    557.33           ! F
  tfuel     565.0            ! K
  modden    0.7441292        ! g/cc
  boron     1321             ! ppmB
  sym       qtr
  feedback  off

  rodbank
   AO 264
   MA 264
   MB 264
   MC 264
   MD 264
   M1 264
   M2 264
   S1 264
   S2 264
   S3 264
   S4 264

[CORE]
  size   15           ! Assemblies across core
  apitch 21.50        ! All dimensions cm
  height 479.88       !
  ratd   3400         ! MW

  baffle ss 0.127 2.54

  lower_plate ss  4.44  0.68
  upper_plate ss  7.62  0.59
  lower_ref   mod 2.54  1.0

 core_shape             ! 1=assembly,
0=nothing/reflector (depending on other parameters)
    0 0 0 0 0 0 1 1 1 0 0 0 0 0 0
    0 0 0 0 1 1 1 1 1 1 1 0 0 0 0
    0 0 0 1 1 1 1 1 1 1 1 1 0 0 0
    0 0 1 1 1 1 1 1 1 1 1 1 1 0 0
    0 1 1 1 1 1 1 1 1 1 1 1 1 1 0
    0 1 1 1 1 1 1 1 1 1 1 1 1 1 0
    1 1 1 1 1 1 1 1 1 1 1 1 1 1 1
    1 1 1 1 1 1 1 1 1 1 1 1 1 1 1
    1 1 1 1 1 1 1 1 1 1 1 1 1 1 1
    0 1 1 1 1 1 1 1 1 1 1 1 1 1 0
    0 1 1 1 1 1 1 1 1 1 1 1 1 1 0
    0 0 1 1 1 1 1 1 1 1 1 1 1 0 0
    0 0 0 1 1 1 1 1 1 1 1 1 0 0 0
    0 0 0 0 1 1 1 1 1 1 1 0 0 0 0
    0 0 0 0 0 0 1 1 1 0 0 0 0 0 0

  assm_map
    158E0I
    420E68I  158E0I
    158E0I   420E68I 158E0I
    420E68I  158E0I  420E68I  158E0I
    158E0I   420E68I 158E0I   480E124I 158E0I
    420E68I  158E0I  480E124I 320E0I   320E0I
    480E124I 480E88I 320E0I   074E0I
    320E0I   074E0I

  insert_map
    -
    12W -
    -   12W -
    12W -   12W -
    -   12W -   8W  -
    12W -   8W  - -
    -   4W  -  -
    -   -
```

```
  crd_map
    AIC
    -   AIC
    W   -   W
    -   AIC -   AIC
    AIC -   AIC -   W
    -   AIC -   AIC -
    W   -   AIC -
    -   -

  crd_bank
    AO
    -  S1
    MD -  MA
    -  S3 -  S1
    M1 -  AO -  MC
    -  S2 -  M2 -
    MB -  S4 -
    -  -

 fuel U074   10.28 94.354 / 0.740   u-234=0.0056 u-236=0.00
 fuel U158   10.28 94.354 / 1.580   u-234=0.0130 u-236=0.0019
 fuel U158B  10.30 94.641 / 1.580   u-234=0.0130 u-236=0.0019
 fuel U320   10.28 94.354 / 3.200   u-234=0.0277 u-236=0.0006
 fuel U320B  10.30 94.641 / 3.200   u-234=0.0277 u-236=0.0006
 fuel U320AB 10.37 94.354 / 3.200   u-234=0.0277 u-236=0.0006
 fuel U340   10.28 94.354 / 3.400   u-234=0.0296 u-236=0.0008
 fuel U380   10.28 94.354 / 3.800   u-234=0.0347 u-236=0.0010
 fuel U400   10.28 94.354 / 4.000   u-234=0.0363 u-236=0.0010
 fuel U420   10.28 94.354 / 4.200   u-234=0.0388 u-236=0.0008
 fuel U440   10.28 94.354 / 4.400   u-234=0.0392 u-236=0.0029
 fuel U480   10.28 94.354 / 4.800   u-234=0.0449 u-236=0.0147

  mat zirlo    6.5
  mat zirc4    6.5
  mat he       0.0001786
  mat ifba     3.28 zrb2
  mat ss       7.8
  mat ssspring 1.5 ss
  mat aic      10.1
  mat tungsten 19.2
  mat inc      8.2
  mat waba     2.36
  mat al2o3    2.56

[ASSEMBLY]
  npin 17
  ppitch 1.26

! Guide Tube and Instrument Tube
  cell 011                              0.56134 0.61214 /                    mod   zirlo ! IT, and GT above dashpot
  cell 012                              0.52066 0.61214 /                    mod   zirlo ! GT below dashpot
  cell 013                              0.56134  0.61214 /                   mod   zirlo ! IT
! Fuel, Region A
  cell 111           0.409575           0.41783  0.47498 /         U074      he    zirlo
! Fuel, Region B
  cell 211           0.409575           0.41783  0.47498 /         U158      he    zirlo
! Fuel, Region C
  cell 311           0.409575           0.41783  0.47498 /         U320      he    zirlo
  cell 331           0.409575           0.41783  0.47498 /         U158B     he    zirlo
```

```
! Fuel, Region D
  cell 411           0.409575           0.41783  0.47498 /         U340      he    zirlo
  cell 412           0.409575           0.41783  0.47498 /         U380      he    zirlo
  cell 413           0.409575           0.41783  0.47498 /         U420      he    zirlo
  cell 421           0.409575  0.410083 0.41783  0.47498 /  U340   ifba      he    zirlo
  cell 422           0.409575  0.410083 0.41783  0.47498 /  U380   ifba      he    zirlo
  cell 423           0.409575  0.410083 0.41783  0.47498 /  U420   ifba      he    zirlo
  cell 431           0.409575           0.41783  0.47498 /         U320B     he    zirlo
  cell 432  0.19685  0.409575           0.41783  0.47498 /  he     U320AB    he    zirlo
! Fuel, Region E
  cell 511           0.409575           0.41783  0.47498 /         U400      he    zirlo
  cell 512           0.409575           0.41783  0.47498 /         U440      he    zirlo
  cell 513           0.409575           0.41783  0.47498 /         U480      he    zirlo
  cell 521           0.409575  0.410083 0.41783  0.47498 /  U400   ifba      he    zirlo
  cell 522           0.409575  0.410083 0.41783  0.47498 /  U440   ifba      he    zirlo
  cell 523           0.409575  0.410083 0.41783  0.47498 /  U480   ifba      he    zirlo
  cell 531           0.409575           0.41783  0.47498 /         U320B     he    zirlo
  cell 532  0.19685  0.409575           0.41783  0.47498 /  he     U320AB    he    zirlo

  cell 601 0.47498 / zirlo                                        ! bottomplug
  cell 602 0.35  0.4039 0.41783  0.47498 / he zirlo he zirlo    ! stand off tube
  cell 610 0.1   0.4039 0.417830 0.47498 / he zirlo he zirlo    ! pellet stack base
  cell 603 0.24  0.37   0.417830 0.47498 / he ssspring he zirlo ! plenum
  cell 604 0.47498 / zirlo                                        ! endplug
  cell 605 0.47498 / mod                                          ! topgap

lower_nozzle ss 6.4     6000 ! mat, height, mass (g)
upper_nozzle ss 10.6    8000 ! mat, height, mass (g)
```

```
axial 074E0I
                 6.4
   BOTPLUG       8.6
   BOTSTANDOFF  19.8
   PELLETBASE   20.9
   BOTFUEL1     79.3
   TOPFUEL1    447.6
   PLENUM      464.1
   ENDPLUG     465.2
   TOPGAP      469.3
```

```
axial 158E0I
                 6.4
   BOTPLUG       8.6
   BOTSTANDOFF  19.8
   PELLETBASE   20.9
   BOTFUEL2     79.3
   TOPFUEL2    447.6
   PLENUM      464.1
   ENDPLUG     465.2
   TOPGAP      469.3
```

```
axial 320E0I
                 6.4
   BOTPLUG       8.6
   BOTSTANDOFF  19.8
   PELLETBASE   20.9
   BOTBLK3      41.2
   BOTFUEL3     79.3
   TOPFUEL3    427.3
   TOPBLK3     447.6
   PLENUM      464.1
   ENDPLUG     465.2
   TOPGAP      469.3
```

```
axial 420E68I
                 6.4
   BOTPLUG       8.6
   BOTSTANDOFF  19.8
   PELLETBASE   20.9
   BOTBLK3      41.2
   BOTFUEL3     79.3
   TOPFUEL3    427.3
   TOPBLK3     447.6
   PLENUM      464.1
   ENDPLUG     465.2
   TOPGAP      469.3
```

```
axial 480E88I
                 6.4
   BOTPLUG       8.6
   BOTSTANDOFF  19.8
   PELLETBASE   20.9
   BOTBLK3      41.2
   BOTFUEL3     79.3
   TOPFUEL3    427.3
   TOPBLK3     447.6
   PLENUM      464.1
   ENDPLUG     465.2
   TOPGAP      469.3
```

```
axial 480E124I
                 6.4
   BOTPLUG       8.6
   BOTSTANDOFF  19.8
   PELLETBASE   20.9
   BOTBLK3      41.2
   BOTFUEL3     79.3
   TOPFUEL3    427.3
   TOPBLK3     447.6
   PLENUM      464.1
   ENDPLUG     465.2
   TOPGAP      469.3
```

```
lattice BOTPLUG
  013
  601 601
  601 601 601
  012 601 601 012
  601 601 601 601 601
  601 601 601 601 601 012
  012 601 601 012 601 601 601
  601 601 601 601 601 601 601 601
  601 601 601 601 601 601 601 601 601

lattice BOTSTANDOFF
  013
  602 602
  602 602 602
  012 602 602 012
  602 602 602 602 602
  602 602 602 602 602 012
  012 602 602 012 602 602 602
  602 602 602 602 602 602 602 602
  602 602 602 602 602 602 602 602 602

lattice PELLETBASE
  013
  610 610
  610 610 610
  012 610 610 012
  610 610 610 610 610
  610 610 610 610 610 012
  012 610 610 012 610 610 610
  610 610 610 610 610 610 610 610
  610 610 610 610 610 610 610 610 610

lattice PLENUM
  013
  603 603
  603 603 603
  011 603 603 011
  603 603 603 603 603
  603 603 603 603 603 011
  011 603 603 011 603 603 603
  603 603 603 603 603 603 603 603
  603 603 603 603 603 603 603 603 603

lattice ENDPLUG
  013
  604 604
  604 604 604
  011 604 604 011
  604 604 604 604 604
  604 604 604 604 604 011
  011 604 604 011 604 604 604
  604 604 604 604 604 604 604 604
  604 604 604 604 604 604 604 604 604

lattice TOPGAP
  013
  605 605
  605 605 605
  011 605 605 011
  605 605 605 605 605
  605 605 605 605 605 011
  011 605 605 011 605 605 605
  605 605 605 605 605 605 605 605
  605 605 605 605 605 605 605 605 605

! Fuel, Region A
  lattice TOPFUEL1
  013
  111 111
  111 111 111
  011 111 111 011
  111 111 111 111 111
  111 111 111 111 111 011
  011 111 111 011 111 111 111
  111 111 111 111 111 111 111 111
  111 111 111 111 111 111 111 111 111

  lattice BOTFUEL1
  013
  111 111
  111 111 111
  012 111 111 012
  111 111 111 111 111
  111 111 111 111 111 012
  012 111 111 012 111 111 111
  111 111 111 111 111 111 111 111
  111 111 111 111 111 111 111 111 111
```

```
! Fuel, Region B
  lattice TOPFUEL2
    013
    211 211
    211 211 211
    011 211 211 011
    211 211 211 211 211
    211 211 211 211 211 011
    011 211 211 011 211 211 211
    211 211 211 211 211 211 211 211
    211 211 211 211 211 211 211 211 211

  lattice BOTFUEL2
    013
    211 211
    211 211 211
    012 211 211 012
    211 211 211 211 211
    211 211 211 211 211 012
    012 211 211 012 211 211 211
    211 211 211 211 211 211 211 211
    211 211 211 211 211 211 211 211 211

! Fuel, Region C
  lattice TOPFUEL3
    013
    311 311
    311 311 311
    011 311 311 011
    311 311 311 311 311
    311 311 311 311 311 011
    011 311 311 011 311 311 311
    311 311 311 311 311 311 311 311
    311 311 311 311 311 311 311 311 311

  lattice BOTFUEL3
    013
    311 311
    311 311 311
    012 311 311 012
    311 311 311 311 311
    311 311 311 311 311 012
    012 311 311 012 311 311 311
    311 311 311 311 311 311 311 311
    311 311 311 311 311 311 311 311 311

  lattice TOPBLK3
    013
    331 331
    331 331 331
    011 331 331 011
    331 331 331 331 331
    331 331 331 331 331 011
    011 331 331 011 331 331 331
    331 331 331 331 331 331 331 331
    331 331 331 331 331 331 331 331 331

  lattice BOTBLK3
    013
    331 331
    331 331 331
    012 331 331 012
    331 331 331 331 331
    331 331 331 331 331 012
    012 331 331 012 331 331 331
    331 331 331 331 331 331 331 331
    331 331 331 331 331 331 331 331 331

! Fuel, Region D, 68 IFBA
  lattice TOPFUEL4
    013
    412 423
    412 413 423
    011 412 412 011
    412 413 423 412 412
    412 413 423 412 412 011
    011 412 412 011 412 412 412
    412 412 412 422 412 412 412 422
    421 411 421 411 421 411 421 411 421
  lattice BOTFUEL4
    013
    412 423
    412 413 423
    012 412 412 012
    412 413 423 412 412
    412 413 423 412 412 012
    012 412 412 012 412 412 412
    412 412 412 422 412 412 412 422
    421 411 421 411 421 411 421 411 421
```

```
  lattice TOPBLK4
    013
    431 432
    431 431 432
    011 431 431 011
    431 431 432 431 431
    431 431 432 431 431 011
    011 431 431 011 431 431 431
    431 431 431 432 431 431 431 432
    432 431 432 431 432 431 432 431 432
  lattice BOTBLK4
    013
    431 432
    431 431 432
    012 431 431 012
    431 431 432 431 431
    431 431 432 431 431 012
    012 431 431 012 431 431 431
    431 431 431 432 431 431 431 432
    432 431 432 431 432 431 432 431 432
```

```
  lattice TOPBLK5
    013
    531 531
    531 531 531
    011 531 531 011
    531 531 532 531 531
    531 531 532 531 531 011
    011 531 531 011 531 531 531
    532 531 532 532 531 531 531 531
    532 532 532 532 532 532 531 532 531
  lattice BOTBLK5
    013
    531 531
    531 531 531
    012 531 531 012
    531 531 532 531 531
    531 531 532 531 531 012
    012 531 531 012 531 531 531
    532 531 532 532 531 531 531 531
    532 532 532 532 532 532 531 532 531
```

```
! Fuel, Region E, 88 IFBA
  lattice TOPFUEL5
    013
    512 513
    512 513 513
    011 512 512 011
    512 513 523 512 512
    512 513 523 512 512 011
    011 512 512 011 512 512 512
    522 512 522 522 512 512 512 512
    521 521 521 521 521 521 511 521 511
  lattice BOTFUEL5
    013
    512 513
    512 513 513
    012 512 512 012
    512 513 523 512 512
    512 513 523 512 512 012
    012 512 512 012 512 512 512
    522 512 522 522 512 512 512 512
    521 521 521 521 521 521 511 521 511
```

```
! Fuel, Region E, 124 IFBA
  lattice TOPFUEL6
    013
    512 523
    512 513 513
    011 512 512 011
    512 513 523 512 512
    512 523 523 512 512 011
    011 512 512 011 522 512 512
    522 512 522 522 512 512 512 522
    521 521 521 521 521 521 521 521 521
  lattice BOTFUEL6
    013
    512 523
    512 513 513
    012 512 512 012
    512 513 523 512 512
    512 523 523 512 512 012
    012 512 512 012 522 512 512
    522 512 522 522 512 512 512 522
    521 521 521 521 521 521 521 521 521
```

```
  lattice TOPBLK6
    013
    531 532
    531 531 531
    011 531 531 011
    531 531 532 531 531
    531 532 532 531 531 011
    011 531 531 011 532 531 531
    532 531 532 532 531 531 531 532
    532 532 532 532 532 532 532 532 532

  lattice BOTBLK6
    013
    531 532
    531 531 531
    012 531 531 012
    531 531 532 531 531
    531 532 532 531 531 012
    012 531 531 012 532 531 531
    532 531 532 532 531 531 531 532
    532 532 532 532 532 532 532 532 532


[grid input]
! omitted



[INSERT]
  title "WABA"
  npin 17
  cell 041  0.29 0.34 0.35 0.40386 0.41783 0.48387 / mod
zirc4 he waba he zirc4
  cell 042  0.29 0.34              0.41783 0.48387 / mod
zirc4         he zirc4
  cell 043  0.29                                 0.48387
/ mod                  zirc4
  cell 050  0.54
/  ss
```

```
rodmap  4waba
  -
  -   -
  -   -   -
  -   -   -   -
  -   -   -   -   -
  -   -   -   -   -   041
  -   -   -   -   -   -   -
  -   -   -   -   -   -   -   -
  -   -   -   -   -   -   -   -   -

 rodmap  4top
  -
  -   -
  -   -   -
  -   -   -   -
  -   -   -   -   -
  -   -   -   -   -   042
  -   -   -   -   -   -   -
  -   -   -   -   -   -   -   -
  -   -   -   -   -   -   -   -   -

rodmap  20thimbles4wabas
 -
 -   -
 -   -   -
 050 -   -   050
 -   -   -   -   -
 -   -   -   -   -   042
 050 -   -   050 -   -   -
 -   -   -   -   -   -   -   -
 -   -   -   -   -   -   -   -   -
rodmap  4spacer
  -
  -   -
  -   -   -
  -   -   -   -
  -   -   -   -   -
  -   -   -   -   -   043
  -   -   -   -   -   -   -
  -   -   -   -   -   -   -   -
  -   -   -   -   -   -   -   -   -
```

```
rodmap  8waba
  -
  -   -
  -   -   -
  041 -   -   -
  -   -   -   -   -
  -   -   -   -   -   041
  -   -   -   -   -   -   -
  -   -   -   -   -   -   -   -
  -   -   -   -   -   -   -   -   -

rodmap  8top
  -
  -   -
  -   -   -
  042 -   -   -
  -   -   -   -   -
  -   -   -   -   -   042
  -   -   -   -   -   -   -
  -   -   -   -   -   -   -   -
  -   -   -   -   -   -   -   -   -

rodmap  16thimbles8wabas
 -
 -   -
 -   -   -
 042 -   -   050
 -   -   -   -   -
 -   -   -   -   -   042
 050 -   -   050 -   -   -
 -   -   -   -   -   -   -   -
 -   -   -   -   -   -   -   -   -

rodmap  8spacer
  -
  -   -
  -   -   -
  043 -   -   -
  -   -   -   -   -
  -   -   -   -   -   043
  -   -   -   -   -   -   -
  -   -   -   -   -   -   -   -
  -   -   -   -   -   -   -   -   -
```

```
rodmap  12waba
   -
   -   -
   -   -   -
   041 -   -   -
   -   -   -   -   -
   -   -   -   -   -   041
   041 -   -   -   -   -   -
   -   -   -   -   -   -   -   -
   -   -   -   -   -   -   -   -   -

 rodmap  12top
   -
   -   -
   -   -   -
   042 -   -   -
   -   -   -   -   -
   -   -   -   -   -   042
   042 -   -   -   -   -   -
   -   -   -   -   -   -   -   -
   -   -   -   -   -   -   -   -   -

 rodmap  12thimbles12wabas
  -
  -   -
  -   -   -
  042 -   -   050
  -   -   -   -   -
  -   -   -   -   -   042
  042 -   -   050 -   -   -
  -   -   -   -   -   -   -   -
  -   -   -   -   -   -   -   -   -

  rodmap  12spacer
   -
   -   -
   -   -   -
   043 -   -   -
   -   -   -   -   -
   -   -   -   -   -   043
   043 -   -   -   -   -   -
   -   -   -   -   -   -   -   -
   -   -   -   -   -   -   -   -   -
```

```
 rodmap  8waba4spacer
   -
   -   -
   -   -   -
   043 -   -   -
   -   -   -   -   -
   -   -   -   -   -   041
   041 -   -   -   -   -   -
   -   -   -   -   -   -   -   -
   -   -   -   -   -   -   -   -   -

 rodmap  8waba4top
   -
   -   -
   -   -   -
   042 -   -   -
   -   -   -   -   -
   -   -   -   -   -   041
   041 -   -   -   -   -   -
   -   -   -   -   -   -   -   -
   -   -   -   -   -   -   -   -   -

rodmap  24thimbles
  -
  -   -
  -   -   -
  050 -   -   050
  -   -   -   -   -
  -   -   -   -   -   050
  050 -   -   050 -   -   -
  -   -   -   -   -   -   -   -
  -   -   -   -   -   -   -   -   -

 axial   4W
                        41.2
      4spacer           61.6
      4waba            356.2
      4top             451.0
      20thimbles4wabas 466.6

 axial   8W
                        41.2
      8spacer           61.6
      8waba            356.2
      8top             451.0
      16thimbles8wabas 466.6

 axial  12W
                         41.2
      8waba4spacer       79.3
      12waba            338.4
      8waba4top         427.3
      12top             451.0
      12thimbles12wabas 466.6

axial NW
                        451.0
      24thimbles        466.6

 [CONTROL]

! control rod input section omitted
```

```
[EDITS]
axial_edit_bounds

20.90
32.23
41.22
48.52
55.82
61.54
70.43
79.32
87.36
95.39
103.43
109.14
120.61
132.07
143.53
154.99
160.71
172.17
183.63
195.09
206.55
212.27
223.30
234.34
236.02
247.07
258.11
263.83
274.87
285.90
287.58
298.63
309.68
315.39
326.06
336.72
338.40
347.29
356.18
361.24
366.95
377.99
389.03
390.70
401.75
412.80
418.52
427.30
437.46
447.62

[INSILICO]
    cell_homogenize true
    eq_set        spn_fv
    SPN_order     5
    Pn_order      3
    tolerance     1e-6
    dimension     3
    mesh          2
    Pn_correction true
    mat_library ap1000_mat_r3.h5
    xs_library
lib252_hetbondoneabs-noabssigp
    silo_output denovo_silo_out
    max_delta_z   15.0
    num_blocks_i  32
    num_blocks_j  10
    num_groups    23
    num_sets      1

 new_grp_bounds
    8.2085e+05
    1.1109e+05
    5.5308e+03
    1.8644e+02
    3.7612e+01
    3.5379e+01
    2.7697e+01
    2.1684e+01
    2.0397e+01
    1.5968e+01
    7.1500e+00
    6.7000e+00
    6.3000e+00
    1.0970e+00
    1.0450e+00
    9.5000e-01
    3.5000e-01
    2.0600e-01
    1.0700e-01
    5.8000e-02
    2.5000e-02
    1.0000e-02
    1.0000e-05
```